1994

Direct Determination Of Normal Mode Parameters And Modal Triggering Of Small Aftershocks

Steven Kamal

DIRECT DETERMINATION OF NORMAL MODE PARAMETERS

&

MODAL TRIGGERING OF SMALL AFTERSHOCKS

by

Kamal

Department of Earth Sciences

Submitted in the partial fulfillment
of the requirements for the degree of
Doctor of Philosophy

Faculty of Graduate Studies
The University of Western Ontario
London, Ontario
August 1994

ISBN 0-315-93243-0

ABSTRACT

Free oscillations of the earth (also called normal modes) depend on the shape and structure of the earth. Each mode is a decaying sinusoid, and the modal parameters (frequency, phase, Q and relative amplitudes) may be determined from seismic records of large earthquakes. The observed modal parameters act as constraints on possible earth models. The fine structure of the free oscillation peaks, such as multiplets and split peaks, are a source of information and speculation on second order variations of earth shape and structure, such as departure from sphericity and local homogeneities.

The normal mode parameters have traditionally been estimated through the Short Time Fourier Transform (STFT) method. It is well known, and we demonstrate here, that the STFT method gives the correct frequency (to the nearest Fourier component) but an incorrect amplitude spectrum for decaying sinusoids. We propose an alternative approach for modal parameter determination through a non-linear least-squares fit of wavelets, customized for the normal modes of the earth. Iterative minimization of the error function is carried out through Marquardt's method to obtain the normal mode parameters. This direct computation of parameters through modal fitting is tested with synthetic noise free data and several data sets with varying levels of random Gaussian noise. The values for the noisy data using this method are found to be much closer (within 10%) to the true parameter values than those obtained using the STFT method (which may be off by as much as 500%) for signal to noise ratios as low as 1.3. The method is then tested on the record of the Minahasa Peninsula earthquake of April 18, 1990 (M_S = 7.4). The results obtained for the real data give reasonable values for 50% of the modes only. The possible cause for this may be the splitting of modes and/or source generated nonmodal seismic noise.

The second part of the dissertation reports on the discovery of at least two normal mode periodicities (55.38 minutes, ${}_0S_2$ and 43.2 minutes, ${}_0T_2$) in the aftershock sequence of the Loma Prieta, California, earthquake (October 18, 1989; M_S = 7.1). The evidence for the presence of these two periods has been corroborated by two different methods. A third period, corresponding to ${}_0S_3$ is visible, though the

evidence is not as compelling as the former two periods. It is apparent that the normal modes generated by the earthquake are triggering small aftershocks ($1 \leq M_L \leq 2$). Strong evidence of the triggering of low magnitude aftershocks by normal modes is seen during the first 6 days following the mainshock. After 6 days, the decay of the normal modes and the decrease in number of aftershocks make it difficult to detect such an effect. We speculate on possible mechanisms. A clear understanding of this triggering will enhance our knowledge of focal processes in general.

Large aftershocks ($M_L \geq 3$), both in Loma Prieta earthquake sequence and in a catalog of the aftershocks of all $M_S \geq 7$ earthquakes around the world during the period 1970 to 1990, do not appear to be triggered by normal modes. However, this may simply reflect the fact that there are only a small number of large aftershocks, making the detection of periodicities difficult.

ॐ *

Ommmmmmm

किं कर्म किमकर्मेति कवयोऽप्यत्र मोहिताः ।
तत्ते कर्म प्रवक्ष्यामि यज्ज्ञात्वा मोक्ष्यसेऽशुभात् ॥ १६ ॥

Even the wise are bewildered,
What is Action and what is Inaction?
Understand the nature of Action
And you will be Truely free.

–Bhagvad Gita
Ancient Sanskrit Text, circa 500 BC

*A sacred monosyllable, chanted with resonance and slowly decreasing intensity at the beginning of all endeavours. It brings the blessings of the Holy Trinity of Hinduism, Brahmā (the Creator), Vishnu (the Preserver) and Śiva (the Destroyer) and assures Yogā (union) of the body and the soul with the infinite.

ACKNOWLEDGMENTS

Someone once asked me about my relations with Prof. Lalu Mansinha, my supervisor. "He gets ideas (in the middle of the night) and I implement them (in the morning)." I replied. And that is what this thesis is all about. My sincere thanks to him for guiding me to new horizons of science, geophysics in particular. Without his constant encouragement as well as criticism, I wouldn't be what I am.

Thanks are also to Prof. R.F.Mereu for allowing me to use his workstation for processing my time consuming jobs. Mr. Bernie Dunn smoothed away many computer problems at various stages. I thank Ms. Lynn Dietz of USGS for providing the unique aftershock sequence of the Loma Prieta earthquake.

The Canadian Commonwealth Scholarship played a major role in supporting me financially throughout these studies. Additional supports through Canadian Society of Exploration Geophysicists, Graduate Research Fellowship from University of Western Ontario are also acknowledged.

For last five years, the Department of Geophysics has been just like a family to me. We shared our good and bad times together and I made many good friends during this stay. I will always cherish these memories. Now that we grew up as the Department of Earth Sciences, I hope the old traditions will continue.

I am thankful to Pratibha, my wife, who has always been supportive to me and greeted me with a happy smile in the times of need. This study would not have been completed without her. And of course, there was Ankit, who used to think that my frequency spectra are nothing but "a bunch of grass". I hope I proved it otherwise.

Table of Contents

List of Tables

List of Figures

Prologue

"Where shall I begin, please your Majesty?" he asked.
"Begin at the beginning," the King said, gravely, "and go on till you come to the end: then stop."

Lewis Carroll, *Alice's Adventures in Wonderland.*

This thesis consists of two separate parts, related through the free oscillations (also known as normal modes) of the earth - the ringing of the earth like a bell after large earthquakes. The first part of the thesis presents a new method of determination of the parameters of free oscillation, frequency, amplitude, phase and decay rate (or the quality factor, Q). The second part presents the discovery of three normal mode periodicities (${}_0S_2$, 55.38 minutes; ${}_0T_2$, 43.2 minutes and probably ${}_0S_3$, 36.00 minutes) in the aftershock sequence of the Loma Prieta earthquake (October 18, 1989; M_L = 7.1). Periodicities in the aftershock sequence forces us to conclude that normal modes are triggering, i.e. advancing and retarding the time of occurrence of aftershocks. The evidence for such triggering is quite persuasive.

Chapters 1, 2 and 3 present the work on determinations of modal parameters. The triggering of aftershocks is described in Chapters 4, 5 and 6.

Part I

Determination of Modal Parameters

Chapter 1

Overview

The whole of science is nothing more than a refinement of everyday thinking.

Albert Einstein, *Out of my Later Years*, 1950.

1.1 Introduction

In the last thirty years or so, the free oscillations of the earth have progressed from a curiosity to a sub-discipline "Low frequency seismology". This field now includes the very long period nature of the seismic sources (from the amplitude of the modes), the anelastic structure of the earth (through the measurement of Q) and the lateral elastic variation of continental scale (studying the frequency shifts of the modes from the theoretical values). For any of the above problems, an accurate determination of the modal parameters is a very important step. In this study, we point out some basic problems with current methods (Short Time Fourier Transform [STFT] and various variations) of the determination of the modal parameters. We then try an alternative method, which in a sense, may be considered as a fitting of a customized wavelet, but actually is a method of multiparameter optimization.

We design a set of customized waveforms closely resembling the normal modes, and fit these, in a least-squares sense, to the observed seismogram. The method is very successful on the synthetic data, with and without noise, and found

to be more robust than the traditional STFT method, even with low signal-to-noise ratio.

This chapter presents an overview of the normal modes and some existing methods of parameter estimation. Chapter 2 describes the method of modal fitting. The results from the application of this method are presented in chapter 3 with a comparison with the STFT method of parameter estimation.

1.2 Normal Modes of the Earth

Elastic disturbances in a bounded body (e.g., the earth) can be represented with standing waves as well as travelling waves. For example, Rayleigh waves propagating around the earth surface result in a stationary interference pattern which is equivalent to a system of standing waves. The wavelengths of the standing waves on and in the earth must be an integral submultiple of the circumference of the earth. Only certain wavelengths (hence frequencies) are allowed, which are determined by the boundary conditions. These are the **free oscillations** or **normal modes** of the earth. The complete set of free oscillations can describe any general elastic disturbance in the earth. Any time dependent elastic displacement, be it a surface wave or a body wave, may be written as a superposition of the normal modes and *vice versa.*

Free oscillations are classified into two types of oscillations called **spheroidal** and **torsional** (or **toroidal**) oscillations. This classification is the spherical analogue of P-SV and SH motion for body waves, and Rayleigh and Love motion for surface waves. Torsional modes depend only on the shear velocity, whereas spheroidal modes depend upon both shear and compressional velocities. Torsional modes involve circumferential motion only whereas spheroidal modes are much more complex and involve radial displacement also. The simplest spheroidal mode is called the **breathing** mode which is the uniform expansion and contraction of the earth [Figure 1.1a]; it has a period of 20.08 minutes. The **football** mode, represents the deformation of the earth into the shape of a football [Figure 1.1b]; it has a period of 53.84 minutes. The simplest torsional mode is in fact the earth's rotation. The next mode is one in which two hemispheres rotate in opposite directions [Figure 1.1c], hence the name

torsional. For detailed description of the normal modes, the reader is referred to Aki & Richards (1980), Lapwood & Usami (1981) and Gubbins (1990).

1.2.1 Degeneracy of Modes

Each normal mode is denoted by the symbol of the type ${}_nS_l^m$ (spheroidal mode) or ${}_nT_l^m$ (toroidal mode); n is the **radial order number** and is equal to the number of nodal planes of the oscillations inside the earth. Modes with $n > 0$ are known as **overtones** and they are likely to be excited by deep earthquakes only. **Fundamental modes** ($n = 0$) are the most commonly excited modes and have been well studied in the literature. Theoretical derivations for normal modes use spherical surface harmonics $Y_l^m(\theta, \phi)$ and the Legendre function $P_l^m(\cos\theta)$, where θ and ϕ are the colatitude and the longitude respectively (Figure 1.2); l and m must be integers; l is the **angular order number** of the mode and m the **azimuthal order number.**

Any spherical harmonic Y_l^m has l nodal lines, out of which m pass through the pole, and the remaining $l-m$ are along lines of latitude (pole and latitude refer to the coordinate system). The rotation of the coordinate system will change the value of m but will not affect the total number of nodal lines l. In general, rotation will transform Y_l^m into a linear combination of spherical harmonics with the same l but different values of m. The frequency of the mode does not depend on m in a uniform sphere. All the modes with same angular order number l have the same frequency in a uniform, spherically symmetric earth model, but they can differ in their displacement patterns. This is known as **degeneracy**: several eigenfunctions have the same eigenvalue. This result applies to any spherically symmetric body because the modes with the same angular order number may be converted into each other simply by rotating the axes: rotation of the coordinate system will change displacement patterns (eigenfunctions) but not frequencies (eigenvalues). For each value of l there are $2l + 1$ possible values of m. l can take integer values as 0, 1 , 2, ...and $m = -l, -l + 1, -l + 2, \ldots, l + 1, l$. Such a group is called a **multiplet** and each member of a multiplet is called a singlet.

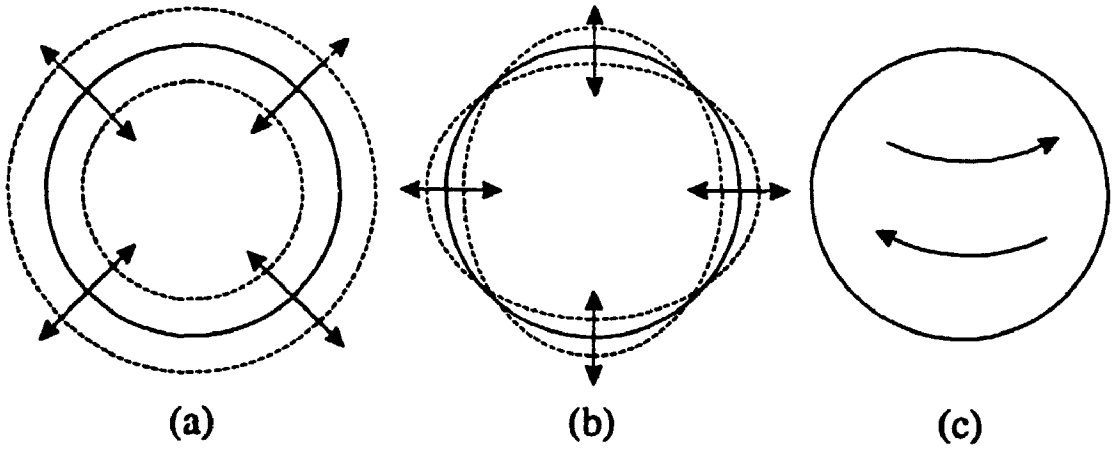

Figure 1.1: Particle motion of the fundamental spheroidal and toroidal modes. (a) the breathing mode, ${}_0S_0$, which has a period of 20.08 minutes, (b) the football mode, ${}_0S_2$, which has a period of 53.84 minutes, and (c) the toroidal mode, ${}_0T_2$, which has a period of 43.84 minutes.

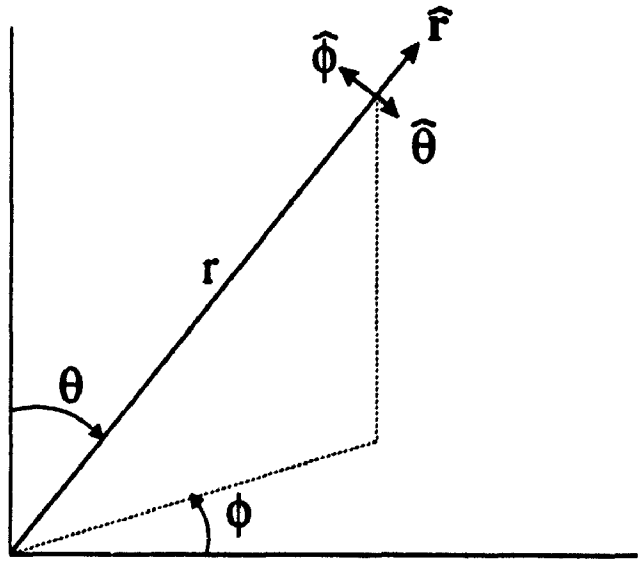

Figure 1.2: Spherical polar coordinates (r, θ, ϕ), with origin at the center of the earth. The line $\theta = 0$ is often taken to pass through a seismic source, in which case (r, θ, ϕ) are known as epicentral coordinates.

1.2.2 Damping of Normal Modes

In the absence of attenuation, the energy of all the earthquakes of the past would still be reverberating throughout the earth today. Attenuation is loss of energy per oscillation, or per wave cycle. When a wave travels through a medium, the energy in the wave is lost by various damping mechanisms. The physical mechanism of attenuation of waves in the earth at long wavelengths is not completely understood in spite of frequent speculation (Knopoff, 1964a; Masters & Gilbert, 1983).

Except for the nonlinear behavior near the focus, seismic strains are small and seismic oscillations take place in the domain of linear elasticity. Attenuation of harmonic signals is therefore exponential, and the rate of attenuation is describable by an exponential rate of decay

$$a(t) = Ae^{-\alpha t}\cos(\omega t + \phi) \tag{1.1}$$

where A is the initial amplitude, ϕ is the initial phase, ω is the frequency of the mode, and α is the attenuation parameter. It is useful to write

$$\alpha = \frac{\omega}{2Q} \tag{1.2}$$

where Q is the quality factor. Note that Q and α are just parameters and say nothing at all about the physical mechanism of attenuation.

1.2.3 Importance of Parameter Estimation

Each normal mode i is associated with four parameters, namely, amplitudes A_i, frequency ω_i, phase ϕ_i, and the quality factor Q_i. The departure of the observed frequencies of normal modes from their theoretical values provides estimates of asphericity, lateral heterogeneity and all other variations from spherical symmetry of the earth (Silver & Jordan,1981; Smith & Masters,1989; Pollitz,1990; Woodward & Masters,1992). Gilbert (1973) and Gilbert & Dziewonski (1975) have shown that the source mechanism (moment tensor) of an earthquake may be computed through model fitting to normal mode amplitudes and phases. Mendiguren (1980) also used the free oscillation data for source moment tensor studies. Anderson & Dziewonski (1982)

inverted the observed frequency shifts of normal modes to constrain upper mantle anisotropy.

Inversion of short period (as compared to the modal periods) seismic waves also provides information on the distribution of density and elasticity in the earth, which in turn shed some light on chemical composition, phase changes and the evolution of structure of the earth. Similarly, distribution of anelasticity provides additional constraints on the working structural models of the earth. Anderson & Archambeau (1964) developed an inversion method to characterize the earth's structure by means of Q values. Dziewonski & Anderson (1981) obtained the Preliminary Reference Earth Model (PREM) by simulating travel time observations, normal mode periods and several normal mode Q values.

1.3 Parameter Estimation and associated Problems

Since the first confirmed normal mode observations after the Great Chilean earthquake of May 20, 1960, several methods have been tried to determine modal parameters. Benioff *et al* (1961) determined Q values by measuring the width of the spectral peaks of normal modes observed in the Fourier spectrum. The half width at the half power level of the theoretical resonant peak is equal to α, from which Q can be calculated using Equation 1.2. However, the observed peaks are usually asymmetric and contaminated with noise, which renders this method of dubious reliability. Q has also been measured by examining the spectral amplitude decay of the modes in the time domain or in the frequency domain. Stein & Geller (1978) and Geller & Stein (1979) applied this technique by isolating different modes through narrow bandpass filtering and studying the amplitude decay of individual modes in the time domain using the Hilbert transform. This method is limited to single mode determinations and splitting of modes may lead to spurious values of Q (Masters & Gilbert, 1983).

Buland & Gilbert (1978) suggested the moment ratio technique for estimating the center frequency and the minimum width technique for measuring Q. The minimum width method involves multiplying the record by a trial growing exponential, $e^{\alpha t}$. The value of α that best cancels the effect of attenuation is the best estimate.

This value should also minimize the width of the spectral peak. Bolt & Brillinger (1979) have described a complex demodulation technique in which they use a least-squares estimator to retrieve the modal properties from the complex demodulator. Hansen (1982) applied this method to 24 long period recordings to estimate several modal Q values.

Simultaneous multimode estimations can be made using autoregressive method of Chao & Gilbert (1980). Values of modal properties can also be found using straight-forward non-linear least-squares fitting of resonance peaks in the frequency domain to narrowly bandpass filtered data for different modes (Masters & Gilbert, 1983).

Recently, Hori *et al* (1989) proposed a method named "Sompi" to estimate the frequencies and decay rates of the free oscillation parameters which is similar to an improved Prony's method described by Price (1979). Lindberg & Park (1987) estimated modal parameters using an extension of the nonparametric multiple taper method of Thomson (1982).

1.4 STFT Method

Despite the many available methods of parameter estimation, the most common technique appears to have been the short time Fourier transform (STFT) method. This method has been used by Alsop *et al* (1961) and Nowroozi (1968) during the early observations of normal modes. For good signal-to-noise ratio, this method works well and was used by Dratler *et al* (1971) to discover high-Q overtone modes. Sailor & Dziewonski (1978) measured Q's of many fundamental modes and overtones by stacking and stripping World-Wide Standard Seismographic Network (WWSSN) data and using STFT method. Kamal & Mansinha (1992) used STFT method to compute normal mode parameters from a recording of the Canadian superconducting gravimeter.

The short time Fourier transform (STFT) method consists of multiplying the signal $f(t)$ with a suitable window function $w(t)$, centered around $t = 0$ and of computing the Fourier coefficients of the product $f(t)\,w(t)$. The coefficients give a value of the frequency content of the signal $f(t)$ in the neighborhood of $t = 0$. This

procedure is then repeated with translated window function, i.e., $w(t)$ is replaced by $w(t + t_0)$, $w(t + 2t_0)$,..., where t_0 is a suitably chosen time shift. This results in a matrix of complex Fourier coefficients

$$C_{mn} = \int_{-\infty}^{\infty} f(t)\, w(t + nt_0)\, e^{im\omega_0 t} dt \tag{1.3}$$

where m,n are integers. The matrix of corresponding amplitude values can be computed from C_{mn}

$$A_{mn} = \sqrt{Re(C_{mn})^2 + Im(C_{mn})^2} \tag{1.4}$$

For any $m = k$, the column vector A_{kn} will provide the temporal variation of the corresponding frequency, $k\omega_0$. This amplitude is assumed to decay exponentially with time,

$$A_t = A_0 e^{-\alpha t} \tag{1.5}$$

$$\text{or} \quad \ln[A_t] = \ln[A_0] - \alpha t$$

The latter is a linear relation in t and the slope of the best line fit to $\ln[A_t]$ or logarithm of A_{kn} would provide the value of α, thus of Q, of the kth mode [Figure 1.3]. The standard deviation of this line fit also indicates the error in the value of Q. The frequency resolution (hence the error in frequency determination) is determined by the length of the segment used for spectrum.

In analysing for normal modes, the first window $w(t)$ is placed on the seismogram well after the subsidence of any saturation, caused during the initial part of the seismogram by the high amplitudes of early Rayleigh phases. Therefore, the time series used for modal analysis do not include early body wave arrivals. The function $w(t)$ is tapered. Well excited normal modes appear as distinct peaks in the amplitude spectrum.

1.4.1 Window length

The width of $w(t)$, or segment length, is critical. The smaller the segment, the more local is the spectrum. The frequency resolution decreases with decreasing segment length. The frequency resolution for 12 hour, 24 hour and 48 hour long segments

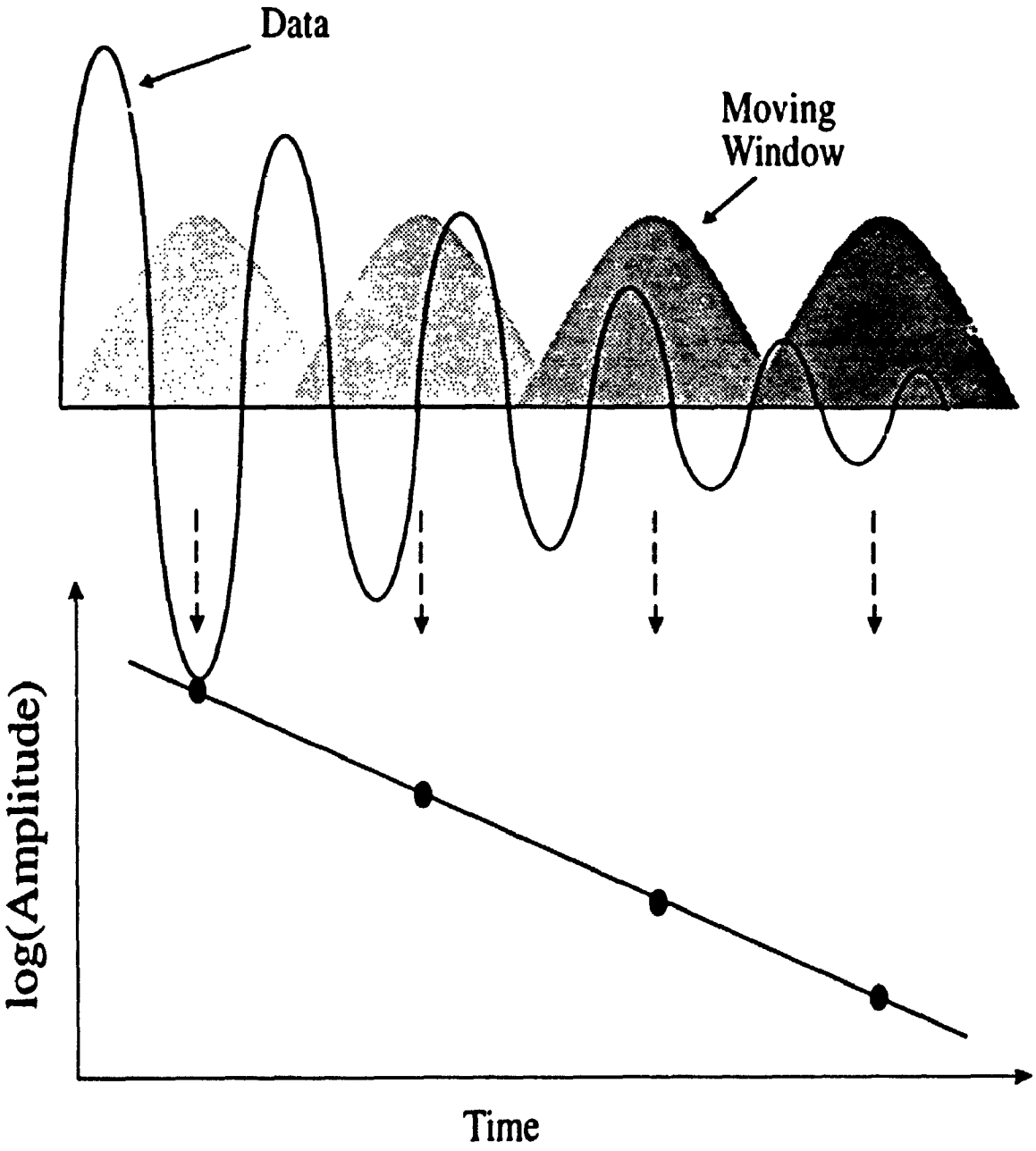

Figure 1.3: Parameter determination by the Short Time Fourier Transform (STFT) method. Amplitudes(A) of the modes are determined in successive windows, and $\log(A)$ is plotted against time. The slope of the best line fit gives the quality factor(Q).

are ~ 0.02 mHz, ~ 0.01 mHz and ~ 0.006 mHz, respectively. The fundamental spheroidal multiplet peaks (from ${}_0S_2$ to ${}_0S_{40}$) are not only closely spaced (~ 0.1 mHz), but also broadened through damping and through artifacts of processing, such as the convolution of the Fourier transform of the window with the true spectrum of the time series. Thus a higher frequency resolution (~ 0.01 mHz or better) than the average frequency separation of the modes (~0.1 mHz) is necessary. Taking a large STFT segment should achieve better resolution. One problem with taking larger segments is the decay of the modes to below the background noise level. As the length of segment is increased, the amplitudes of each multiplet drops and disappears into the ambient seismic noise level. One cannot increase the segment length indefinitely. Another problem is the occurrence of large aftershocks or earthquakes elsewhere. Small aftershocks do not excite normal modes to detectable levels and do not pose a problem. A large aftershock, or an earthquake elsewhere, places an upper limit to the length of a time segment. The singlets in each normal mode multiplet are very closely spaced (~ 3 to 0.01μHz), hence even higher frequency resolution is required to observe splitting of the modes. Very large data segments (100 hours to 3 years) have to be used to get the required frequency resolution. This is not always possible and in most cases the maximum segment length is governed by the background noise level and the time of occurrence of other large earthquakes.

Dahlen (1982) stated that the minimum record length for measuring frequencies and decay rates using a Hann window is $1.1QT$ and for determining amplitudes and phases is $0.5QT$, where T is the period of the mode. If the average value of Q is taken to be 275 and the average period of the modes to be 300 seconds, then a record length of about 23 hours would be sufficient for a good estimate of the frequencies and the decay rates. In the present study, a Hann window is used to determine the spectra with the STFT method.

1.4.2 Problems of STFT Method

Any seismogram can be modeled by a superposition of an appropriate number of normal modes. The seismogram can be thought of as a sum of exponentially decaying sinusoids (normal modes) and background seismic noise. The implicit assumption for

the amplitude determination through the Fourier transform is that any function $f(t)$ can be decomposed into a set of time-invariant sinusoids. The recorded seismogram is not time-invariant. The decay of normal modes (hence the seismogram) makes it inevitable that the amplitude, frequency and phase determined through Fourier transform will be incorrect. Figure 1.4 is a simple illustration of this effect.

Any standard spectral estimation technique requires apodization, i.e., applying a suitable taper to the data set prior to the transformation. This reduces the spectral leakage from the neighboring peaks in the frequency domain. Dahlen (1982) compared the use of several windows to taper the data segment for determination of free oscillation parameters. All tapers truncate the data set at both ends. If the data set is time-invariant, tapering does not affect the data set adversely. But, in case of the normal modes, most of the information is contained in the initial part of the data set (where it has the maximum amplitude), which is truncated by the operation of tapering. This results in loss of information at the ends of the data set, which in turn will reflect in the amplitude determination. A diagram in Figure 1.5 explains this effect.

Figures 1.6, 1.7 and 1.8 show an example of amplitude determination through Fourier transform method. A synthetic data set consisting of 35 normal mode frequencies is shown in Figure 1.6(a). All the modes in the data set have the same initial amplitude [Figure 1.6(b)] but different quality factor Q's [Figure 1.6(c)]. Figures 1.7(a) and 1.7(b) show untapered (or Boxcar) and a Hann windowed spectra of this time series respectively. It can be seen that the amplitude values for different frequencies are different in the spectra even if all the modes have same initial amplitude in the original data set. It appears from the spectrum that the amplitude decreases as the frequency increases. It is also to be noted that the tapered spectrum shows further decrease in the computed amplitudes. Figure 1.8 shows the error in peak amplitudes when Hann window is used to compute the spectrum. In the case of the data with added noise (real data), this decrease in amplitude will result in loss of signal-to-noise ratio (if the background noise is considered to be time-invariant). As a consequence, it will be difficult to identify the spectral peaks above the noise level.

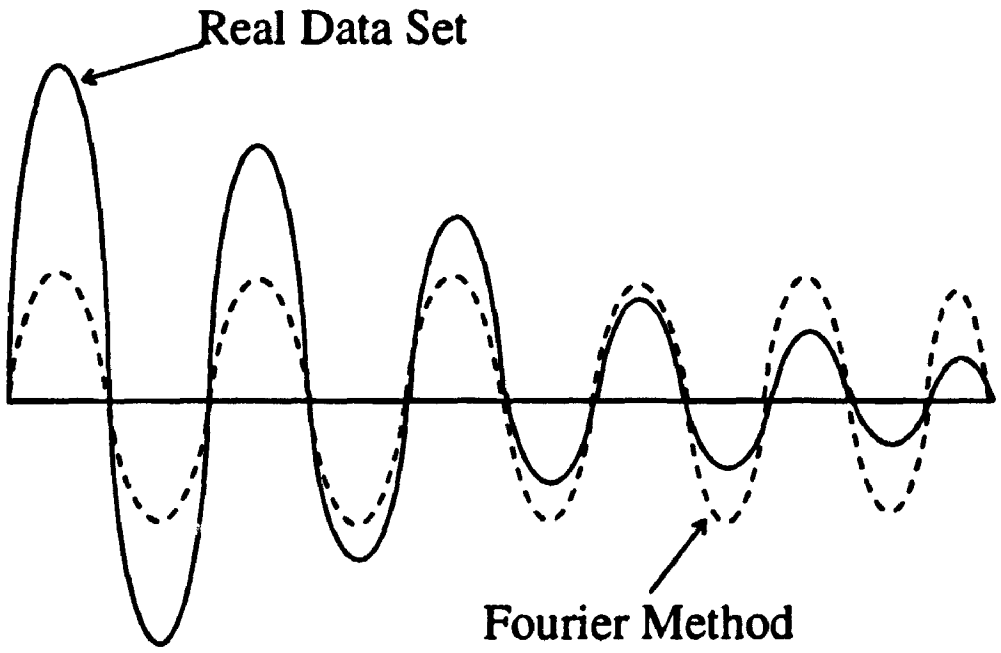

Figure 1.4: The effect of fitting a nondecaying sinusoid to a decaying signal. The amplitude of the corresponding frequency is not the true initial amplitude.

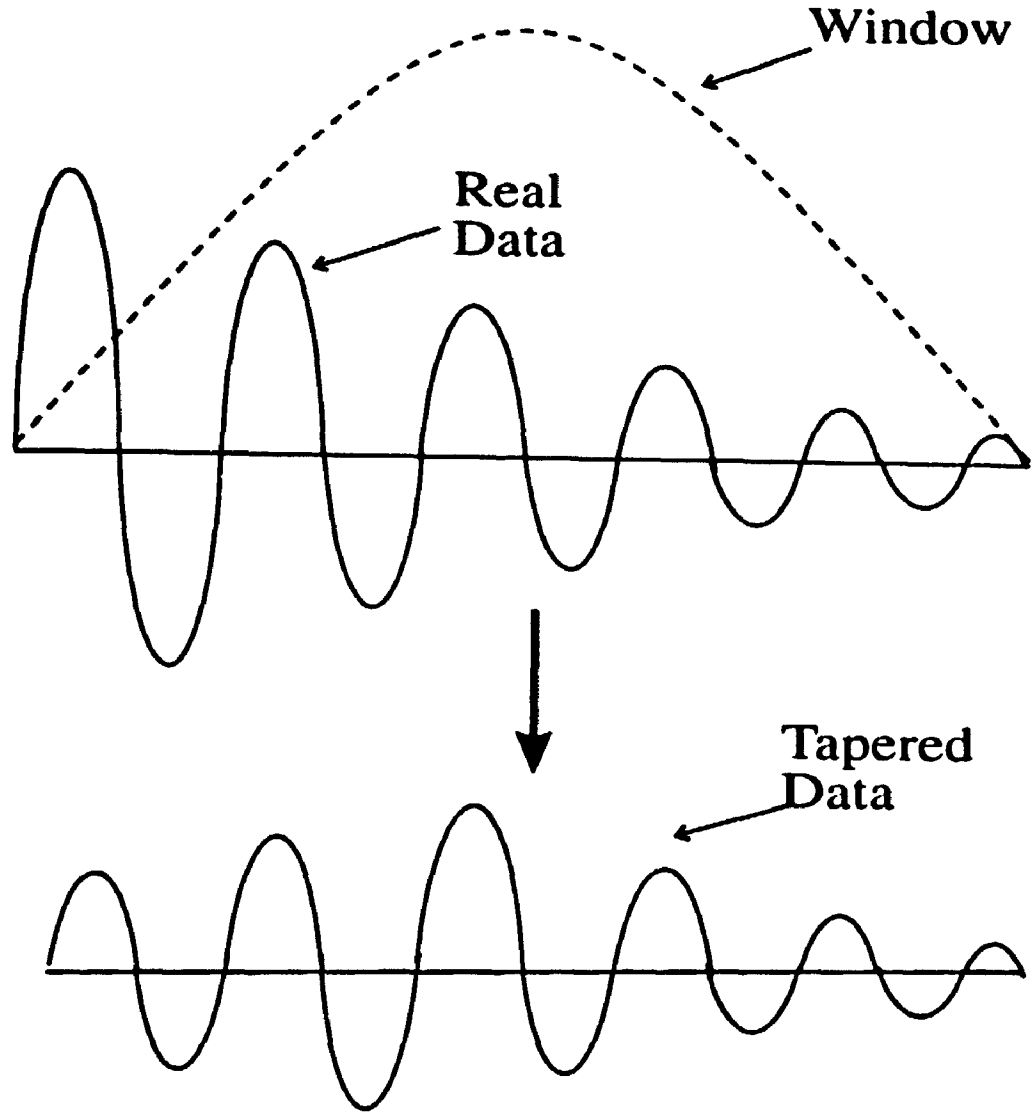

Figure 1.5: The effect of tapering on amplitude determination. Any taper truncates the ends of the data set, resulting in a severe loss of information (normal modes have important information at the front end).

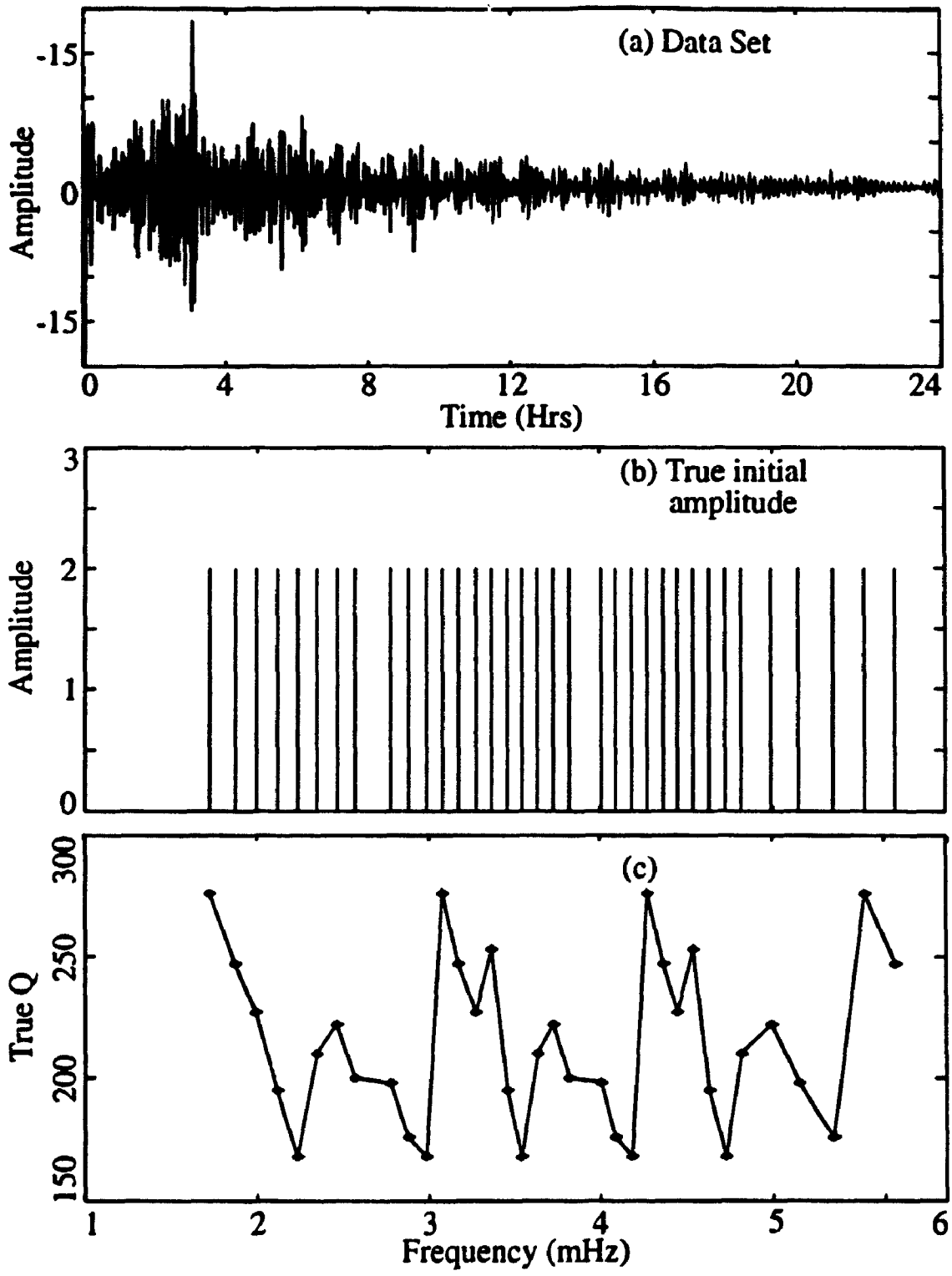

Figure 1.6: (a) A time series with 35 normal modes with equal initial amplitude. (b) the true initial amplitude values, and (c) the Q values for different frequencies.

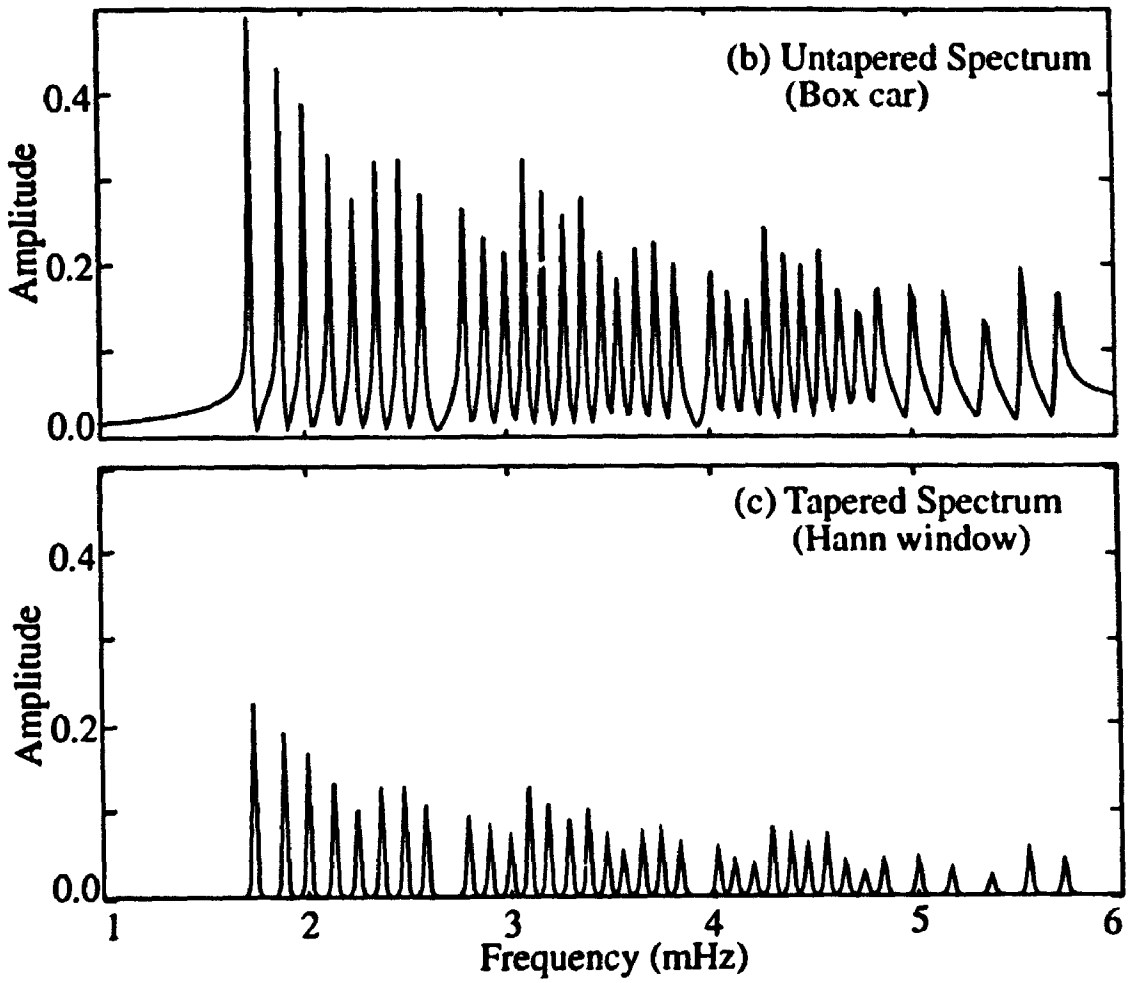

Figure 1.7: (a) The amplitude values for different frequencies differ from each other in untapered (Boxcar) spectrum. (b) Tapering of the data set with Hann window further reduces the amplitudes.

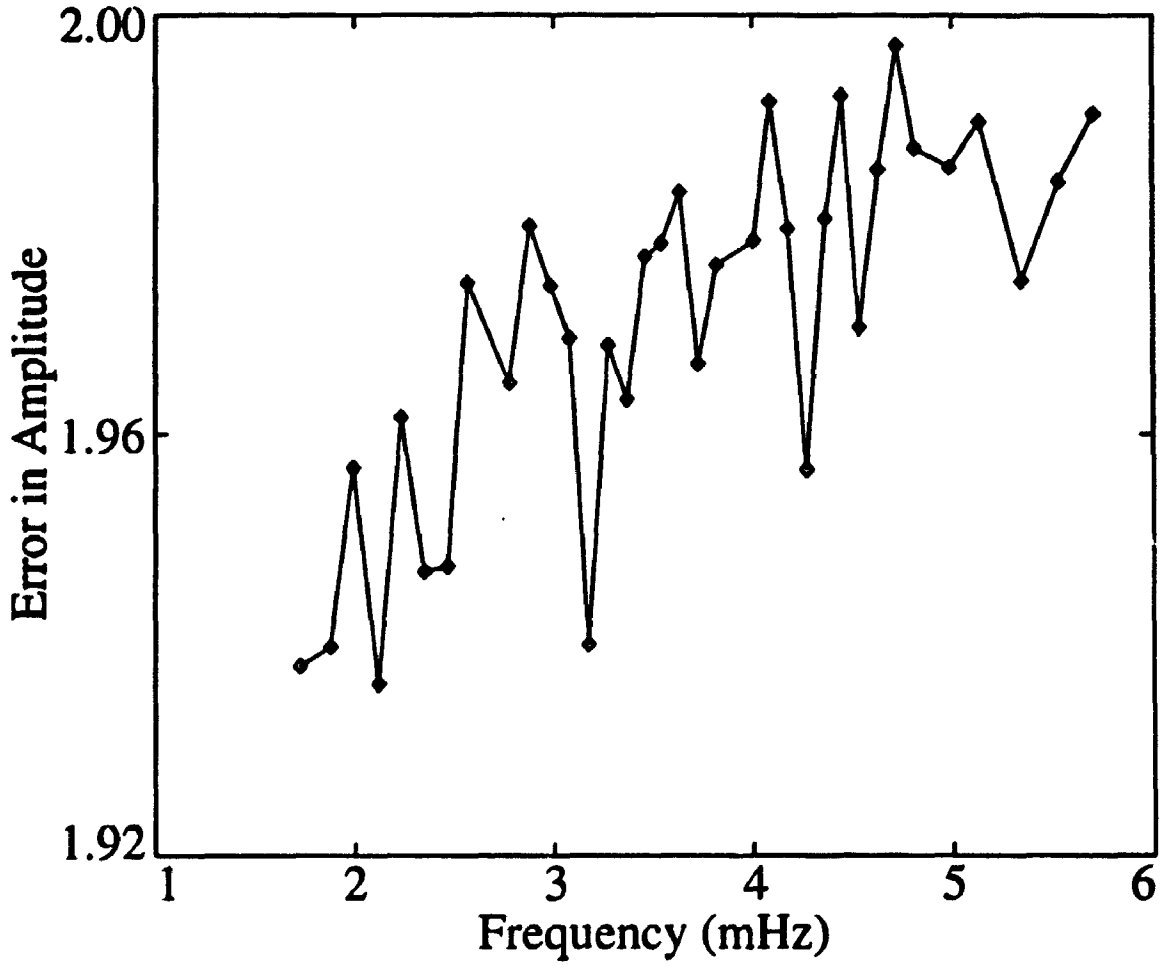

Figure 1.8: The error in peak amplitudes for different frequencies using Hann window.

1.5 Revival of an old method

To avoid the difficulties associated with the STFT method and to provide accurate values of the normal mode parameters, we investigate here the possibility of computing the parameters through a non-linear least-squares fitting of a set of functions to seismic time series. Each normal mode is associated with four parameters, namely, initial amplitude, initial phase, frequency and the quality factor which controls the decay of the mode. For each mode, we define an initial wavelet, a decaying sinusoid with best guess values of these parameters. A model is then fitted to the data set such that the difference between the model and the observations is minimized.

The method has one advantage over STFT method in that it requires much less data length to determine the modal parameters. With the STFT method, one has to consider several time windows, separated in time, utilising a much larger data set to determine Q. Also, the frequency values obtained from the STFT method are accurate only to the closest Fourier frequency. Since there is an inherent error in the amplitudes from the STFT method, the true initial amplitude of the modes cannot be determined from this method reliably. Our method of modeling of the normal modes removes many of these shortcomings of the STFT method and provides direct determination of the modal parameters.

Chapter 2

Modal Fitting (Inversion)

*α'γεωμέτρητος μηδεὶς εἰ'σίτω.**

- Inscription on Plato's door.

This method is basically a least-squares fit of a model of normal modes to the observed data set. Iterative adjustments in the parameters of the modes are made to minimize the discrepancy between the model response and the observations. This is a three step procedure:

- Define a good starting model closely representing the currently known normal mode parameters.
- Define a merit function, the criterion for discrepancy between the model response and the observed response.
- Search for the absolute minimum value of the merit function by successive adjustments in the parameters of the model function.

The set of parameters that minimizes the discrepancy between the model response and the observations is the best determined set of the modal parameters.

*Let no one enter my door, who is ignorant of geometry (mathematics).

2.1 The Model

Any observed seismogram can be modeled as the superposition of an infinite set of modes and any free oscillation mode can be represented as an exponentially decaying sinusoid. For a given source-receiver geometry, the amplitude response due to the kth mode at time t, $A_k(t)$, can be written as

$$A_k(t) = A_k(0)\cos(\omega_k t + \phi_k)e^{-\frac{\omega_k t}{2Q_k}} \tag{2.1}$$

where $A_k(0)$ is the initial amplitude at time $t = 0$. ω_k, ϕ_k and Q_k are frequency, initial phase and the quality factor, respectively, for the kth mode. One can model the observed seismogram as a function of modal parameters and time

$$f(\xi_i, t) = \sum_{i=1}^{N} A_i \cos(\omega_i t + \phi_i)e^{-\frac{\omega_i t}{2Q_i}} \tag{2.2}$$

where N is the number of modes (wavelets) to satisfactorily model the seismogram, and each ξ_i represents four parameters corresponding to the mode. The number of parameters in this model will therefore be $4N$. For the discrete case, the model function can be written as

$$f(\xi_i, t_j) = \sum_{i=1}^{N} A_i \cos(\omega_i t_j + \phi_i)e^{-\frac{\omega_i t_j}{2Q_i}} \quad j = 1 \ldots M \tag{2.3}$$

$f(\xi_i, t_j)$ in this equation is the model function or the objective function. In this case, the model consists of the $4N$ parameters and the model response is the seismogram constructed with (2.2).

2.2 The Merit Function

The merit function is a measure of departure of the model response from a perfect fit to the observed data. It can be defined as the sum of differences between the model response and the observed data, y_{obs} at all sample points, M. Therefore, the merit function χ can be written as

$$\chi = \sum_{j=1}^{M} \left\{ y_{obs}(t_j) - \sum_{i=1}^{N} f(\xi_i, t_j) \right\} \tag{2.4}$$

This form of the merit function might result in cancellation of the positive and negative errors at different points and may produce a small value of χ, even if there is a large discrepancy between the two. This is not a desirable property, hence we chose a merit function, which is a sum of the squares of the difference (error) between the two responses at all points of observation

$$\chi^2 = \sum_{j=1}^{M} \left\{ y_{obs}(t_j) - \sum_{i=1}^{N} f(\xi_i, t_j) \right\}^2 \tag{2.5}$$

Our goal is to achieve the global minimum of the merit function χ^2 by adjusting the parameter set ξ_i.

2.3 Minimization

At every minimum, the derivative with respect to each ξ_i of the merit function should vanish, i.e.

$$\frac{\partial \chi^2}{\partial \xi_i} = \frac{\partial}{\partial \xi_i} \sum_{j=1}^{M} \left\{ y_{obs}(t_j) - \sum_{i=1}^{4N} f(\xi_i, t_j) \right\}^2 = 0 \tag{2.6}$$

$$\text{or} \quad \sum_{j=1}^{M} \left[y_{obs}(t_j) - \sum_{i=1}^{4N} f(\xi_i, t_j) \right] \frac{\partial}{\partial \xi_i} f(\xi_i, t_j) = 0 \tag{2.7}$$

Taking partial derivatives with respect to each of the parameters $\xi_i, i = 1 \ldots 4N$, will yield $4N$ coupled equations in $4N$ unknown parameters ξ_i.

Since $f(\xi_i, t_j)$ is not a linear function of the parameters ξ_i, these $4N$ equations will not be linear in parameters. This system of equations cannot be solved analytically, so we have to consider methods of iterative approximations. The $4N$ dimensional parameter space has to be searched for the global minimum of χ^2. Under certain restrictive assumptions, the function χ^2 can be approximated analytically by a suitable function to locate the minimum.

2.3.1 Grid Search Method

This is a very simple and intuitive method and can be applied to almost any problem when the number of parameters to be searched is small and all the parameters

ξ_i's are independent of each other (Bevington, 1969). The lowest value of the merit function χ^2 is found by minimising it with respect to each parameter independently. Iterative local minimization of χ^2 for each parameter in succession leads to locating the absolute minimum. The basic procedure is as follows.

First, a physically permissible range of each parameter ξ_i is divided into p equal intervals $\Delta\xi_i$, so that the $4N$ parameter space is divided into $\prod_{i=1}^{4N} p_i$ hypercubes. A corner of one of the hypercubes is chosen as the starting guess values of parameters ξ_i's and value of χ^2 is computed at this grid point. Then, one parameter ξ_k is incremented by a quantity $\pm\Delta\xi_k$. The sign of $\Delta\xi_k$ is chosen such that the value of χ^2 decreases. This parameter is incremented until χ^2 stops decreasing. This indicates that the search has encountered a local minimum. The last three values of ξ_k and χ^2 are then used to determine true local minimum. It can be assumed that the variation of χ^2 near the minimum can be approximated by a parabolic function of the parameter ξ_k. If the last three values of ξ_k are $\xi_k(1)$, $\xi_k(2)$ and $\xi_k(3)$ where

$$\chi^2(3) > \chi^2(2) \leq \chi^2(1)$$

then the minimum of the parabola is given by the following (Bevington, 1969)

$$\xi_k(min) = \xi_k(3) - \Delta\xi_k \left[\frac{\chi^2(3) - \chi^2(2)}{\chi^2(3) - 2\chi^2(2) + \chi^2(1)} + \frac{1}{2} \right] \tag{2.8}$$

This is a local minimum in χ^2 with respect to each parameter ξ_k [Figure 2.1]. In the same manner, χ^2 is minimized for each parameter in turn. This procedure is repeated until χ^2 shows a negligible decrease (one can define the desired accuracy here).

The procedure is definitely very easy to implement, but only valid when the parameters are mutually independent. If this condition is not met, the convergence to the minimum is very slow. The method is good only for a moderate number of parameters. As the number of parameters increases, the method becomes much more complex and time consuming. In case of normal mode parameters, each mode is associated with four parameters. For a moderate earthquake ($M_S \geq 6.5$), the spectrum of the observed seismogram will show 30 to 40 spectral peaks on the average. Therefore, the number of parameters will generally be very large (> 100). Due to the large number of parameters, this method is not suitable for the present study.

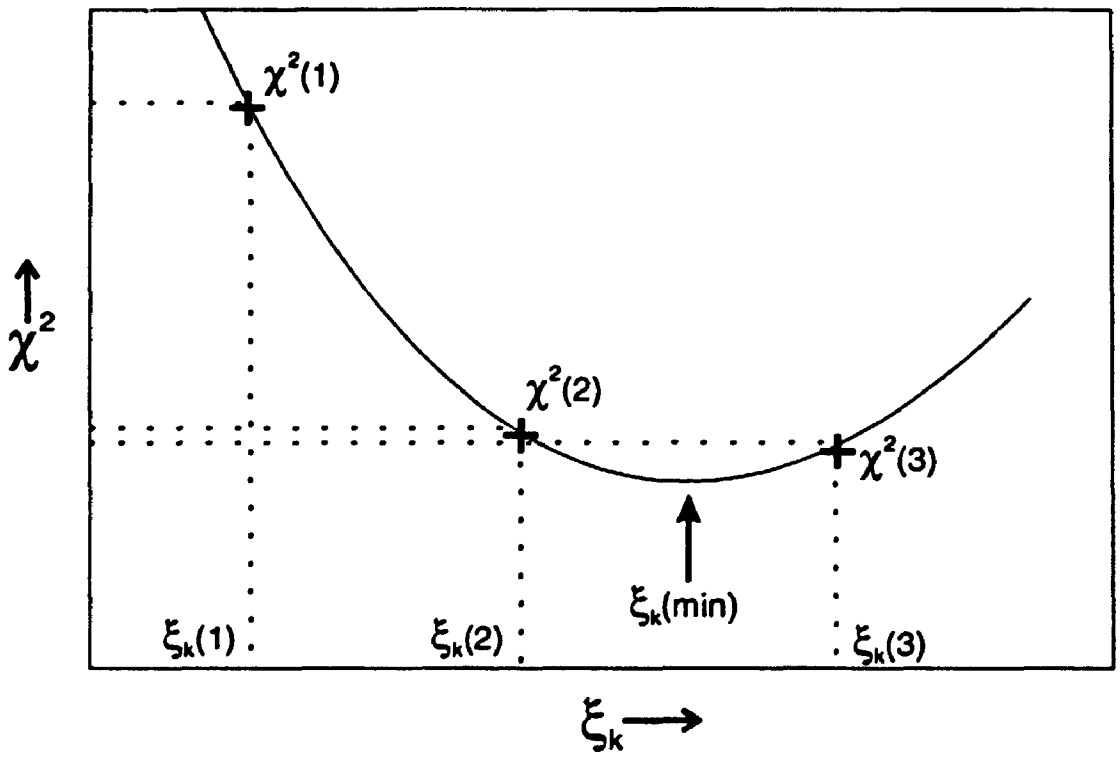

Figure 2.1: Approximation of the merit function χ^2 near a local minimum with respect to the parameter ξ_k.

2.3.2 Gradient Search Method

A more direct method of approaching the absolute minimum of the merit function χ^2 is the gradient search method. The method was originally proposed by Cauchy (1848) for the solution of a system of nonlinear equations. In this method, all the parameters ξ_i are adjusted simultaneously, with the relative magnitudes chosen such that the resultant direction of travel in parameter space is along the direction of maximum variation (the gradient) of χ^2. The gradient vector $\nabla\chi^2$ has components in parameter space equal to the rate of change of χ^2 along each axis.

$$\nabla\chi^2 = \sum_{i=1}^{4N}\left[\frac{\partial\chi^2}{\partial\xi_i}\hat{\xi}_i\right]$$

where $\hat{\xi}_i$ is a directional unit vector of the ξ_i coordinate axis. The partial derivatives with respect to parameters ξ_i can be numerically estimated as

$$\left(\nabla\chi^2\right)_i = \frac{\partial\chi^2}{\partial\xi_i} \simeq \frac{\chi^2(\xi_i + s\Delta\xi_i) - \chi^2(\xi_i)}{s\Delta\xi_i} \tag{2.9}$$

where s is a fraction of the step size $\Delta\xi_i$ to estimate the derivative by the forward difference scheme (other difference schemes may also be utilised). Usually, dimensions of various parameters are different, so the components of the gradient $\nabla\chi^2$ do not have the same dimensions either. The step sizes $\Delta\xi_i$'s can be used as a scaling constant to define dimensionless parameters η_i where

$$\eta_i = \frac{\xi_i}{\Delta\xi_i}$$

The derivatives with respect to η_i will then be

$$\frac{\partial\chi^2}{\partial\eta_i} = \frac{\partial\chi^2}{\partial\xi_i}\Delta\xi_i$$

It can numerically be estimated as

$$\begin{aligned}\frac{\partial\chi^2}{\partial\eta_i} &\simeq \frac{\chi^2(\xi_i + s\Delta\xi_i) - \chi^2(\xi_i)}{s\Delta\xi_i}\Delta\xi_i \\ &= \frac{\chi^2(\xi_i + s\Delta\xi_i) - \chi^2(\xi_i)}{s}\end{aligned} \tag{2.10}$$

A dimensionless gradient γ, with unit magnitude, may then be defined as

$$\gamma_i = \frac{\partial\chi^2/\partial\eta_i}{\sqrt{\sum_{i=1}^{4N}\left(\frac{\partial\chi^2}{\partial\eta_i}\right)^2}}$$

The gradient search method follows the direction of steepest descent, which is the direction opposite to the gradient γ. All the parameters are incremented by an amount $\delta\xi_i$ with magnitude equal to the size constant $\Delta\xi_i$ in direction opposite to the gradient γ_i

$$\delta\xi_i = -\gamma_i \Delta\xi_i = \frac{-\left(\frac{\partial\chi^2}{\partial\xi_i}\right)\Delta\xi_i^2}{\sqrt{\sum_{i=1}^{4N}\left\{\left(\frac{\partial\chi^2}{\partial\xi_i}\right)\Delta\xi_i\right\}^2}}$$

The minus sign ensures the decrease in χ^2. A search is carried out in the direction of the gradient, calculating the values of χ^2 at each step until χ^2 increases again (Powell, 1975). The gradient is computed again at this point and the search for the absolute minimum is continued in a new direction of gradient, until the absolute minimum is found.

This method becomes less efficient as the search approaches a minimum because the gradient changes only slightly near a minimum and the computation of derivatives in equation(2.10) requires taking differences between nearly equal numbers. At the minimum, this difference should be zero. Therefore, alternate methods are suggested in the regions close to the minimum.

2.3.3 Function Linearisation

One of the alternate methods to determine step size $\Delta\xi_i$ is through analytical approximation of the fitting function (the model function), proposed by Hartley (1961). The model function $f(\xi_i, t)$ can be expanded in parameters ξ_i and the parameter increments $\Delta\xi_i$ can be estimated using the method of linear least-squares. If the starting guess values for ξ_i are very close to a minimum, then the higher order terms in the Taylor series expansion of $f(\xi_i, t)$ can be neglected. This expansion about the point ξ_i' can be written as

$$f(\xi_i, t) \simeq f(\xi_i', t) + \sum_{i=1}^{4N}\left[\frac{\partial f(\xi_i', t)}{\partial\xi_i}\delta\xi_i\right] \qquad (2.11)$$

where $\delta\xi_i = \xi_i - \xi_i'$ and $f(\xi_i', t)$ is the model response with parameters ξ_i'. This equation is linear in the parameter increments $\delta\xi_i$ and can be solved by using the method of linear least-squares. The merit function χ^2 can be written as a function of

parameter increments $\delta\xi_i$

$$\chi^2 = \sum_{j=1}^{M} \left\{ y_{obs}(t_j) - f(\xi_i', t_j) - \sum_{i=1}^{4N} \left[\frac{\partial f(\xi_i', t_j)}{\partial \xi_i} \delta\xi_i \right] \right\}^2 \tag{2.12}$$

Minimising the χ^2 with respect to $\delta\xi_i$ requires that derivatives $\partial\chi^2/\partial\delta\xi_i$ are zero.

$$-2 \sum_{j=1}^{M} \left(\left\{ y_{obs}(t_j) - f(\xi_i', t_j) - \sum_{i=1}^{4N} \left[\frac{\partial f(\xi_i', t_j)}{\partial \xi_i} \delta\xi_i \right] \right\} \frac{\partial f(\xi_i', t_j)}{\partial \xi_k} \right) = 0 \tag{2.13}$$

This results in a set of $4N$ simultaneous linear equations in $\delta\xi_i$, which can be written as

$$\beta_k - \sum_{i=1}^{4N} \delta\xi_i \alpha_{ik} = 0, \quad k = 1 \ldots 4N \tag{2.14}$$

$$\text{where} \quad \beta_k \equiv \sum_{j=1}^{M} \left[y_{obs}(t_j) - f(\xi_i', t_j) \right] \frac{\partial f(\xi_i', t_j)}{\partial \xi_k} \tag{2.15}$$

$$= -\frac{1}{2} \frac{\partial \chi_0^2}{\partial \xi_k}$$

$$\chi_0^2 = \sum_{j=1}^{M} \left[y_{obs}(t_j) - f(\xi_i', t_j) \right]^2 \tag{2.16}$$

$$\text{and} \quad \alpha_{ik} \approx \sum_{j=1}^{M} \left[\frac{\partial f(\xi_i', t_j)}{\partial \xi_i} \frac{\partial f(\xi_i', t_j)}{\partial \xi_k} \right] \tag{2.17}$$

This reduces to a matrix equation

$$\underline{\beta} = \delta\underline{\xi} \cdot \underline{\alpha} \tag{2.18}$$

$$\delta\underline{\xi} = \underline{\beta} \cdot \underline{\alpha}^{-1} \tag{2.19}$$

$\underline{\beta}$ and $\delta\underline{\xi}$ are row vectors and $\underline{\alpha}$ is a symmetric matrix of order $4N$. The matrix $\underline{\alpha}$ also measures the curvature of the χ^2 hypersurface.

This method is very accurate and precise if the initial guess values are close to a minimum. If the starting values are far away, then the approximation of the χ^2 hypersurface is not valid and the result will be erroneous.

2.3.4 Marquardt Method

As we noted in section 2.3.2, the gradient search method is good for locating the minimum when the starting guess values are far from the minimum but the method

becomes inefficient near the minimum. On the other hand, the Taylor expansion (section 2.3.3) does not provide good results far from the minimum, but is efficient near the minimum. What we need is a combination of the above two methods, which can switch from one approach to the other, depending on the initial value (whether it is far from or near the minimum).

Marquardt (1963) proposed such an algorithm, combining the best of both the methods. A factor $(1+\lambda)$ is introduced in the diagonal terms of the curvature matrix $\underline{\alpha}$. The Marquardt factor controls the interpolation of the algorithm between the two methods.

Combining the Marquardt factor, equation (2.18) can be written as

$$\underline{\beta} = \delta\underline{\xi} \cdot \underline{\alpha}'$$

$$\text{where} \quad \alpha_{ik}' = \begin{cases} \alpha_{ik}(1+\lambda) & \text{for } i = k \\ \alpha_{ik} & \text{for } i \neq k \end{cases} \tag{2.20}$$

when λ is very small, these equations behave as the equation (2.18), which were developed using the linearisation of the model function $f(\xi_i', t_j)$. As λ becomes very large, the diagonal terms of the matrix $\underline{\alpha}$ are large compared to the off-diagonal terms and the matrix equations degenerate into $4N$ separate equations

$$\beta_i \simeq \lambda\, \delta\xi_i\, \alpha_i \tag{2.21}$$

which gives the parameter increment vector $\delta\underline{\xi}$ in the direction same as the vector $\underline{\beta}$ (or opposite to the gradient of χ^2). The parameter increment vector $\delta\underline{\xi}$ can be obtained by matrix inversion

$$\delta\underline{\xi} = \underline{\beta}\,\underline{\alpha}^{-1} \tag{2.22}$$

For a given initial guess value for the parameter $\underline{\xi}$, following recipe has been proposed by Marquardt (1963):

1. Compute $\chi^2(\xi)$,
2. Choose a small value of λ, say 0.001,
3. Solve for $\delta\xi$ and evaluate $\chi^2(\xi + \delta\xi)$,

4. If $\chi^2(\xi + \delta\xi) \geq \chi^2(\xi)$, increase λ by a suitable factor and repeat step 3.

5. If $\chi^2(\xi + \delta\xi) \leq \chi^2(\xi)$, decrease λ by the factor, update the trial solution $\xi \leftarrow \xi + \delta\xi$, and go back to step 3.

A condition for convergence is also needed to stop the iterations. One can put a lower bound on the change in the value of χ^2 as a convergence condition. Once an acceptable minimum is found, λ is set to zero and the matrix $\underline{\alpha}^{-1}$ is computed, which is the estimated covariance matrix of the errors in the fitted parameters ξ.

The Marquardt's method is used on a number of synthetic data sets (with and without noise) and a real data set acquired on the Canadian superconducting gravimeter. The results from these data sets are discussed in next chapter.

Chapter 3

Application of the Method

*Muss es sein? Es muss sein.**

Ludwig Van Beethoven, *Epigraph to String Quartet in F Major*, Opus 135

Modal fitting was applied to invert synthetic as well as real seismic data sets to compute normal mode parameters.

3.1 Synthetic Data

Four different synthetic time series were generated at 10 second sampling interval using the following components:

Series I. Four different periods corresponding to ${}_0S_{13}$, ${}_0S_{19}$, ${}_0S_{26}$, and ${}_0S_{32}$ (Table 3.1). The values of Q for these modes are taken from Sailor & Dziewonski (1978). These modes were assigned different amplitudes, based on the relative amplitude values in the spectrum of the record of the Minahasa Peninsula earthquake of April 18, 1990. All frequencies were assigned zero phase.

Series II. Two periods and Q corresponding to ${}_0S_{13}$ and ${}_0S_{26}$, each consists of two singlets about 0.5 seconds apart (Table 3.2). The value of Q for each singlet

*Must it be? It must be.

was perturbed from that of the corresponding multiplet in Series I. The STFT method requires several segments of this time series, 120 hours (5 days) each, to determine the parameters of all the singlets (section 1.4.1).

Series III. Only one spheroidal mode ${}_0S_{19}$ with four closely spaced singlets about 0.04 to 0.3 seconds apart (Table 3.3). The Q values are perturbed from that of ${}_0S_{19}$ in Series I. This time series requires at least 840 hours (35 days) of data to be analysed in order to resolve all the singlets. Such a long series cannot be used for real seismic data because of the decay of the modes (section 1.4.1).

Series IV. 35 spheroidal modes in the period range of 150 seconds to 600 seconds (${}_0S_7$ to ${}_0S_{43}$). This seismogram and its spectrum are shown in Figure 3.1. These modes are among the most commonly excited normal modes observed on a long period vertical seismometer after large earthquakes. The frequencies and the Q values of these modes were perturbed from the values observed for the Minahasa Peninsula earthquake of April 18, 1990 (Kamal & Mansinha, 1992).

To obtain the free oscillation parameters from the data set, we start with an initial guess model

$$\left.\begin{aligned} A_i &= 1.0 \\ \phi_i &= 0.0 \\ Q_i &= 100.0 \end{aligned}\right\} \quad i = 1 \ldots N \tag{3.1}$$

where N is the number of modes that we fit to the given time series. The initial values for the frequencies ω_i are set in the following manner. An FFT routine FOURG (Childers & Durling, 1975) is used to compute amplitude spectra of these synthetic series. Prior to computing the Fourier transform, a Hann window is used to taper the time series. All the frequency peaks (these peaks will be at the nearest Fourier component to the true frequency) above the noise level are identified in the spectra and are considered as the starting guess values [Figure 3.1(b)]. With this set of starting values for the parameters, the search for the minimum of the merit function χ^2 is carried out.

Physically impossible results are occasionally encountered during the search for the minimium. Therefore, it is necessary that some limits be imposed on

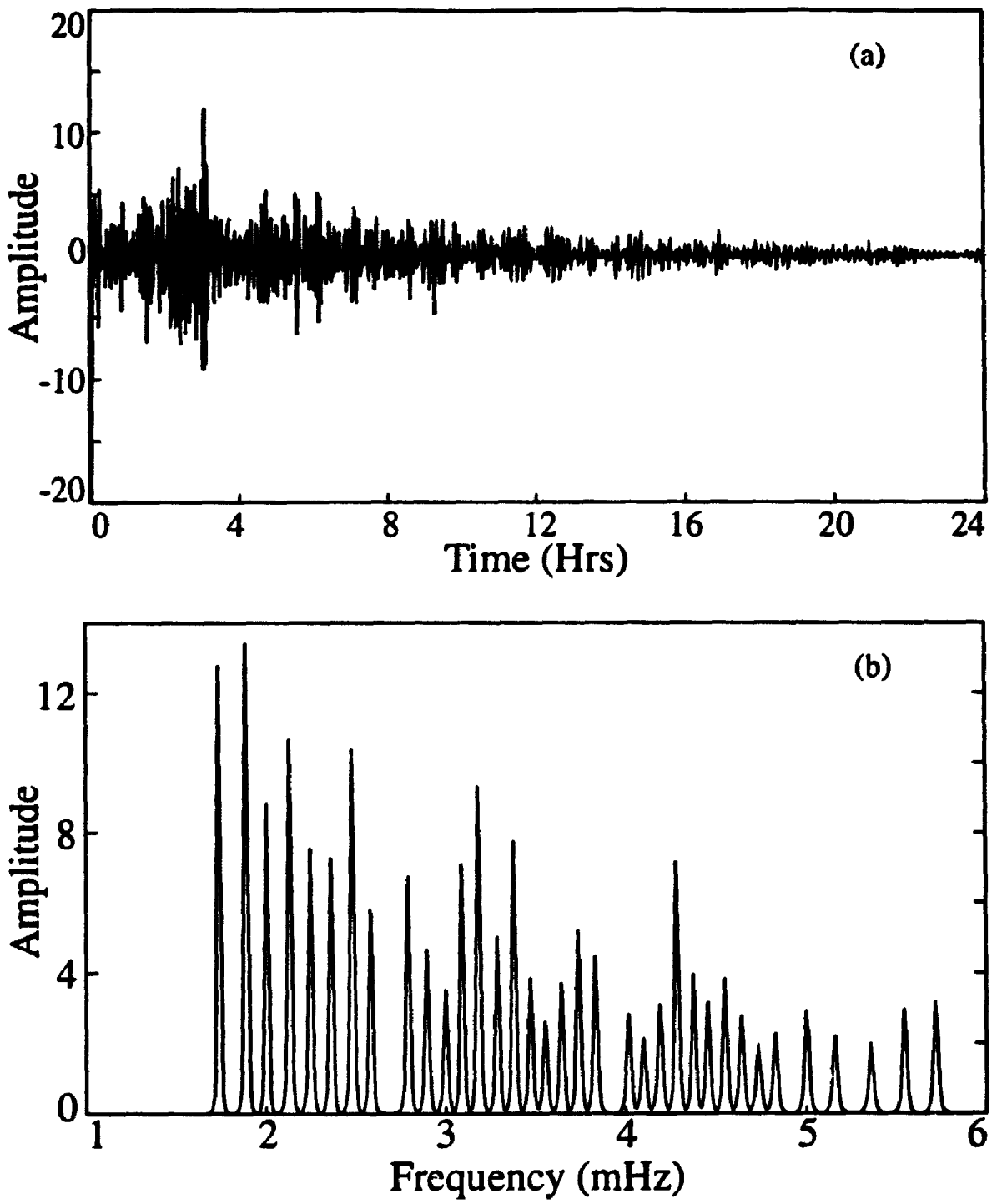

Figure 3.1: (a) A 24 hour long noise free synthetic record of 35 fundamental spheroidal modes (Series IV). (b) Spectrum of the above record using a Hann window.

the allowable range of the parameters:

- Amplitudes $A_i > 0$.
- Each frequency ω_i is allowed to vary only between the two adjacent starting values of the frequencies, ω_{i-1} and ω_{i+1}. If three consecutive modes in the starting model have frequencies ω_1, ω_2 and ω_3, then the value of ω_2 in the solution is allowed to vary between ω_1 and ω_3 only.

$$\omega_1 < \omega_2 \leq \omega_3$$

- Phase $-\pi \leq \phi_i \leq \pi$.
- A negative quality factor corresponds to a exponentially increasing mode, which is not physically possible. Also, normal modes are known to be moderately decaying phenomena, therefore a very high Q value, which implies an almost nondecaying signal, is discarded as the background noise.

$$0 < Q_i < 10000$$

These conditions are implemented in the computer routine used for the purpose.

Kamal & Mansinha (1992) used STFT method to compute the modal parameters, therefore their frequency values will only be accurate to the nearest Fourier frequencies determined by the time length of the window. To check the validity of the inversion method for non-Fourier frequencies, we perturbed the frequencies of the modes (within the adjacent Fourier frequencies for a given length of the time series) from those computed by Kamal & Mansinha (1992) in Series IV.

Modal fitting is used to compute the modal parameters from the first few hours of data. The results are compared with those obtained using STFT method. For the STFT method, a 24 hour Hann window is used to compute the spectra in succession, each separated by 4 hours in time (At least 6 such segments are needed to determine Q values). The modal fitting requires only 6 hours of data to determine the modal parameters from the noise free data set. Tables 3.1, 3.2, 3.3 and 3.4 show the computed modal parameters using the modal fitting and those obtained with the STFT method.

${}_0S_n$	Period (seconds)			Q		
	True	STFT	Modal Fit	True	STFT	Modal Fit
13	473.55	474.73	473.55	276	275.32	275.99
19	360.21	360.00	360.21	168	168.10	168.00
26	289.78	289.93	289.78	165	164.92	164.99
32	250.46	250.43	250.46	150	150.01	150.00

Table 3.1: The periods and Q determined for four synthetic spheroidal modes each consisting of a single peak each (Series I).

${}_0S_n$	Period (seconds)			Q		
	True	STFT	Modal Fit	True	STFT	Modal Fit
13	473.55	474.73	473.55	276	244.16	275.72
	473.04		473.04	270		269.64
26	290.02	289.93	290.02	170	158.23	169.97
	289.78		289.78	165		164.95

Table 3.2: The periods and Q determined for two synthetic spheroidal modes each consisting of two singlets (Series II).

${}_0S_n$	Period (seconds)			Q		
	True	STFT	Modal Fit	True	STFT	Modal Fit
19	360.36	360.00	360.38	180	156.72	182.35
	360.21		360.24	168		156.96
	360.17		360.17	170		190.13
	359.84		359.87	160		161.29

Table 3.3: The periods and Q determined for a single synthetic spheroidal mode consisting of four singlets of different frequency and Q (Series III).

Period (seconds)			Initial Amplitude			Q		
True	STFT	Modal Fit	True	STFT	Modal Fit	True	STFT	Modal Fit
579.80	579.86	579.80	1.140		1.140	276.00	275.97	276.00
533.30	533.33	533.30	1.402		1.402	247.00	246.98	247.00
502.30	502.32	502.30	1.060		1.060	227.00	226.98	227.00
472.10	472.13	472.10	1.620		1.620	195.00	194.98	195.00
447.60	447.66	447.60	1.490		1.490	168.00	167.98	168.00
425.60	425.61	425.60	1.145	N	1.145	210.00	209.99	210.00
405.60	405.63	405.60	1.620	o	1.620	222.00	221.96	222.00
389.10	389.18	389.10	1.093		1.093	200.00	199.92	200.00
360.00	360.00	360.00	1.440		1.440	198.00	197.96	198.00
346.90	346.98	346.90	1.264		1.264	176.00	175.83	176.00
334.80	334.88	334.80	1.085		1.085	168.00	167.99	168.00
324.80	324.81	324.80	1.113	E	1.113	276.00	275.93	276.00
315.30	315.32	315.30	1.753	s	1.753	247.00	246.93	247.00
305.30	305.30	305.30	1.122	t	1.122	227.00	226.88	227.00
296.90	296.90	296.90	1.533	i	1.533	253.00	252.94	253.00
288.90	288.96	288.90	1.194	m	1.194	195.00	194.73	195.00
282.30	283.27	282.30	1.111	a	1.111	168.00	166.90	168.00
275.10	275.15	275.10	1.101	t	1.101	210.00	209.93	210.00
268.30	268.32	268.30	1.474	e	1.474	222.00	221.96	222.00
261.80	261.81	261.80	1.571		1.571	200.00	200.01	200.00
249.70	249.71	249.70	1.105		1.105	198.00	197.70	198.00
244.70	244.75	244.70	1.090		1.090	176.00	175.51	176.00
239.30	239.33	239.30	1.824		1.824	168.00	168.23	168.00
234.10	234.14	234.10	1.772		1.772	276.00	275.81	276.00
229.10	229.17	229.10	1.224		1.224	247.00	246.51	247.00
225.00	224.41	225.00	1.172		1.172	227.00	227.46	227.00
220.40	220.40	220.40	1.203		1.203	253.00	252.85	253.00
216.00	216.54	216.00	1.476		1.476	195.00	194.80	195.00
211.70	211.76	211.70	1.364		1.364	168.00	168.13	168.00
207.60	207.69	207.60	1.140		1.140	210.00	209.77	210.00
200.40	200.46	200.40	1.402		1.402	222.00	221.90	222.00
194.20	194.59	194.20	1.419		1.419	198.00	197.63	198.00
187.00	187.01	187.00	1.620		1.620	176.00	175.98	176.00
180.70	180.75	180.70	1.145		1.145	276.00	275.88	276.00
175.20	174.25	175.20	1.620		1.620	247.00	246.90	246.99

Table 3.4: The parameters (period, initial amplitude and quality factor) of the normal modes used in the synthetic data set (Series IV).

In the absence of background noise, both methods provide good and similar Q values for the modes well separated in frequency [Figure 3.2]. The analysis of multiplets is difficult with STFT method as one requires longer time series to achieve a good resolution for closely spaced singlets. Tables 3.2 and 3.3 show that the STFT method provides average values of the parameters of various multiplets, whereas modal fitting gives parameters for all the singlets separately and accurately. True initial amplitudes cannot be obtained from the STFT method (because these are decaying sinusoids), but modal fitting provides initial amplitudes also. The frequency values from the STFT method are only good up to the nearest Fourier frequency. However, modal fitting gives value closer to the true frequency present in the data. Figure 3.2 compares the Q values obtained by both methods.

3.2 Synthetic data with Noise

Seismic time series always contain background noise. Therefore, the modal fitting was tested on more realistic data sets. These data sets are formed by adding variable noise to the synthetic data set shown in Figure 3.1 (Series IV). The noise series were generated using the rou·ine **gasdev** (Press *et al*, 1992). The Fourier amplitude spectra of these time series were determined using the Hann window. Three such series with their respective amplitude spectra are shown in Figures 3.3, 3.4 and 3.5. The average noise level is different in these series. The signal-to-noise ratio, defined as the ratio of peak amplitude to the average noise level in the near vicinity of the peak, varies from ~ 30 (for lower frequencies) to ~ 1.3 (for higher frequencies).

The parameter values from these noisy data sets provide very exciting results. Tables 3.5 to 3.10 show modal parameters obtained with the STFT method and those by modal fitting. The Tables 3.6, 3.8 and 3.10 also show the estimated errors in Q values obtained using both methods. In STFT method, the error in Q is the standard deviation of the best line fit in equation(1.5). For modal fitting, the error is computed from the inverse of the curvature matrix α in equation(2.22). Note that the errors in Q determined by modal fitting are in a reasonable range (~10%). On the other hand, for low S/N ratios, the error in Q determined with STFT method are very

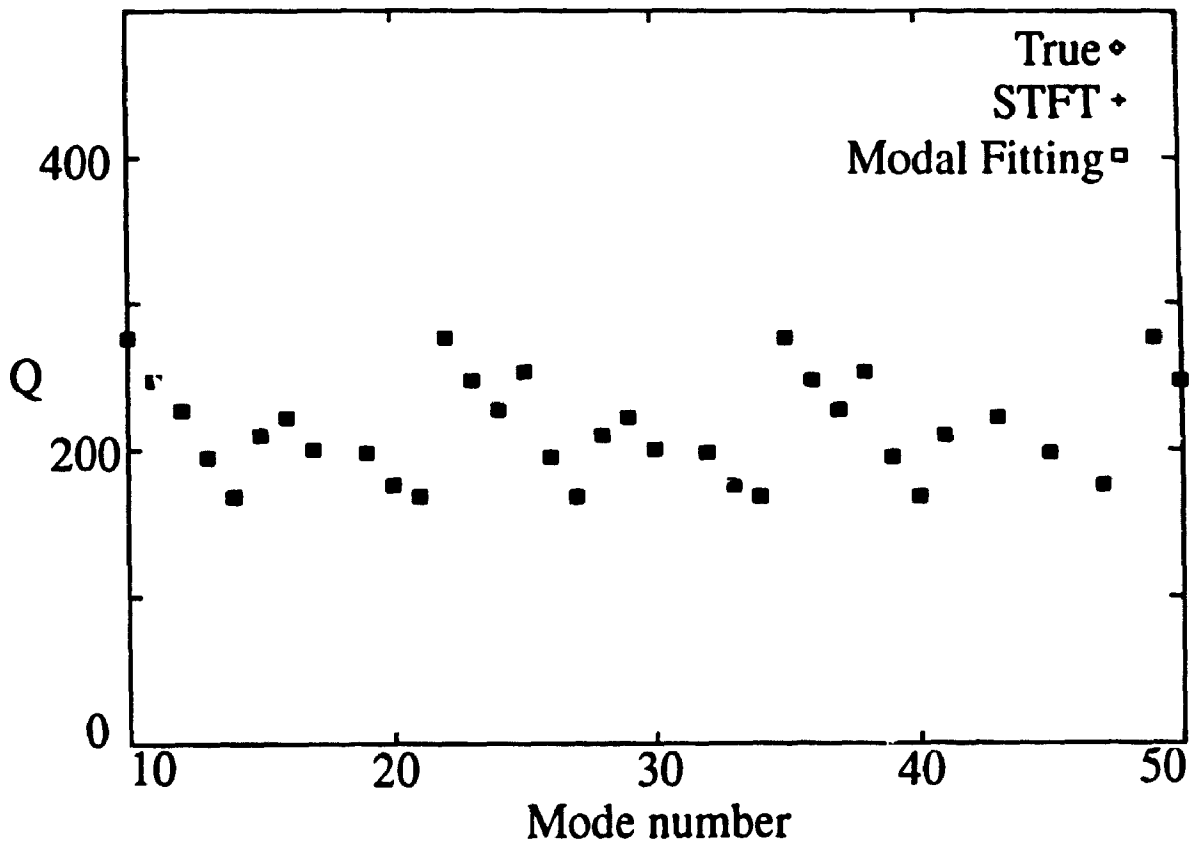

Figure 3.2: Comparison of the Q values in noise free data set using modal fitting and STFT method. The modal fitting method and the STFT method provide similar results with noisefree data.

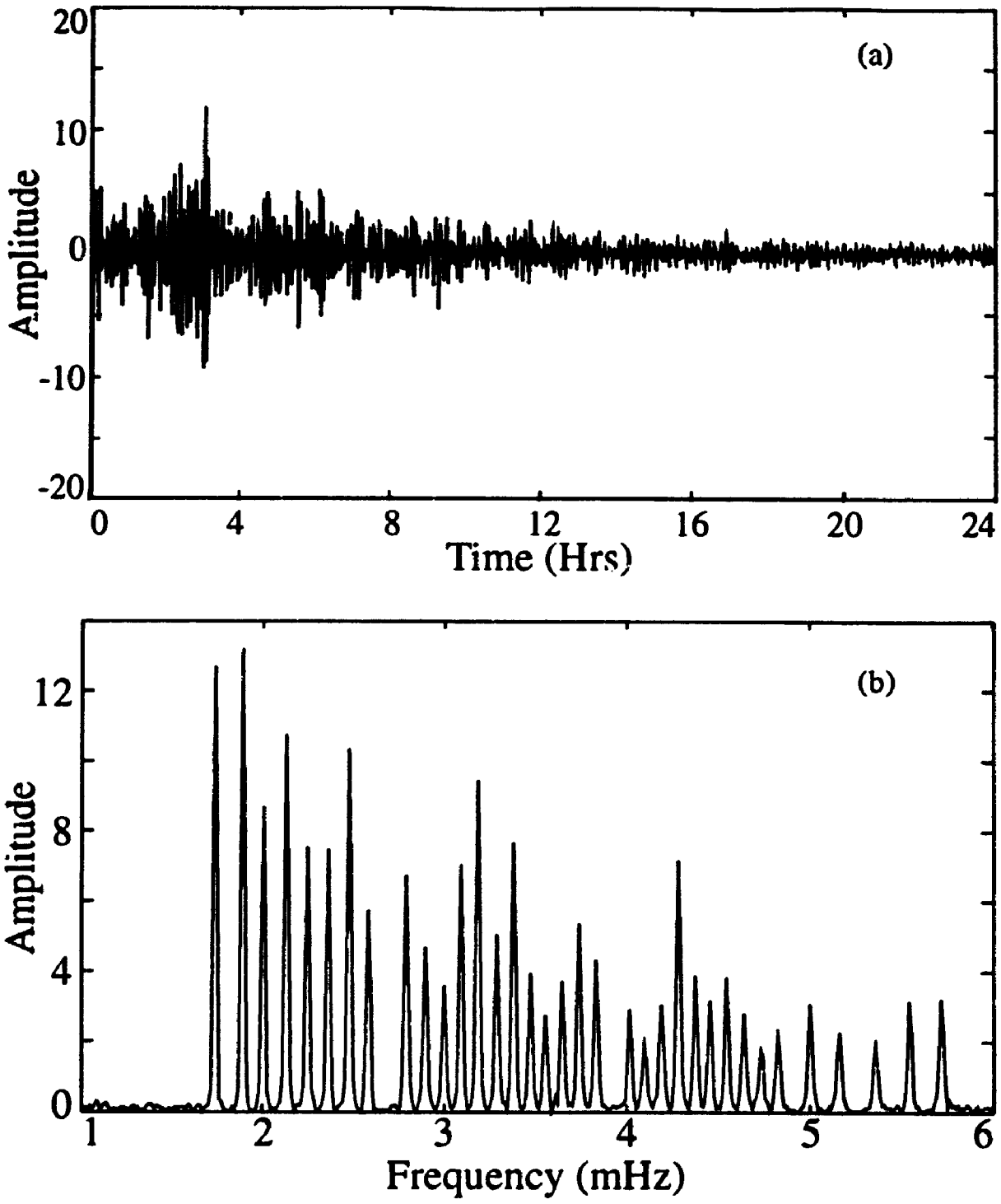

Figure 3.3: (a) A 24 hour long synthetic record of 35 spheroidal modes with added gaussian random noise. (b) Spectrum of the above record using a Hann window.

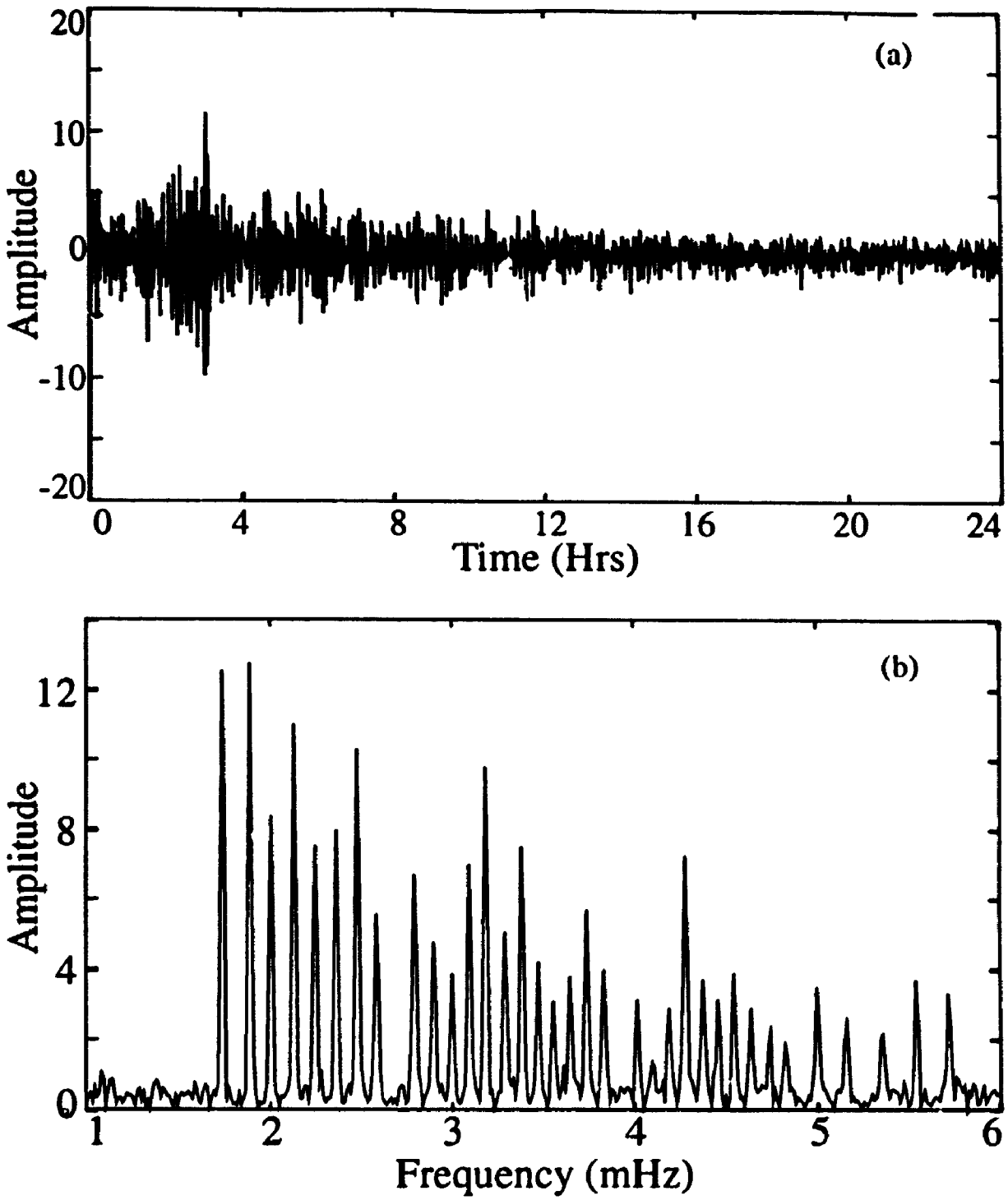

Figure 3.4: (a) A 24 hour long synthetic record of 35 spheroidal modes with added gaussian random noise. Noise magnitude is more than that of Figure 3.3. (b) Spectrum of the above record using a Hann window.

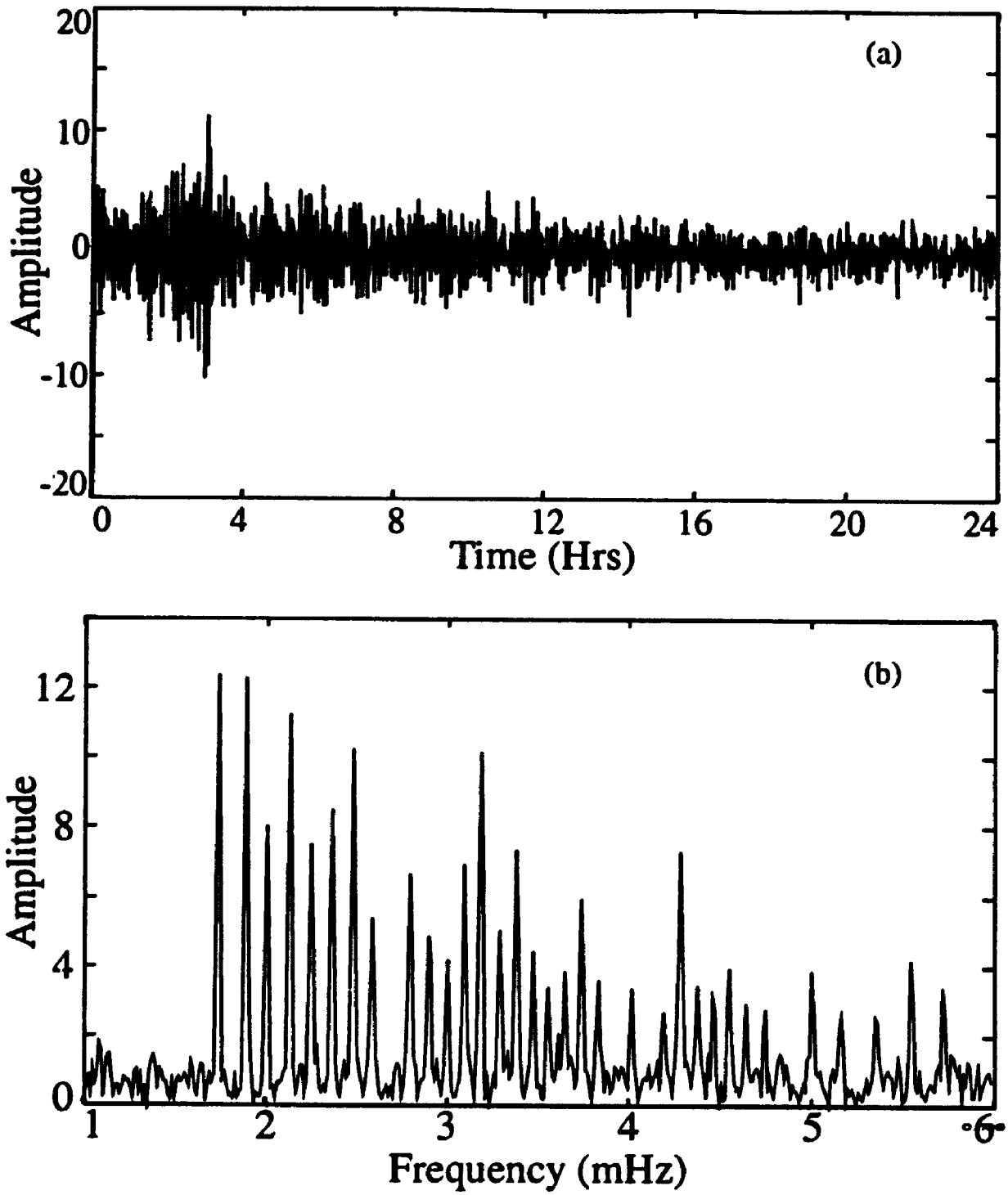

Figure 3.5: (a) A 24 hour long synthetic record of 35 spheroidal modes with added gaussian random noise. Noise magnitude is more than those of Figures 3.3 and 3.4. (b) Spectrum of the above record using a Hann window.

high and unacceptable.

The most astonishing results are the values of the quality factors Q for low signal-to-noise ratio (S/N). Figures 3.6, 3.7 and 3.8 show that for low frequencies (where S/N ratio is generally higher), the Q values from both the methods are close to the true values, which is expected. As the S/N ratio drops, the inaccuracy in STFT method increases severely (note the difference in parameters determined by STFT towards the higher frequencies). However, the modal fitting still provides reliable and accurate Q values even for the modes which are hardly detectable in the spectrum. In addition, modal fitting also gives the initial amplitude values corresponding to the modes, which is very useful for the source moment tensor studies (Gilbert, 1973). The values of the normal mode parameters for the noisy data set indicates the superiority of the modal fitting over the STFT method.

3.3 Application to Real Data

The Minahasa Peninsula earthquake occurred on April 18, 1990 (M_S = 7.4) at 1.186°N, 122.857°E. This event was recorded on the Canadian superconducting gravimeter (SG) installed at Cantley, Quebec, Canada. This earthquake was not preceded or followed by any large earthquakes within 7 days of its occurrence. Therefore, we have a very clean record of this earthquake, well suited for the normal mode study. A 24 hour time series was chosen well after the subsidence of high amplitude surface waves (3 hours after the first P phase). This segment is then tapered using a Hann window of 24 hour length and the spectrum is calculated using FOURG (Childers & Durling, 1975). The periods of the multiplets (they are not split in 24 hour spectrum) are read from this spectrum. The modes were identified using the periods earlier observed by Sailor & Dziewonski (1978) and Masters & Gilbert (1983). Figure 3.9 shows a 24 hour recording of this earthquake and the corresponding amplitude spectrum.

Filtering. Prior to modal fitting, a bandpass filter is applied to remove (i) the tides and (ii) the periods below 100 seconds, to permit resampling. A 8^{th} order Chebyshev filter is used. The Frequency response of this filter is shown in Figure 3.10.

S/N	Period (seconds)			Phase (radians)		Initial Amplitude	
	True	STFT	Modal Fit	True	Modal Fit	True	Modal Fit
28.2	579.80	579.86	579.78	0.00	0.000	1.140	1.1420
20.1	533.30	533.33	533.29	0.00	-0.006	1.402	1.4000
20.4	502.30	502.32	502.32	0.00	0.022	1.060	1.0738
16.2	472.10	472.13	472.12	0.00	0.014	1.620	1.6034
11.0	447.60	447.66	447.60	0.00	-0.011	1.490	1.4992
17.9	425.60	425.61	425.59	0.00	-0.006	1.145	1.1562
13.2	405.60	405.63	405.62	0.00	0.008	1.620	1.6127
12.5	389.10	389.18	389.03	0.00	-0.026	1.093	1.0861
10.4	360.00	360.00	359.99	0.00	-0.000	1.440	1.4529
9.3	346.90	346.98	346.89	0.00	-0.006	1.264	1.2571
8.4	334.80	334.88	334.81	0.00	0.021	1.085	1.1098
13.3	324.80	324.81	324.81	0.00	0.004	1.113	1.1193
14.7	315.30	315.32	315.31	0.00	0.007	1.753	1.7396
10.8	305.30	305.30	305.28	0.00	-0.031	1.122	1.1236
10.3	296.90	296.90	296.90	0.00	0.001	1.533	1.5325
7.4	288.90	288.96	288.87	0.00	-0.009	1.194	1.2218
4.4	282.30	283.27	282.33	0.00	0.025	1.111	1.1246
7.3	275.10	275.15	275.09	0.00	0.000	1.101	1.1146
7.9	268.30	268.32	268.29	0.00	0.007	1.474	1.4749
7.0	261.80	261.81	261.81	0.00	0.015	1.571	1.5607
6.4	249.70	249.71	249.70	0.00	-0.011	1.105	1.0992
3.2	244.70	244.75	244.69	0.00	-0.015	1.090	1.1331
4.7	239.30	239.33	239.32	0.00	0.024	1.824	1.8469
9.5	234.10	234.14	234.10	0.00	0.019	1.772	1.7656
5.4	229.10	229.17	229.09	0.00	-0.002	1.224	1.2478
4.6	225.00	224.41	225.01	0.00	0.018	1.172	1.1793
7.7	220.40	220.40	220.41	0.00	0.020	1.203	1.2272
5.3	216.00	216.54	216.01	0.00	0.016	1.476	1.4986
3.8	211.70	211.76	211.71	0.00	0.019	1.364	1.3273
4.3	207.60	207.69	207.60	0.00	-0.010	1.140	1.1465
5.4	200.40	200.46	200.41	0.00	0.013	1.402	1.3562
1.7	194.20	194.59	194.22	0.00	-3.112	1.419	1.4142
5.1	187.00	187.01	186.99	0.00	-0.004	1.620	1.6234
8.2	180.70	180.75	180.70	0.00	0.012	1.145	1.1648
6.2	175.20	174.25	175.20	0.00	-0.004	1.620	1.6316

Table 3.5: Parameter values of the noisy synthetic data set (shown in Figure 3.3) obtained by modal fitting and STFT method.

S/N	Q				
	True	STFT		Modal Fit	
		Value	Error	Value	Error
28.2	276.00	270.11	0.02	276.84	24.71
20.1	247.00	242.96	4.22	251.28	17.42
20.4	227.00	234.11	18.83	222.25	19.60
16.2	195.00	195.42	0.83	195.14	11.47
11.0	168.00	167.09	1.85	167.37	10.80
17.9	210.00	212.59	0.11	203.84	17.09
13.2	222.00	215.92	1.47	224.66	13.02
12.5	200.00	195.50	7.99	203.41	17.26
10.4	198.00	201.34	9.84	195.91	13.03
9.3	176.00	162.97	10.58	180.01	14.53
8.4	168.00	172.10	2.31	162.27	16.04
13.3	276.00	274.47	15.67	273.59	24.15
14.7	247.00	248.97	9.57	248.28	13.91
10.8	227.00	237.67	7.31	225.62	20.10
10.3	253.00	246.01	2.60	250.87	16.43
7.4	195.00	192.83	0.70	188.42	17.57
4.4	168.00	193.52	7.54	162.72	18.10
7.3	210.00	208.79	3.11	205.79	20.55
7.9	222.00	212.69	1.30	222.98	16.26
7.0	200.00	206.33	12.81	200.49	14.13
6.4	198.00	180.83	25.38	204.04	21.39
3.2	176.00	208.51	31.00	170.93	20.15
4.7	168.00	177.19	25.37	166.72	12.14
9.5	276.00	266.72	6.70	276.92	16.63
5.4	247.00	245.32	28.80	243.09	22.01
4.6	227.00	204.00	12.95	223.74	22.88
7.7	253.00	290.11	52.58	241.25	23.27
5.3	195.00	179.69	10.62	190.63	17.00
3.8	168.00	213.09	50.70	171.09	18.44
4.3	210.00	213.96	10.30	206.09	22.56
5.4	222.00	239.70	17.68	231.71	19.21
1.7	198.00	278.61	164.4	197.29	17.13
5.1	176.00	209.03	32.89	177.07	14.27
8.2	276.00	280.07	10.91	272.04	16.97
6.2	247.00	330.55	143.4	243.89	25.07

Table 3.6: Values of Q and associated errors determined by modal fitting and STFT method for the data set shown in Figure 3.3.

S/N	Period (seconds)			Phase (radians)		Initial Amplitude	
	True	STFT	Modal Fit	True	Modal Fit	True	Modal Fit
15.4	579.80	579.86	579.77	0.00	-0.005	1.140	1.1629
10.1	533.30	533.33	533.26	0.00	-0.025	1.402	1.4182
14.2	502.30	502.32	502.43	0.00	0.075	1.060	1.1196
11.6	472.10	472.13	472.14	0.00	0.051	1.620	1.5653
5.3	447.60	447.66	447.54	0.00	-0.041	1.490	1.5191
11.0	425.60	425.61	425.56	0.00	-0.021	1.145	1.1764
7.1	405.60	405.63	405.64	0.00	0.031	1.620	1.6243
6.2	389.10	389.18	388.93	0.00	-0.089	1.093	1.1073
5.9	360.00	360.00	359.98	0.00	-0.006	1.440	1.5098
5.4	346.90	346.98	346.85	0.00	-0.025	1.264	1.2741
5.1	334.80	334.88	334.82	0.00	0.073	1.085	1.1855
6.5	324.80	324.81	324.81	0.00	0.018	1.113	1.1452
10.3	315.30	315.32	315.33	0.00	0.031	1.753	1.7405
6.4	305.30	305.30	305.20	0.00	-0.101	1.122	1.1622
5.5	296.90	296.90	296.90	0.00	0.005	1.533	1.5742
6.4	288.90	288.96	288.82	0.00	-0.034	1.194	1.3447
3.3	282.30	283.27	282.43	0.00	0.105	1.111	1.1890
3.0	275.10	275.15	275.08	0.00	0.021	1.101	1.1785
4.2	268.30	268.32	268.28	0.00	0.044	1.474	1.5156
4.3	261.80	261.81	261.83	0.00	0.076	1.571	1.5742
3.5	249.70	249.71	249.70	0.00	-0.039	1.105	1.1488
2.1	244.70	244.75	244.70	0.00	-0.001	1.090	1.3427
2.7	239.30	239.33	239.41	0.00	0.129	1.824	1.9625
6.9	234.10	234.14	234.12	0.00	0.095	1.772	1.8161
3.0	229.10	229.17	229.12	0.00	0.039	1.224	1.3863
3.6	225.00	224.41	225.07	0.00	0.143	1.172	1.2384
5.9	220.40	220.40	220.47	0.00	0.154	1.203	1.3235
3.6	216.00	216.54	216.08	0.00	0.171	1.476	1.6193
2.2	211.70	211.76	211.84	0.00	0.267	1.364	1.2340
2.3	207.60	207.69	207.67	0.00	0.128	1.140	1.0273
3.8	200.40	200.46	200.53	0.00	0.330	1.402	1.1810
3.7	187.00	187.01	186.84	0.00	-0.279	1.620	1.6488
7.4	180.70	180.75	180.64	0.00	-0.013	1.145	1.2756
3.8	175.20	174.25	175.20	0.00	-0.143	1.620	1.6898

Table 3.7: Parameter values of the noisy synthetic data set (Figure 3.4) obtained by modal fitting and STFT method. The S/N ratio is lower than in Table 3.5.

S/N	Q				
	True	STFT		Modal Fit	
		Value	Error	Value	Error
15.4	276.00	266.31	7.38	264.94	23.25
10.1	247.00	236.19	9.61	250.93	17.44
14.2	227.00	260.80	81.16	207.04	17.42
11.6	195.00	197.91	1.62	195.19	11.71
5.3	168.00	168.44	6.76	168.67	10.63
11.0	210.00	221.17	3.11	197.10	15.92
7.1	222.00	205.53	6.61	223.51	13.00
6.2	200.00	199.48	5.80	199.50	17.01
5.9	198.00	227.14	66.70	187.23	12.15
5.4	176.00	147.37	22.26	182.64	14.63
5.1	168.00	221.80	63.56	150.15	14.25
6.5	276.00	276.71	55.60	268.87	23.11
10.3	247.00	259.20	42.44	245.24	13.86
6.4	227.00	289.82	41.46	216.00	19.01
5.5	253.00	234.00	6.858	238.97	15.58
6.4	195.00	195.71	9.094	168.48	15.32
3.3	168.00	335.80	73.44	148.97	16.61
3.0	210.00	264.64	73.72	190.66	18.71
4.2	222.00	202.25	12.71	218.19	15.75
4.3	200.00	231.28	45.13	195.98	13.91
3.5	198.00	200.51	36.77	208.42	20.98
2.1	176.00	399.84	821.68	149.41	16.28
2.7	168.00	301.71	521.51	159.95	11.45
6.9	276.00	258.86	36.11	264.68	15.98
3.0	247.00	322.99	385.45	218.28	19.15
3.6	227.00	241.80	35.38	209.20	21.32
5.9	253.00	545.74	1284.3	213.79	20.22
3.6	195.00	241.12	73.96	173.81	15.32
2.2	168.00	351.66	374.20	178.59	20.29
2.3	210.00	304.57	42.47	218.36	25.50
3.8	222.00	295.61	73.33	264.95	23.35
3.7	176.00	320.48	224.00	171.99	20.54
7.4	276.00	306.75	30.30	245.28	13.62
3.8	247.00	651.36	880.16	236.04	15.96

Table 3.8: Values of Q and associated errors determined by modal fitting and STFT method for the data set shown in Figure 3.4. The S/N ratio in the time series is lower than in Table 3.6.

S/N	Period (seconds)			Phase (radians)		Initial Amplitude	
	True	STFT	Modal Fit	True	Modal Fit	True	Modal Fit
8.1	579.80	579.86	579.74	0.00	-0.007	1.140	1.1600
6.3	533.30	533.33	533.24	0.00	-0.042	1.402	1.4216
10.3	502.30	502.32	502.53	0.00	0.130	1.060	1.1204
9.2	472.10	472.13	472.19	0.00	0.089	1.620	1.5168
3.1	447.60	447.66	447.50	0.00	-0.077	1.490	1.5390
7.7	425.60	425.61	425.58	0.00	-0.045	1.145	1.1926
4.8	405.60	405.63	405.69	0.00	0.049	1.620	1.6060
4.0	389.10	389.18	388.89	0.00	-0.175	1.093	1.1120
4.0	360.00	360.00	359.98	0.00	-0.014	1.440	1.5081
3.7	346.90	346.98	346.85	0.00	-0.053	1.264	1.2761
3.9	334.80	334.88	334.86	0.00	0.107	1.085	1.2230
4.3	324.80	324.81	324.88	0.00	0.013	1.113	1.1289
8.1	315.30	315.32	315.32	0.00	0.043	1.753	1.6705
4.4	305.30	305.30	305.17	0.00	-0.196	1.122	1.1451
3.5	296.90	296.90	296.90	0.00	-0.003	1.533	1.5609
5.5	288.90	288.96	288.76	0.00	-0.080	1.194	1.3772
2.7	282.30	283.27	282.51	0.00	0.118	1.111	1.1256
2.0	275.10	275.15	275.01	0.00	-0.044	1.101	1.1773
2.9	268.30	268.32	268.25	0.00	0.025	1.474	1.5148
2.9	261.80	261.81	261.83	0.00	0.072	1.571	1.5327
2.5	249.70	249.71	249.71	0.00	-0.024	1.105	1.1244
1.3	244.70	244.75	244.68	0.00	-0.011	1.090	1.3905
2.0	239.30	239.33	239.46	0.00	0.184	1.824	1.9159
4.9	234.10	234.14	234.11	0.00	0.136	1.772	1.7837
2.0	229.10	229.17	229.11	0.00	0.046	1.224	1.3840
2.6	225.00	224.41	225.07	0.00	0.202	1.172	1.1924
4.7	220.40	220.40	220.43	0.00	0.233	1.203	1.2761
2.6	216.00	216.54	216.05	0.00	0.226	1.476	1.6291
1.4	211.70	211.76	211.77	0.00	0.341	1.364	1.1433
1.4	207.60	207.69	207.58	0.00	-0.001	1.140	1.1643
3.1	200.40	200.46	200.42	0.00	0.361	1.402	1.1488
2.0	194.20	194.59	194.28	0.00	-2.845	1.419	1.4087
3.0	187.00	187.01	186.96	0.00	-0.274	1.620	1.6346
4.1	180.70	180.75	180.67	0.00	0.016	1.145	1.6353
2.6	175.20	174.25	175.22	0.00	-0.161	1.620	1.2772

Table 3.9: Parameter values of the noisy synthetic data set obtained by modal fitting and STFT method (Figure 3.5). The S/N ratio is lower than in Tables 3.5 and 3.7.

S/N	Q				
	True	STFT		Modal Fit	
		Value	Error	Value	Error
8.1	276.00	267.62	18.13	266.04	23.00
6.3	247.00	233.65	9.06	254.74	18.21
10.3	227.00	299.76	155.94	212.84	16.48
9.2	195.00	205.32	6.52	196.17	12.45
3.1	168.00	172.45	8.77	167.48	11.06
7.7	210.00	231.24	9.90	188.43	15.79
4.8	222.00	200.62	14.86	228.95	13.62
4.0	200.00	207.89	4.66	195.93	18.29
4.0	198.00	264.83	185.05	189.94	12.18
3.7	176.00	151.91	26.00	182.81	16.10
3.9	168.00	325.88	417.05	142.68	14.29
4.3	276.00	283.16	87.70	271.92	24.47
8.1	247.00	278.26	103.06	255.94	14.92
4.4	227.00	346.58	96.18	217.98	21.06
3.5	253.00	227.93	6.86	233.25	16.56
5.5	195.00	217.99	60.35	160.61	16.00
2.7	168.00	515.90	202.06	152.12	19.41
2.0	210.00	452.04	887.07	185.73	20.70
2.9	222.00	207.18	42.44	216.98	17.81
2.9	200.00	266.65	83.60	198.21	16.17
2.5	198.00	246.21	23.85	219.95	26.86
1.3	176.00	712.98	5972.68	146.80	19.01
2.0	168.00	469.14	1560.05	167.17	13.70
4.9	276.00	255.73	69.74	266.23	18.00
2.0	247.00	475.89	1586.58	219.61	21.16
2.6	227.00	451.03	1017.44	208.40	25.34
4.7	253.00	1529.3	26801.0	212.24	22.11
2.6	195.00	336.77	315.43	168.71	17.39
1.4	168.00	519.20	1007.07	190.61	27.32
1.4	210.00	513.97	584.97	189.51	30.14
3.1	222.00	372.50	206.63	288.30	31.46
2.0	198.00	2253.1	88240.0	192.22	21.11
3.0	176.00	440.53	500.32	184.06	14.67
4.1	276.00	342.05	44.57	247.42	16.73
2.6	247.00	1312.0	767.26	248.91	21.33

Table 3.10: Values of Q and associated errors determined by modal fitting and STFT method for the data set shown in Figure 3.5. The S/N ratio in the time series is lower than in Tables 3.6 and 3.8.

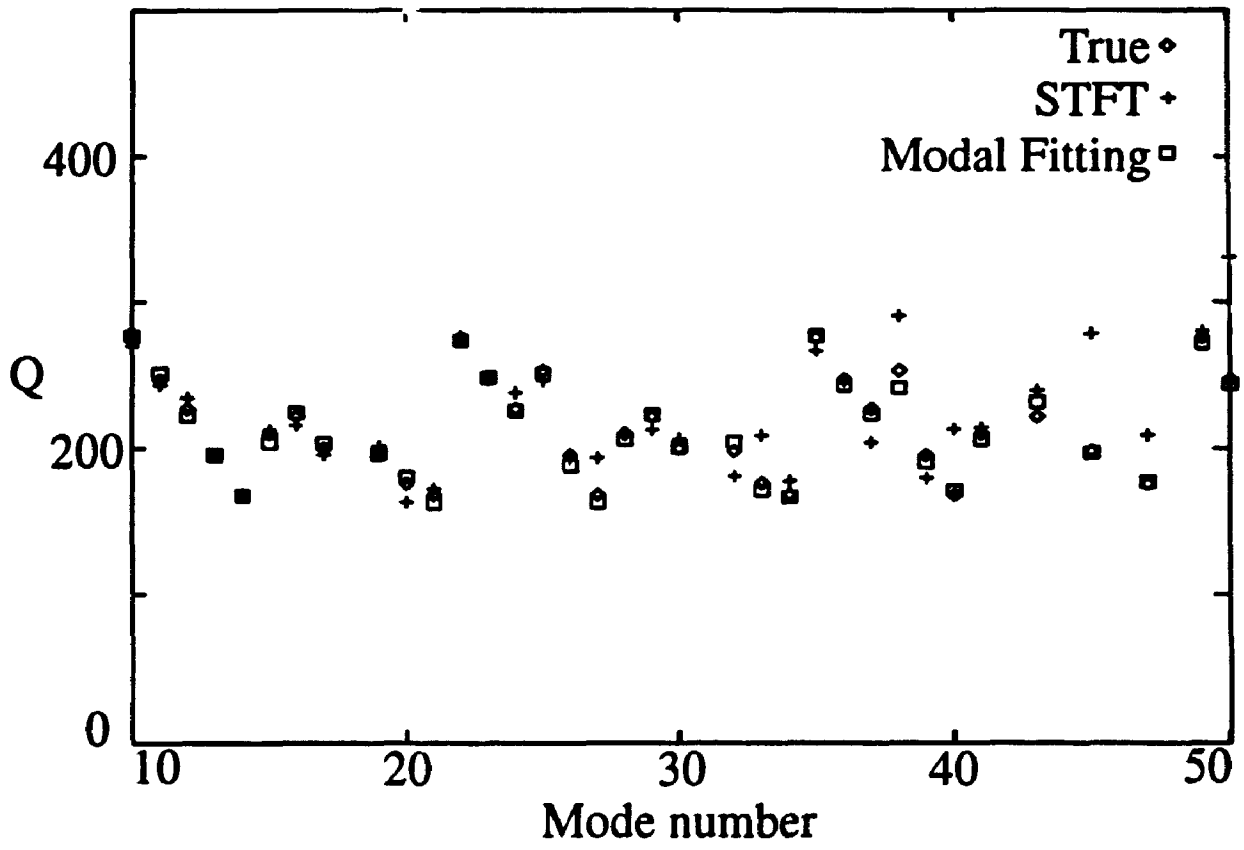

Figure 3.6: Comparison of the Q values in noisy data set Table 3.6 using modal fitting and STFT method. With noisy data, modal fitting gives better values of Q than does STFT.

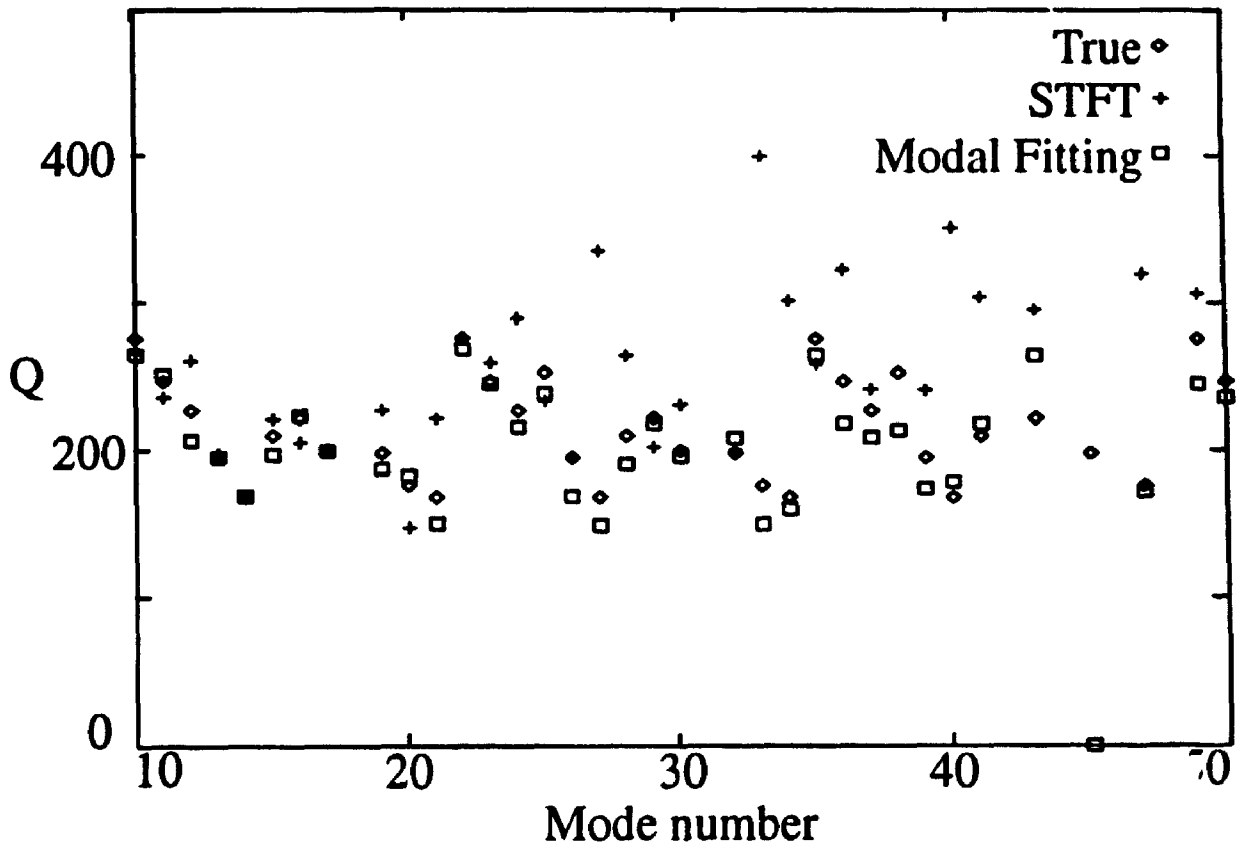

Figure 3.7: Comparison of the Q values in noisy data set Table 3.8 using modal fitting and STFT method. The difference between the true values and those obtained using the STFT method increases as the S/N ratio decreases.

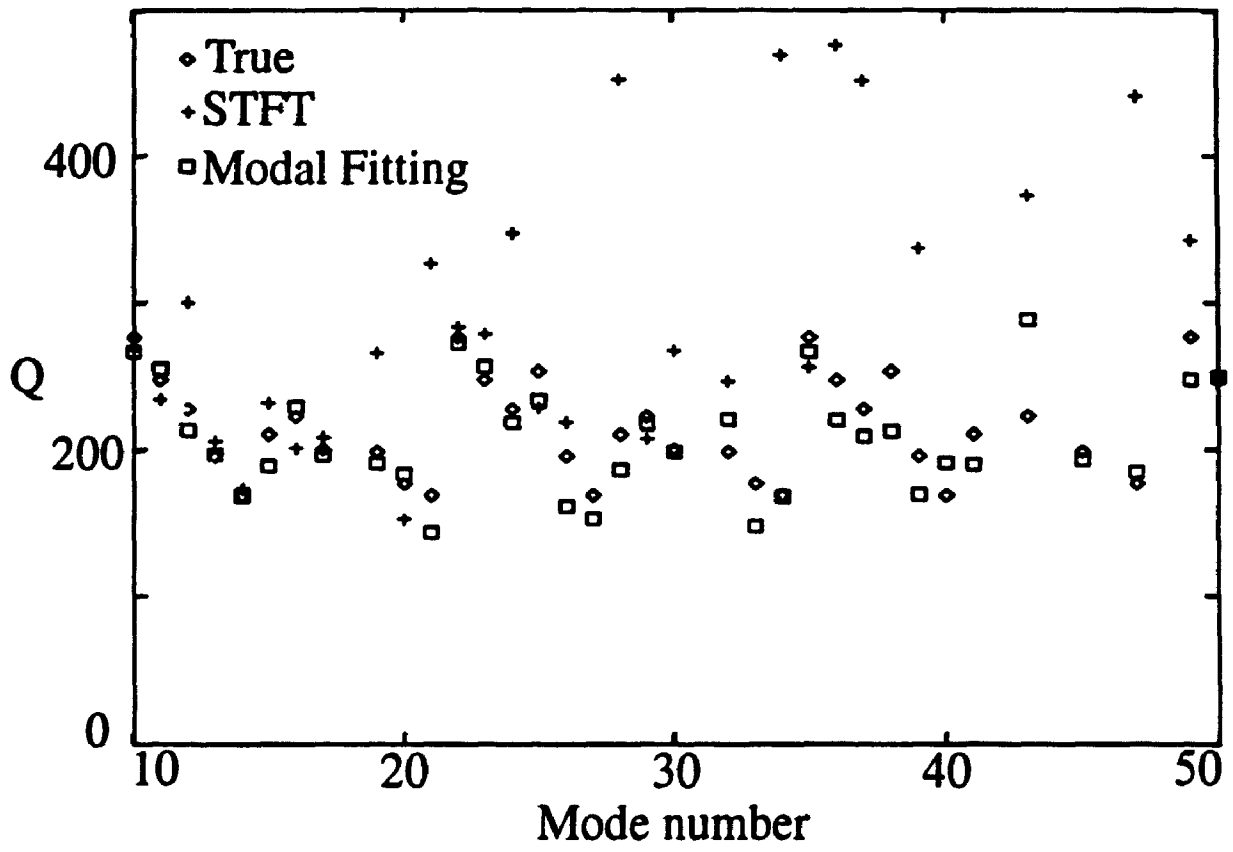

Figure 3.8: Comparison of the Q values in noisy data set Table 3.10 using modal fitting and STFT method. The difference between the true values and those obtained using the STFT method increases as the S/N ratio decreases.

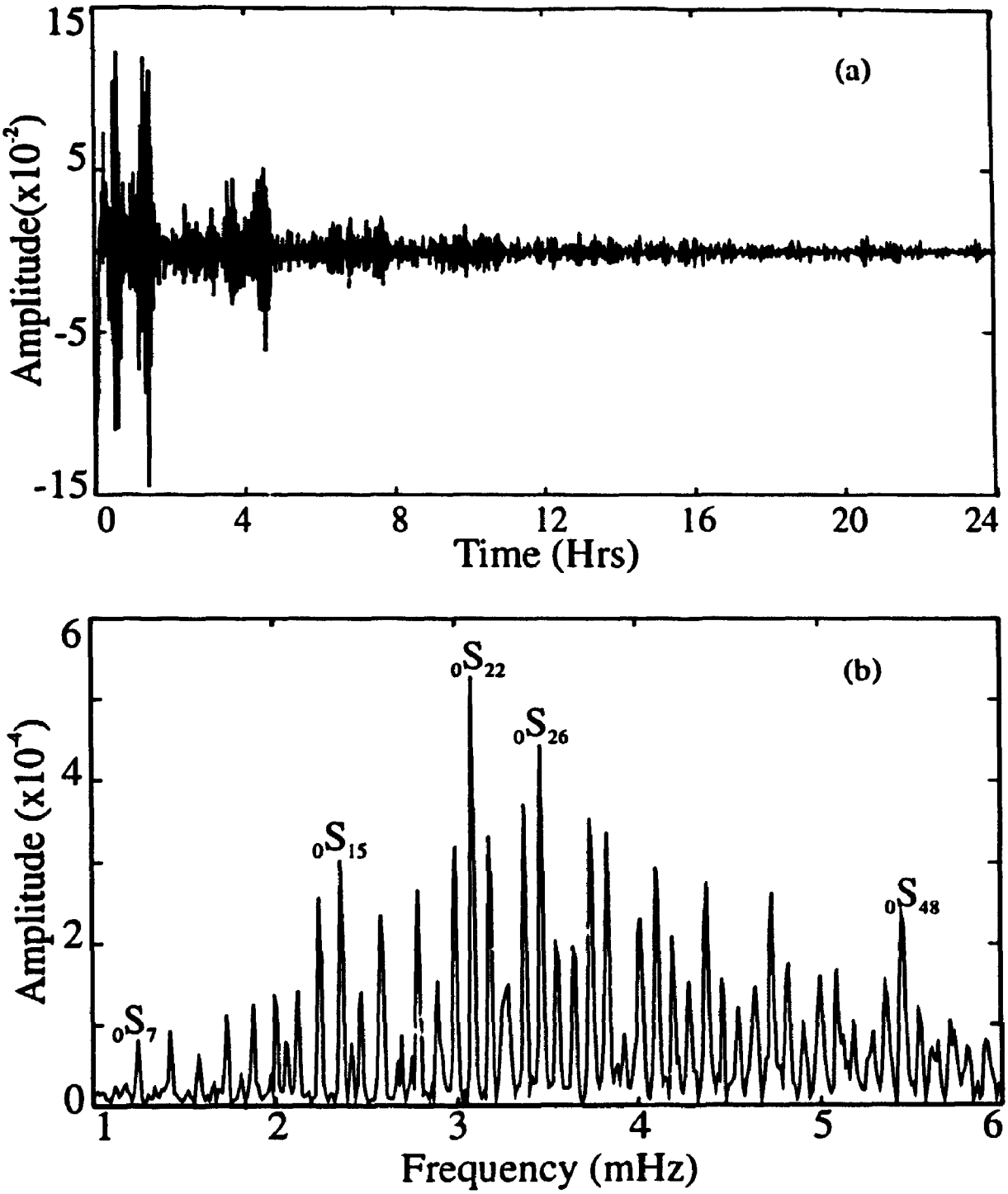

Figure 3.9: (a) A record of the April 18, 1990, Minahasa Peninsula earthquake, (b) Amplitude spectrum computed from the record using a Hann window.

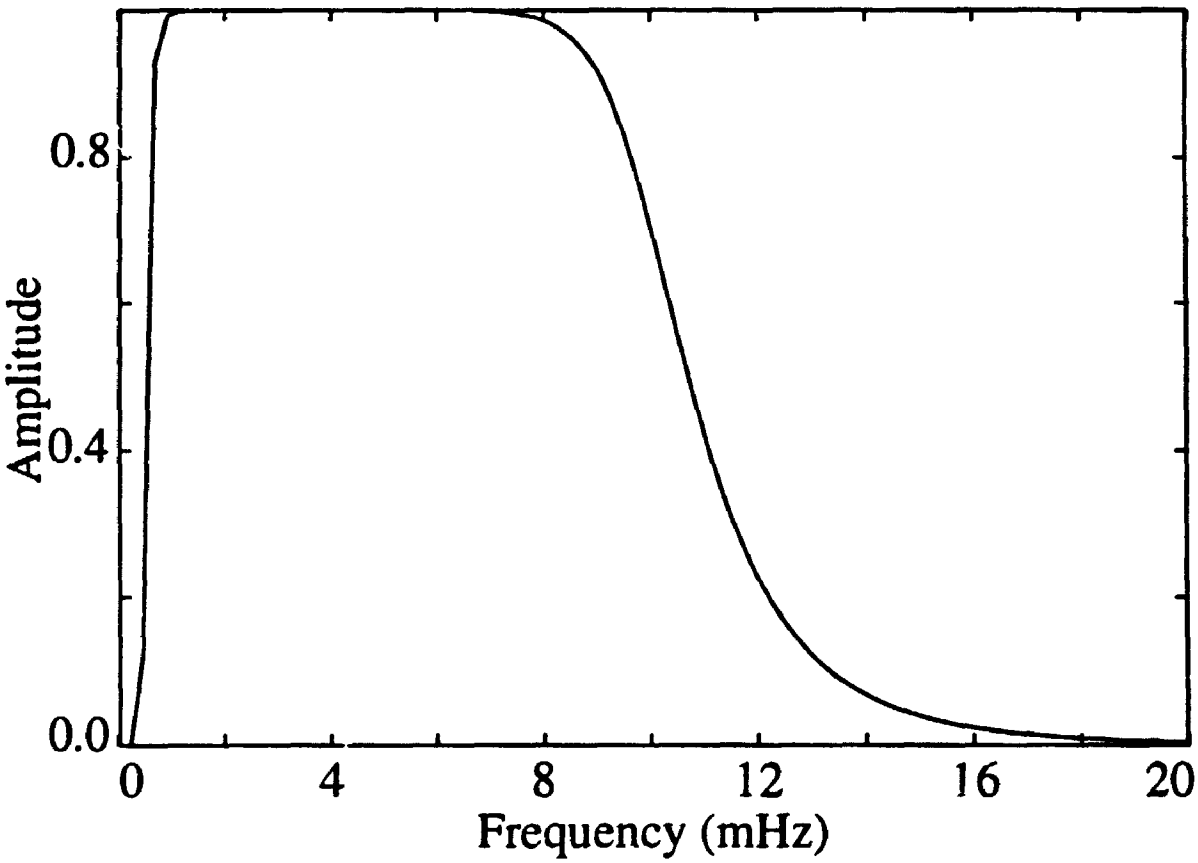

Figure 3.10: Frequency response of 8^{th} order Chebyshev filter used to bandpass filter the SG record.

Resampling. The data set is recorded on the SG at a rate of 1 sample/sec. This gives 86400 data points per day, which is a large number of values for the modal fitting method. The period range of normal modes varies between 5 minutes to 1 hour. Therefore, a data set with a 10 second sampling rate (Nyquist period 20 seconds) is sufficient for the modal analysis. This is the standard sampling rate for all the International Deployment of Accelerometers (IDA) instruments. The filtered time series is resampled at 10 seconds interval.

Guess parameters. The starting guess values were chosen in the same manner as for the synthetic data. By examining the Fourier spectrum of the first 24 hours of the recorded seismogram (excluding the initial saturated part), all the spectral peaks above the ambient noise level were identified (number of modes to be considered for fitting). As before, the Fourier periods are used as the initial guess periods. Starting amplitudes of all the modes are taken as unity and the phase as zero. The guess for the Q values is 100.0.

3.3.1 Results

The real data do not show as good results as compared with that from synthetic data. We have not been able to satisfactorily fit the model to the real data set using the modal fitting. In all, thirty five modal peaks were identified in the spectrum of the time series above the background seismic noise level.

1. All 140 parameters, corresponding to 35 modal peaks, were fitted at the same time. This provides reasonable values of periods and phases for all the peaks. Some of the higher order modes (lower periods) give reliable Q and amplitude values, but the values for the lower order modes are not realistic [Table 3.11]. Lower order modes usually decay slowly (higher Q), but Table 3.11 indicates low Q values for these modes.

   The method does provide Q values in a physically reasonable range for about 50% of the modes. These Q values are not the same as those obtained by Kamal & Mansinha (1992) using the STFT method. But this does not indicate that

Period	Amplitude	Phase (radians)	Q
815.094	0.0014	3.13	9.55
635.294	0.0017	2.62	114.42
579.866	0.0024	3.14	103.50
536.646	0.0111	4.04	101.02
502.326	0.0087	2.48	234.63
472.131	0.0008	3.13	5.56
447.668	0.0040	3.16	>10000
425.616	0.0114	1.92	181.55
405.634	0.0058	3.77	396.55
389.189	0.0018	2.89	>10000
372.414	0.0116	3.73	206.45
360.000	0.0158	3.03	155.28
346.988	0.0017	3.82	150.48
334.884	0.0170	3.41	298.11
324.812	0.0301	2.54	435.31
315.328	0.0216	4.00	380.35
305.300	0.0018	3.14	2.37
296.907	0.0233	2.99	448.47
288.963	0.0402	4.06	301.44
281.433	0.0077	3.12	247.14
275.159	0.0014	5.76	>10000
267.492	0.0348	3.73	278.87
261.818	0.0021	3.08	61.77
255.621	0.0117	3.11	68.43
249.711	0.0536	2.85	183.43
244.759	0.0564	3.93	210.73
238.674	0.0320	3.29	212.56
234.146	0.0329	3.20	211.52
229.787	0.0571	3.47	195.22
224.416	0.0341	3.18	194.45
220.408	0.0442	3.49	168.18
216.541	0.0350	3.05	239.99
212.285	0.0617	3.13	210.43
208.193	0.0528	3.61	180.74
204.255	0.0079	2.64	899.47

Table 3.11: Parameter values for the Minahasa Peninsula earthquake obtained by modal fitting (these values are not at the absolute minimum of the merit function). The method provides reasonable Q values for about 50% of the modes.

these values are wrong. We have demonstrated that the STFT method may provide incorrect values of the parameters for low S/N ratio, therefore the values determined by modal fitting cannot be discarded.

2. Instead of fitting all the parameters together, we tried to partially fit these parameters in turn. Keeping $\alpha_i = 0$ (no decay) for all i, the amplitudes, frequencies and phases of the modal peaks were computed. This procedure is identical to fitting for nondecaying modes (as is done in Fourier transform). It is assumed that this will provide reasonable values of frequency and phase (not amplitude). In the next step, ω_i and ϕ_i were kept fixed at these preliminary values and a fit is obtained only for amplitudes A_i and quality factors Q_i. Again, ω_i and ϕ_i were modified in the next step by keeping A_i and Q_i fixed at their most recent values. This is repeated until the error between the time series and the model response reaches a threshold minimum. This procedure also provides similar results for the parameters.

3.3.2 Possible causes of misfit

The algorithm used for least-squares minimization does get stuck in a local minimum and gives incorrect values for some of the parameters. The quality factor Q is the most sensitive parameter of all and has an exponential dependence in the model. It is very likely that several combination of Q and amplitude give the same merit function.

Another problem associated with the data set may be the splitting of the modes. As discussed in section 1.2.1, for a laterally homogeneous earth, all the singlets of a mode are degenerate and produce a multiplet. Due to the lateral heterogeneity, some of these singlets appear as a separate peak in the spectrum and the mode is said to be split. The frequency resolution in the Fourier transform is not enough to resolve these split modes, hence these split peaks will appear as a single broad peak in the spectrum. The modeling of this peak as a single frequency will not be correct and the fitting of this model will provide incorrect values of the parameters corresponding to this mode.

The presence of seismic noise in the modal band may also cause the

misfit. It is almost impossible to filter this noise from the time series. The only remedy may be to properly model the noise and subtract it from the data prior to the modal fitting.

3.4 Concluding Remarks

The least-squares fitting of customized wavelets works very well on the synthetic data consisting of single modal peaks. Even in the presence of large random noise ($S/N \approx 1.3$), the method provides much more reliable values of the parameters than those from the STFT method. Before it can be applied to the real data set, more work is required. A more realistic model of split modes may provide better values for the parameters. Proper modeling of the unwanted (non modal) signal and removing this from the data set may improve the results.

Part II

Do Normal Modes Trigger Aftershocks?

Answer: Yes

Chapter 4

Why Ask?

'Curiouser and curiouser!' cried Alice.

Lewis Carroll, *Alice's Adventures in Wonderland.*

An earthquake is the process of release and radiation of strain energy by rupture. This process may also be described as the creation of a new fault and/or as a slip of a prexisting fault. Prior to the quake, energy is stored as elastic strain in the rocks. When the strain builds to a level that exceeds the strength of a weak region, such as along an existing fault, opposite sides of the fault suddenly slip, producing an earthquake (or earthquakes). Part of the released energy is in the form of elastic waves. In an idealized model of an earthquake source, rupture of the fault begins at a point on the fault surface called the *hypocenter.* The rupture then spreads at a certain velocity and finally stops when the remaining energy is insufficient to create new fault surface.

4.1 Rupture

In a simplistic time predictable earthquake model, stresses on an existing fault slowly increase over time until a critical limit is reached and then rupture occurs. The stress discontinuity at the point of initiation of rupture is the critical factor. Normal tensile stresses or opposing shear stresses are necessary for initiation and continuation of

rupture.

Let us first consider the rupture process with the simple case of tensile fracture. The process of tensile fracture is easier to understand and model than shear fracture (earthquake fault). Figure 4.1 shows a standard mechanical test on a rod. The rod is subjected to constant tensile stress T. Initially, the rod deforms elastically [Figure 4.1(a)]. After reaching a critical stress, there is plastic deformation [Figure 4.1(b)], and finally rupture occurs [Figure 4.1(c)].

Figure 4.2(a) shows a medium with a crack subjected to tensile stress T. The difference from the case of a rod is that there is a stress concentration at the tip of the crack. If the crack can be approximated by a flattened ellipse, the expression of the stress concentration at the tips of the crack, σ, can be given by (Scholz, 1990)

$$\sigma = T\left(1 + \sqrt{\frac{a}{\rho}}\right) \tag{4.1}$$

where a is the length of the semi-major axis (half length of the crack) and ρ is the radius of curvature at the end of the crack. Clearly, this stress concentration σ can become very large in case of sharp ends of the crack ($\rho \rightarrow 0$). The stress in the neighborhood of the tip varies as inverse of the square root of the distance from the tip. In the immediate vicinity of the tip, the stress becomes very high. Extension (or growth) of an existing crack is facilitated by the stress pattern near the tip.

For shear fracture [Figure 4.2(b)], the problem is very similar if one assumes that the crack surface is friction free. Growth of the shear crack is then controlled by the stress amplification near the tip. With friction, there is a resistance to slip of one side against the other. In the earth, the two opposing fault surfaces are rarely smooth. The roughness increases friction. Large scale protrusions of the fault surface are called "asperities". Friction, asperities and the energy needed to create new fault surface are the factors which oppose shear crack growth. Superposition of all these factors determine a critical stress S_c. Only if the applied forcing stress S_f exceeds this value, will there be fault growth. To restate

- Earthquake occurs if $S_f \geq S_c$.
- Earthquake does not occur if $S_f < S_c$.

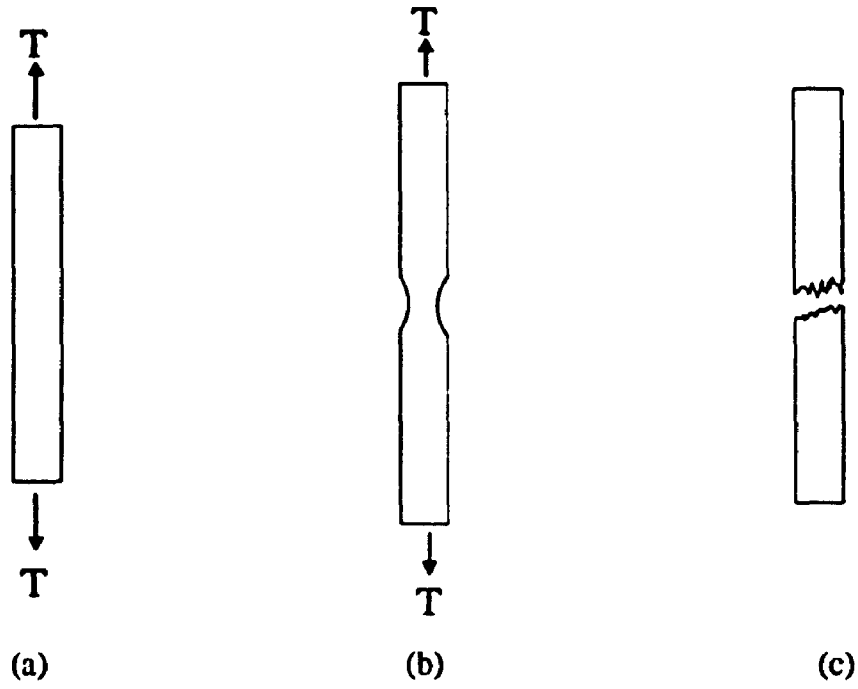

Figure 4.1: The process of rupture in a rod under tensile stress. (a) Elastic deformation, (b) plastic deformation and (c) rupture.

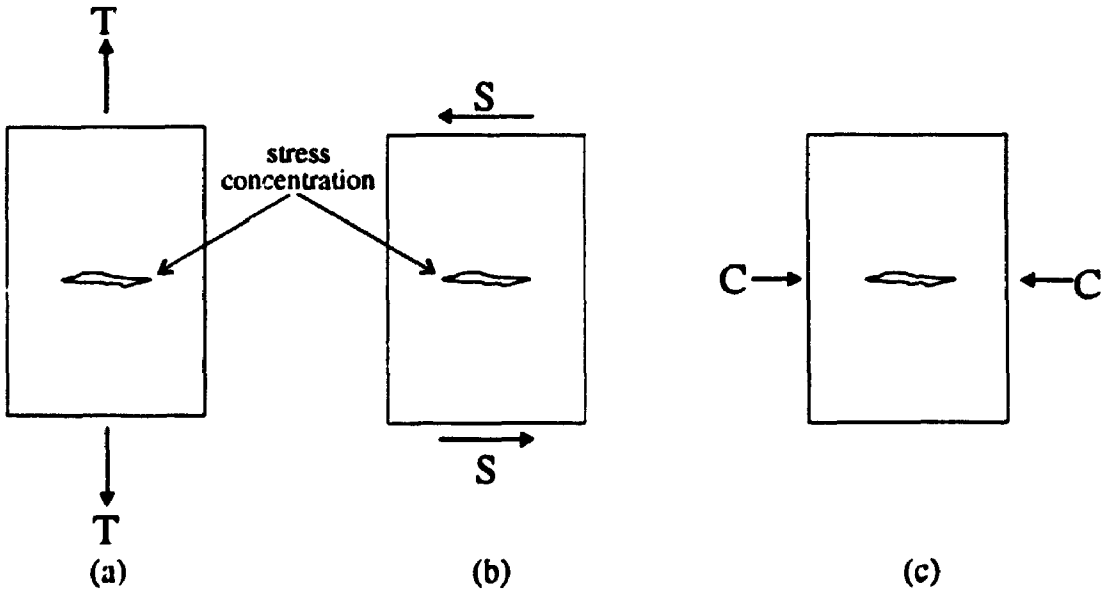

Figure 4.2: Effect of different type of stresses on an existing crack. (a) tensile stress, which opens the crack (b) shear stress, which affect the shear rupture and (c) compressive stress does not affect the crack at all.

Any trigger mechanism for an earthquake functions either by increasing S_f or decreasing S_c. The process of retardation of an earthquake also falls under triggering. In this case, S_f is decreased or S_c is increased. A trigger can advance or retard the onset of an impending earthquake.

The process of decreasing the critical stress S_c is now well documented for man-induced earthquakes. Injection of fluids can cause decrease of friction (Healy *et al*, 1968). Earthquakes under large reservoirs (Gupta & Rastogi,1976; Simpson,1986; Simpson *et al*, 1988) are good example of this effect. Another method of reducing S_c is through the application of a small normal stress to the fault surface. A separation of the fault faces which is greater than the biggest asperity will result in a total decrease of frictional forces. A partial separation will produce a partial drop of friction.

4.1.1 Aftershocks

Aftershocks violate logic. If aftershocks were not observed, we would not be able to predict their occurrence. After all, the large earthquake occurs to relieve stored strain energy. Once the energy is released, there should be no strain energy left for more earthquakes, however small. But aftershocks continue on for years. It is clear that the process of strain energy release during the major earthquake is incomplete, or that the slippage along fault during the quake is non-uniform and gives rise to local strain fields.

Let us look at one plausible mechanism. Think of the fault surface as a fractal (Mandelbrot, 1983). The nature of asperities of the fault surface is independent of scale. Thus each large asperity, and the space between, is made up of self-similar smaller asperities, which in turn are again made up of even smaller asperities and so on [Figure 4.3(a)]. During the earthquake faulting, we have two opposing fractal surfaces [Figure 4.3(b)]. One can intuitively see that this is not a minimum energy stable configuration. If, with some mechanism, one surface is slightly shifted [Figure 4.3(c)], then the fault achieves a lower energy, more stable configuration. The smaller scale asperities will similarly find their own equilibrium. With time, the two sides will gradually adjust until most of the asperities are matched and the two sides are "locked", i.e., a maximum number of positive asperities are matched with negative

ones of the other side.

Aftershocks may be considered as continuous readjustment of the scale independent asperities. Seismic waves are essentially "noise" or "sound" waves generated by the process of fault growth or relative slip of the two opposite side of the fault. Conceptually, this is akin to generation of waves in the air by a disturbance. Any disturbance generates air waves. One cannot have any motion without the generation of air waves. Similarly, any motion or disturbance in the focal region of an earthquake generate seismic waves.

Average Slip & Earthquake Magnitude

Kanamori & Anderson (1975) provided an empirical relationship between magnitude (M_S), fault dimension (L), average slip (Δu) and radiated seismic energy (E_S)

$$\begin{aligned} M_S &\sim 2\log L, \text{and} \quad 1.5M_S + 11.5 \sim \log E_S \quad (M_S \geq 5) \\ M_S &\sim 3\log L, \text{and} \quad M_S + 11.5 \sim \log E_S \quad (M_S < 5) \\ \Delta u &\sim 10^{-5} L \end{aligned} \tag{4.2}$$

where Δu, L are in meters and E_S is in ergs. If these relations also hold for very low magnitude earthquakes (this is not checked for), one can quantify the slip, fault area, fault dimension and radiated energy for various magnitude aftershocks. For example, the following table compares several parameters for an earthquake in case of a square shaped fault:

Magnitude	Fault dimension (m)	Fault area	Slip (cm)	Radiated energy (ergs)
7.0	~ 3000	~ 9 km^2	~ 3	~ 10^{22}
5.0	~ 300	~ 0.1 km^2	~ 0.3	~ 10^{19}
3.0	~ 10	~ 100 m^2	~ 0.01	~ 10^{14}
2.0	~ 5	~ 25 m^2	~ 0.004	~ 10^{13}
1.0	~ 2	~ 4 m^2	~ 0.001	~ 10^{12}

The slip for magnitude 1 is at least 3 orders of magnitude smaller than for magnitude 7. We can see that at the low magnitudes, the dimensions of the fault and the energy released are small.

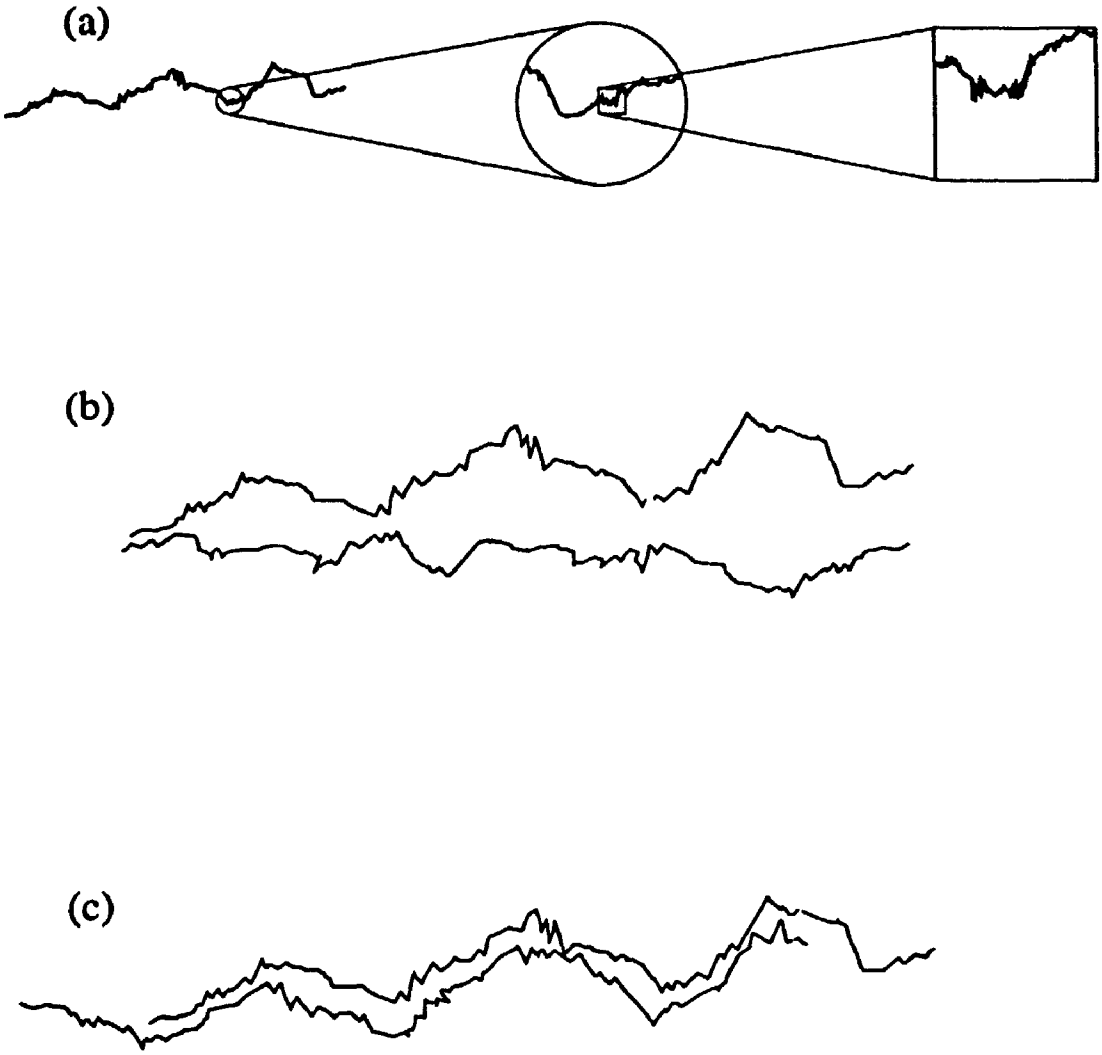

Figure 4.3: A plausible mechanism for continuous aftershock occurrence. (a) Self similarity in a fault surface, (b) Opposing fault surfaces in an unstable environment following a large earthquake and (c) "Locking" of two opposite surface.

This study deals with aftershocks in the magnitude range 1 and 2. It is useful to have some idea of the dimension of the slip and the active area of the aftershock.

4.2 Objectives of the Present Study

A variety of physical processes, such as the gravitational attraction of the Moon, fluid flow through rock fractures, volcanism etc., can cause and may also affect the stress S_c or S_f in the focal region, and thus can change the time of occurrence of the about-to-occur earthquake. The gravitational attraction of the Moon (or the Sun) may act as a trigger by causing appropriately oriented forces on the two sides of a fault. For maximum triggering effect, the orientation of the fault and the potential slip direction should be optimum with respect to the direction of the Moon.

Since fault orientation can be considered to be random, on a global scale there would be no detectable correlation between tides and earthquakes. In any case, the small number of earthquakes per tidal cycle would make such correlation very difficult to detect. This is borne out by numerous unsuccessful efforts to find correlation between tides and earthquakes (See section 4.3.1).

Earthquake swarms, volcanic tremors and aftershock sequence are very local in nature. The source (fault) mechanism is more homogeneous. A large number of events occur per tidal cycle. Therefore, if the tides act as a trigger, it could be easier to detect the correlation in such sequences.

4.2.1 Why Loma Prieta

The Loma Prieta earthquake (M_S = 7.1) occured at 37.036°N, 121.883°W on October 18, 1989. In a year, 10374 aftershocks ($0 < M_L \leq 5.5$) were recorded. Commonly, it is almost impossible to record all the aftershocks (especially in the low magnitude range) of a large earthquake. The reason is the absence of stations near the epicentral region. It takes time to set up portable systems around the epicenter. Even then, small aftershocks during the first few days are not recorded due to the logistics. The seismic stations far from the epicenter will not detect small aftershocks. Therefore, most of

the aftershock sequences are only complete for the events of magnitude 3 and greater. Fortunately, the Loma Prieta earthquake occurred in a very well instrumented zone operated by Northern California Seismic Network (NCSN). By virtue of this an almost complete, unique catalog of the aftershocks ($M_L \geq 1$) is available.

Our initial objective was to examine the Loma Prieta aftershock sequence for tidal periodicities. Like others before us (section 4.3.1), we did not find any strong evidence of correlation with the tides. However, we were astonished to find strong peaks at the periods of two fundamental free oscillations of the earth, ${}_0S_2$ and ${}_0T_2$, ~55.4 minutes and ~43.2 minutes respectively. Therefore, our final objective became the search for the modal periodicities in this sequence. With detailed investigation using a method developed by us (the KORRECT method), we can see evidence of triggering (both advancement and retardation of the onset of rupture) at some phases of modal cycles.

The modal triggering hypothesis was also tested on larger aftershocks ($3 \leq M_L < 7$) from all major global earthquakes ($M_S > 7.0$) occurring in the period 1970–1990, but strong evidence for triggering, such as for the Loma Prieta sequence, was not found.

4.3 Search for Triggering Agents: Review

Until mid eighteenth century, earthquakes were viewed largely as "acts of God" in retribution for misbehaviour of mankind; afterward, they were studied more as natural phenomena, and knowledge of earthquakes grew gradually but steadily as a result of careful observations. Since the late nineteenth century, systematic efforts have been made to associate earthquake occurrences to other naturally occuring phenomena, such as sunspot activity, planetary influences, magnetic and electric disturbances, Chandler Wobble, and solid earth tides.

The search for correlation between earthquakes and sunspot activity dates back to Wallis (1905) and Davison (1927). Using statistical analysis, Davison (1927) reported that just before the minimum in sunspot activity, there is a peak in the frequency of destructive earthquakes. The data used in this study do not have

many events so as to conclusively prove the correlation. Recently, Gribbin (1971) attributed this correlation to be an indirect effect in the sense that the solar activity may be linked to sudden changes in the earth's rate of rotation, and that the latter may initiate earthquakes. Meeus(1976) found no relation at all between the solar activity and the number of big earthquakes ($M > 7.7$) occurred during the period 1905 to 1964.

Since earthquakes were believed to be caused by some forces outside the earth, there have been studies on their association with certain planetary configurations. Such configurations may be the passage of a single planet through a specific longitude or other celestial mark. Delauney (1880), from a catalog of earthquakes from 1750 to 1842, found high earthquake activities at times when Jupiter reaches the mean longitude of 265° and 135° and when Saturn reaches the same longitudes. Tomashek (1959) studied 134 great earthquakes ($M > 7.8$) occurred during the period 1904-1950 and reported that at the time of some earthquakes, Uranus was very near its upper or lower transit. Such studies do not indicate a positive correlation and were counterattacked by Burr (1960) as a coincidence, because no physical mechanism is offered. Gravitational forces associated with planetary configurations are far too small. Most controversial of the planetary influences is the so called *Jupiter effect*, a term coined by Gribbin & Plagemann (1974) for the heliocentric alignment of all the planets on the same side of the sun, which can cause abnormal solar activity; the resultant movement of large atmospheric masses will agitate the geologically unstable regions and trigger earthquakes. On the other hand, Ip (1976) and Hughes (1977) found that planetary alignment is not associated with increase in earthquake activity.

Changes in local terrestrial magnetic field prior to, during and after earthquakes have been observed. Early observations (Lake, 1875; Lamont, 1892; Hazard, 1909) were explained by Reid (1914) as mechanical disturbances in the recording instruments caused by earthquakes. Better instrumentation, however, has shown that the effect is real and the study of earthquake magnetism has been revived. Moore (1964) noted that about 1 hour before the 1964 Alaskan earthquake, earth's magnetic field intensity increased by 100γ at a station 30 km *NW* of the fault zone. Smith & Johnston (1976) and Johnston (1978) noted dramatic changes in the local geomag-

netic field with an array of seven proton precession magnetometers along the San Andreas fault, before an earthquake (M = 5.2) near Hollister, California in 1974. This was attributed to a piezomagnetic effect, which implies that the magnetic field changes represent changes in stress in rocks near the station. An increase in the ULF ($0.01 - 10Hz$) magnetic field is noted near the epicenters of Ms = 6.9 Spitak earthquake and Ms = 7.1 Loma Prieta earthquake (Fraser-Smith *et al*,1990; Molchanov *et al*,1992). It should be noted that the increase in the magnetic field is only a precursory phenomenon, not a trigger.

The correlation of earthquake activity with the 14 month Chandler Wobble is a classical "chicken-egg" mystery. Mansinha & Smylie (1967; 1968) made detailed calculations of the energy involved in a sudden large scale movement of a great fault and proposed that this energy is sufficient to provide the impetus for the Wobble. However, it is not inconceivable that Chandler Wobble may excite earthquakes (Pines & Shaham, 1973). Kanamori (1976) and O'Connell & Dziewonski (1976) used the geometries of great earthquakes predicted by plate tectonics and computed the cumulaive effects of the earthquakes on polar motion. These studies concluded that earthquakes represent the major factor in wobble excitation. On the other hand, Ben-Menahem & Israel (1970) state that even under most favorable conditions, earthquakes could account for only 30% of the Chandler Wobble. Meyerson (1970) compared yearly earthquake counts with the yearly means of the Chandler amplitude and found that earthquakes are associated with the wobble, but he claimed that this is a parallel effect rather than a cause. Press & Briggs (1975) applied a pattern recognition algorithm to the seismicity of earthquake belts, to the amplitudes of Chandler wobble, to the changes in the rotational velocity of the earth for the years 1901-1964, and found that all these phenomena are related.

The most investigated and important phenomenon related to earthquake triggering is the effect of periodic stresses induced by the gravitational attraction of the sun and moon, because they are the largest forces which subject the earth to large oscillatory stresses.

4.3.1 Tidal Triggering

During the past century and a half there have been many attempts to detect a correlation between solid earth tides and the occurrence times of earthquakes. The reason behind the search for correlation is intuitive. Gravitational attraction of the sun and the moon subject the earth to large oscillatory stresses which can be observed in the form of solid earth tides. Crustal stresses due to solid earth tide are of the order of 3×10^4 dynes/cm^2 (0.03 bar), which is about $1/100^{th}$ to $1/1000^{th}$ of the average stress drop of earthquakes (Kanamori,1977; Hanks,1977). In order to trigger earthquakes, the tidal stresses must be oriented in a manner that will reduce critical stress S_c or increase forcing stress S_f (section 4.1). It is worth noting that any stress system generated by the tides must have a stress discontinuity across fault surface, i.e., shear or tensile stress must act in opposite direction on both sides of the fault. Tidal stresses are large and vary according to location on and within the earth. On a preexisting fault, only that part of the tidal stress, which can produce a discontinuity or a differential stress across the fault, may act as an effective trigger.

The tides repeat (though not exactly) at 24, 12 and 8 hour periods. Only a few large earthquakes take place during a very large number of tidal cycles. The problem of searching for a correlation is not trivial. One can only search for earthquake occurences at some preferred tidal phase. By and large the correlations between the earthquakes and tides, if found, have been marginal at best. The first systematic investigation of the possible correlation between earthquake occurrence and tidal stresses in the lithosphere was carried out by Alexis Perrey (1847). Perrey considered the then current doctrine of a fluid nucleus for the earth; he argued that the fluid mass, like the ocean waters, must be subjected to tidal movements and hence would disturb the solid crust. This was later proved to be untrue, but his method of tackling the problem influenced most subsequent workers. Before losing his sight, he wrote several papers on the subject (Perrey, 1864; 1875). The investigations of earthquake periodicities were continued by John Milne (1886) and Knott(1886). Knott (1897) tabulated earthquakes according to 5 different lunar months and using harmonic analysis, he found monthly, fortnightly and weekly periods. These results were

challenged by Arthur Schuster (1897), who claimed that even purely random events would have given results similar to those of Knott (1897).

Oldham (1902) investigated the great Assam earthquake of 1897 and its aftershocks and recognized that the tidal effect on the earthquakes may be due to the change in time rates of stress rather than actual stresses. By this time, scientists had catalogs of instrumentally recorded earthquakes. Oldham (1903) pointed out that for north latitudes, when the sun is in north declination, the rate of change in the tidal stress is greater during the day than during the night; an examination of the records of the Shillong seismograph showed that the ratio of day and night shocks in summer is greater than in winter. Omori (1904), investigating the aftershocks of the Mino-Owari and the Hokkaido earthquake, found an occurrence of two seismic maxima at a mean interval of 12 hours approximately at or a little after, the meridian passages of the moon. These hypotheses were found to be questionable on the basis of several statistical tests (Phillips,1917; Shaw,1917).

Davison (1934; 1935) found that 482 aftershocks of the 1927 Tango earthquake and all the earthquakes recorded at the Tokyo University observatory during 1927 to 1933 show a peak frequency at 14.8 day intervals, at the new and full moons. Allen (1936) studied 1216 earthquakes occurring in southern California and using Schuster's criteria, found lunar triggering effects in this catalog. On the other hand, Knopoff (1964b) found that a data set consisting of random events can give similarly significant correlation with the tides. Later, Knopoff (1969) found a significant correlation at 99% confidence level between the fortnightly earth tide and world wide occurring larger earthquakes ($M_S > 6$), but when aftershocks were eliminated from the data, the correlation fell below 75% confidence level, implying that the initial quakes are not triggered by tidal stress.

Tides and Moonquakes

During Apollo missions spanning 1969 to 1972, long period seismometers were installed on the moon as part of Apollo Lunar Surface Experiment Package (ALSEP). Using ALSEP data, G. Latham with his colleagus reported a striking correlation between the moonquakes and the tides on the moon induced by the earth. Latham *et al*

(1971) observed that moonquakes occur at monthly intervals near the time of perigee and apogee of the earth-moon system and show correlations with seven month lunar gravity variations. Lammlein *et al* (1974) found 14 day and 206 day periodicities in the sequence of moonquakes (magnitude 0.5 to 1.3) recorded at 4 Apollo stations. Since the moon is not a tectonically very active body, the strain energy due to gravitational tides of the earth-moon system seems to be the dominant source of energy released by the moonquakes. Goulty (1979) analysed deep moonquakes from 80 repeating sources. These moon quakes also displayed tidal periodicities in their origin times. This discovery stimulated the search for a similar effect on the earthquakes (Shlien,1972; Heaton,1975; Klein,1976; Young & Zürn,1979). Heaton (1975), using a catalog of 107 worldwide earthquakes, found that only shallow (< 30km) large earthquakes are likely to be triggered by the tides. On the basis of a model of tectonic and tidal stress rates, he concluded that small earthquakes (magnitude < 3) should not correlate with tidal stress. Kilston & Knopoff (1983) tested this hypothesis on the large earthquakes in Southern California but did not find a positive correlation.

Tides and Aftershock sequences

When many globally distributed earthquakes are considered, no signficant periodicities were seen because of a multiplicity of source fault orientations and stress regimes (section 4.2). On the other hand, small regions present a situation which may be much more homogeneous. Therefore, the earthquake catalog from a relatively small region (aftershock sequences or earthquake swarms) is a better candidate for a possible tidal correlation. It was realised that in order to prove (or reject) the tidal triggering hypothesis, one requires a data set with large number of events per tidal cycle. With the advancement in instrumentation within last 30 years, there has been an enormous increase in the number of earthquakes detected in the low magnitude ranges. As a result, a large number of sequences of earthquake swarms, volcanic tremors and aftershocks of large earthquakes became available. The search for correlation in these sequences presents a different picture. There are a large number of events per tidal cycle. Standard methods of correlation can be applied. However, analysis of an aftershock sequence from Shikotan (Kurile Islands) earthquake (mainshock Au-

gust 11, 1969) did not provide any significant tidal correlation (Shlien, 1972). Klein (1976) analysed swarm clusters from many sequences in the Reykjanes Peninsula in Iceland, the central mid-atlantic ridge, the Imperial valley and northern Gulf of California over a span of several years. Significant (> 95%) tidal correlations were found in these swarm clusters except for the Matsushiro Japan swarm of 1965-1967. Young and Zürn (1979) studied earthquakes in the Swabian Jura, but found no significant triggering effects. Mohler (1980) found very little correlation between earth tides and earthquakes in the Susanville, California, earthquake sequence of June-July 1976. By and large, the results of such studies are inconclusive. Recently, a diurnal (24 hours) periodicity has been reported in a catalog of volcanic shocks at Mount Merapi (Fadeli *et al*, 1991), but the absence of a semidiurnal periodicity (semidiurnal tide is the largest in amplitude) has led to the suspicion that the diurnal periodicity is due to cultural noise.

4.4 Normal Modes as a Trigger?

After a large earthquake, many of the earth's normal modes are excited and are detectable for a long time on long period seismometers and accelerometers. These modes are exponentially decaying sinusoids and can be observed as distinct spectral peaks in the spectra of the recorded seismograms (Alsop,1964; Block *et al*,1970; Gilbert & Dziewonski,1975). These modes have distinct stress and displacement patterns in the earth. Under favorable conditions, the nature of the stress due to some of the normal modes may contribute to the forcing stress S_f and act as a trigger. Similarly, it can also act to decrease the critical stress S_c in the vicinity of a number of newly developed cracks in the focal region.

If sufficiently excited, the modes with high quality factor ($Q > 2000$) e.g., ${}_0S_0$ ($Q = 5700$), ${}_6S_2$ ($Q = 2900$) etc., can be observed for months on sensitive instruments. On the average, the normal modes last for about one week or so after the earthquake before disappearing into the ambient seismic noise level. Therefore, the triggering effect of the normal modes, if any, should be prominent in an aftershock sequence during the first few days only.

Was it missed before?

Davison* (1934; 1935) analysed an aftershock catalog for the Tango earthquake of March 7, 1927 during the period of March, 1927 to July, 1928. He mentioned a 42 minute periodicity in the occurrence times of about 400 aftershocks during the month of March and April, 1927. Davison attributed this effect to the surface waves travelling to the antipodes and coming back. At the time, normal modes of the earth had not been observed on instruments; even though the theory for the free oscillations of an elastic sphere had been developed (Lamè,1853; Kelvin, 1864; Lamb,1882; Love,1911). However, in the absence of knowledge of an earth model, the periods of these oscillations were only approximately known. Davison did not realise that this 42 minute period is strikingly close to the period of the second order fundamental torsional mode, ${}_0T_2$.

What follows is a description of a method of analysis (KORRECT) (Chapter 5) and its application (together with spectral analysis) to two aftershock data sets in a search for the tidal and modal periodicities (Chapter 6).

*We found this reference after discovering the modal periodicities in the Loma Prieta aftershock sequence.

Chapter 5

Data and Analysis

It is a capital mistake to theorize before one has data.

Arthur Conan Doyle

Two sets of aftershock data were analysed to check for the triggering effect. The first one is an almost complete aftershock sequence from the Loma Prieta, California earthquake; another data set was constructed by comparing the recorded large ($M_L \geq 3$) aftershocks from all the major earthquakes ($M_S > 7$) around the world that occurred during the 21 year period January 1970 to December 1990.

5.1 The Loma Prieta Earthquake Sequence (Sequence I)

The Loma Prieta, California, earthquake ($M_S = 7.1$) occurred beneath the Santa Cruz mountains at 00:04:15.2 UT on October 18, 1989. This was the biggest earthquake to occur on San Andreas fault since the great 1906 earthquake. Microseismicity studies twenty years prior to this earthquake show a quiescent period (McNally *et al*, 1989). This quiescent period was followed by the aftershocks of the Loma Prieta earthquake.

Since the late 1960's the United States Geological Survey (USGS) has operated a dense seismic network (CALNET) along San Andreas fault on Santa Cruz mountains which consists of high gain vertical component seismometers (Eaton *et al*,1970). The seismometers are Electrotech EV17 (and EV17H) 500-ohm coil electro-

magnet instruments operated at critical damping. The signal from the seismometer is amplified by UED 210A amplifiers, which have a maximum gain of 100 db within a passband of 0.5 to 17 cps. Primary timing is provided by recording the WWVB digitally coded radio time signal. As a result of this network, an aftershock data set of uncomparable quality had been acquired. This data set is unique in the sense that no other data set is complete for such low magnitude aftershocks ($M_L > 1$).

During the year following the Loma Prieta mainshock, 10374 aftershocks, M_L ranging from 0 to 5.5, have been recorded with the CALNET. As usual with all the aftershock sequences, the number of events decay with time. The overall appearance of the data set is that of a decaying random noise sequence. About half of these aftershocks, occurred during the first 20 days following the mainshock. Figure 5.1 shows a part of the data set as number of aftershocks per hour occurring after the mainshock. The data set consists of origin times, locations, depths, and magnitudes of the aftershocks. The distribution of aftershocks with respect to magnitude is shown in Figure 5.2. It is to be noted that as time goes on, the probability of occurrence of larger aftershocks becomes smaller. A majority of the aftershocks are in the magnitude range 1-2. The depths are confined to within 20 km (Figure 5.3). Most of the aftershocks are in the 5-15 km region, which defines the fault plane for this study. Instrumental problems in the epicentral region hindered the recording of the aftershocks during the first 24 hours following the mainshock. From the second day onwards, the data set is complete for the aftershocks of magnitude $M_L \geq 1$ (Dietz & Ellsworth, 1990).

The magnitudes and locations of aftershocks in this catalog were determined using P-wave data (Dietz & Ellsworth, 1990) with the program HYPOINVERSE (Klein, 1989). The aftershocks of the Loma Prieta earthquake exhibit a wide variety of mechanisms (Oppenheimer, 1990) including reverse, right-lateral, left-lateral and normal motion on planes subparallel to the mainshock rupture plane.

The mainshock of the sequence occurred at 37.036°N, 121.883°W, at a depth of 15 km. Through body wave analysis of teleseismic data, Kanamori & Satake(1990) determined the focal mechanism to be dip= 70°, rake= 138°, strike= 128° and the rupture length= 35 km. There is some discrepancy on the vertical extent

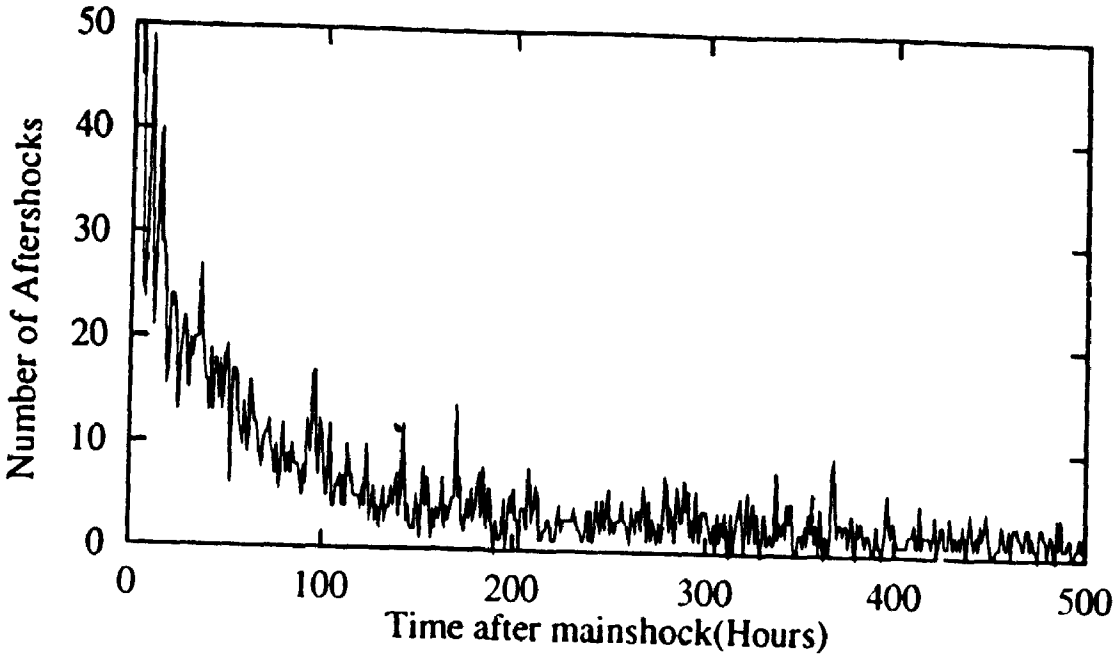

Figure 5.1: Number of events per hour vs. time for the Loma Prieta aftershock sequence.

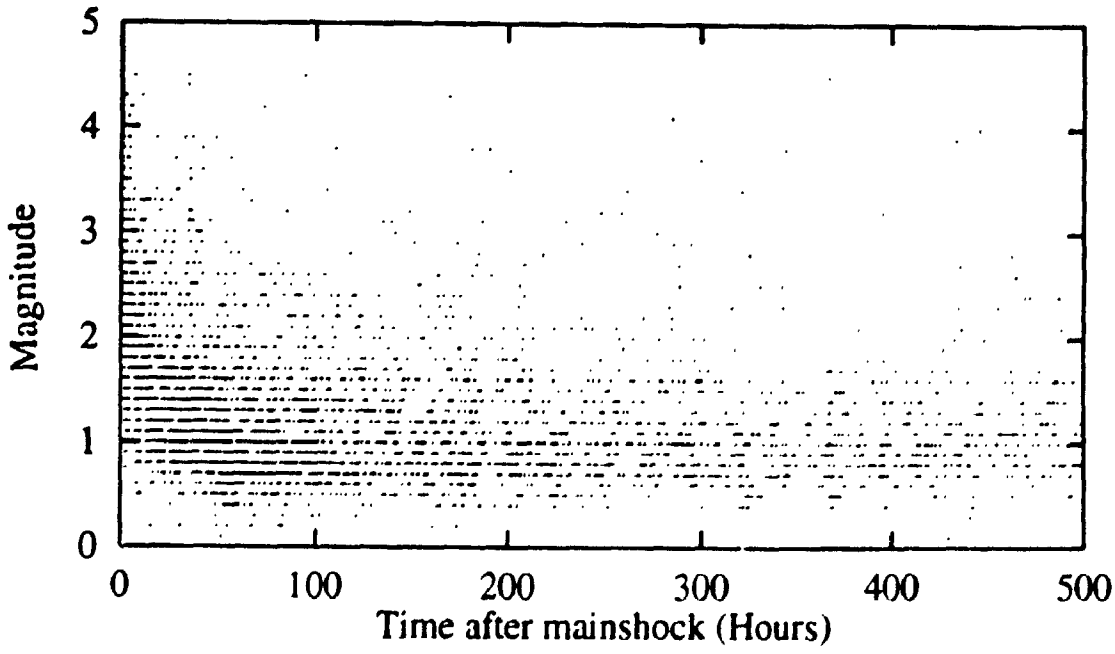

Figure 5.2: Magnitude distribution of Loma prieta aftershocks with time. Note that the number of aftershocks decreases as the magnitude increases.

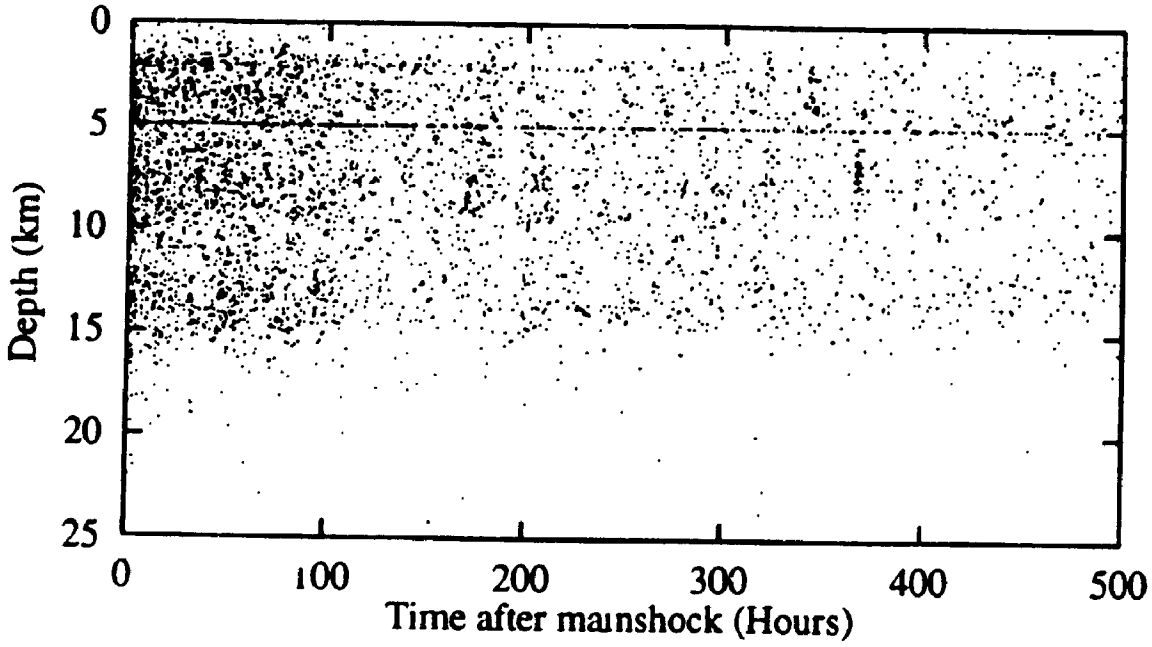

Figure 5.3: Depth distribution of the aftershocks of the Loma Prieta earthquake. Note the clustering of earthquakes between 2 to 15 km depth.

of the fault zone calculated by different methods. Hartzell *et al*(1991) and Steidl *et al*(1991), through the modelling of radiation field for the high frequency body waves (>0.1 Hz) determined a vertical extent of 2 to 19 km. The analysis of the broad band body waves and long period surface waves (Wallace *et al*, 1991) show a vertical extent of 5 to 18 km. A vertical extent of 4.8 to 15.1 km explains the co-seismic horizontal displacements (Snay *et al*, 1991). On the other hand, Modeling of co-seismic elevation data from geodetic levelling surveys (Marshall *et al*, 1991) provides a vertical extent of fault plane as 4 to 15 km. As a working compromise, we have chosen the vertical extent of the fault plane to be 5 to 15 km.

5.2 Global Aftershock Data Set (Sequence II)

The second data set used in the study is extracted from the GLOBAL HYPOCENTER DATA BASE CD-ROM using the software EPIC. The catalog contains earthquakes located by USGS National Earthquake Information Center (NEIC) and its predecessors in the United States Coast and Geodetic Survey. For the 21 year period 1970-1990, 273 large earthquakes ($M_S \geq 7$) were identified (Appendix A). For each of these earthquakes, all the aftershocks (magnitude $3 \leq M_L \leq 6$) occurring from time $t = 0$ (time of mainshock) to $t = 30$ days (720 hours) were extracted. Since the fault dimensions related to the mainshocks were not available, we used a circular area of 100 km radius from the epicenter of each mainshock as the aftershock zone. In this manner, the aftershocks series are formed for all 273 earthquakes ($M_S \geq 7$) and these series are combined to form a global aftershock sequence. The number of aftershocks for each of these earthquakes vary from no aftershocks to 234 aftershocks. In all, this sequence has 7864 aftershocks for the 30 day period.

The data sets, consisting of the occurrence times of aftershocks, were analysed. Since the aftershocks do not occur at regular time intervals, special processing is required before applying standard spectral analysis. Also, commonly used statistical tests of significance of high peaks in the spectra are not valid here (for the reasons mentioned in section 5.3); an independent method in the time domain is developed for the analysis. The methods of analysis are discussed next.

5.3 Spectral Analysis

In a routine method of detecting periodicities in a time series, the data are transformed into the frequency domain through a fast Fourier transform. Dominant frequencies present in the data set will appear as distinct peaks above the noise level. There are two basic requirements for commonly used spectral analysis

- Data should be sampled at regular intervals.
- Each sample point should have an associated amplitude.

The aftershock sequences do not satisfy either of these conditions. The aftershocks of an earthquake do not occur at regular time intervals. Therefore the time series resulting from the event sequence will be irregularly sampled. Also, one cannot associate any amplitude with the occurrence of an aftershock. To solve this problem, an equispaced time series is formed by binning the sequence at regular intervals. The time axis is divided into fixed width bins, and the number of events are counted in each bin. This number is ascribed to the midpoint of the bin as its amplitude (Figure 5.4). The bin width is analogous to the sampling interval in a regular time series.

Tides (Diurnal, semi-diurnal and ter-diurnal) are long period phenomena, while the normal modes (< 1 hour) are shorter period. Therefore, larger bin widths (15 minutes-1 hour) are used to investigate tidal triggering, whereas shorter bin widths (5 minutes-15 minutes) are necessary for the analysis of modal triggering. A bin width shorter than 5 minutes is not suitable in the present study as it results in a large number of bins with no events, i.e. zero amplitude. The spectrum will be distorted by convolution with the resultant sync functions. On the other hand, a very wide bin (>1 hour) does not provide enough resolution to distinguish between different tidal periodicities (if they are present at all).

Any standard spectral estimation method require tapering of the data set prior to transformation into the frequency domain. This is necessary to prevent the spectral leakage. Several tapers are available for this purpose. Each has its merits and demerits. Most commonly used tapers are Hann, Hamming, Tukey, Blackman-Harris, Kaiser etc. (Childers & Durling,1975). Since the overall appearance of the

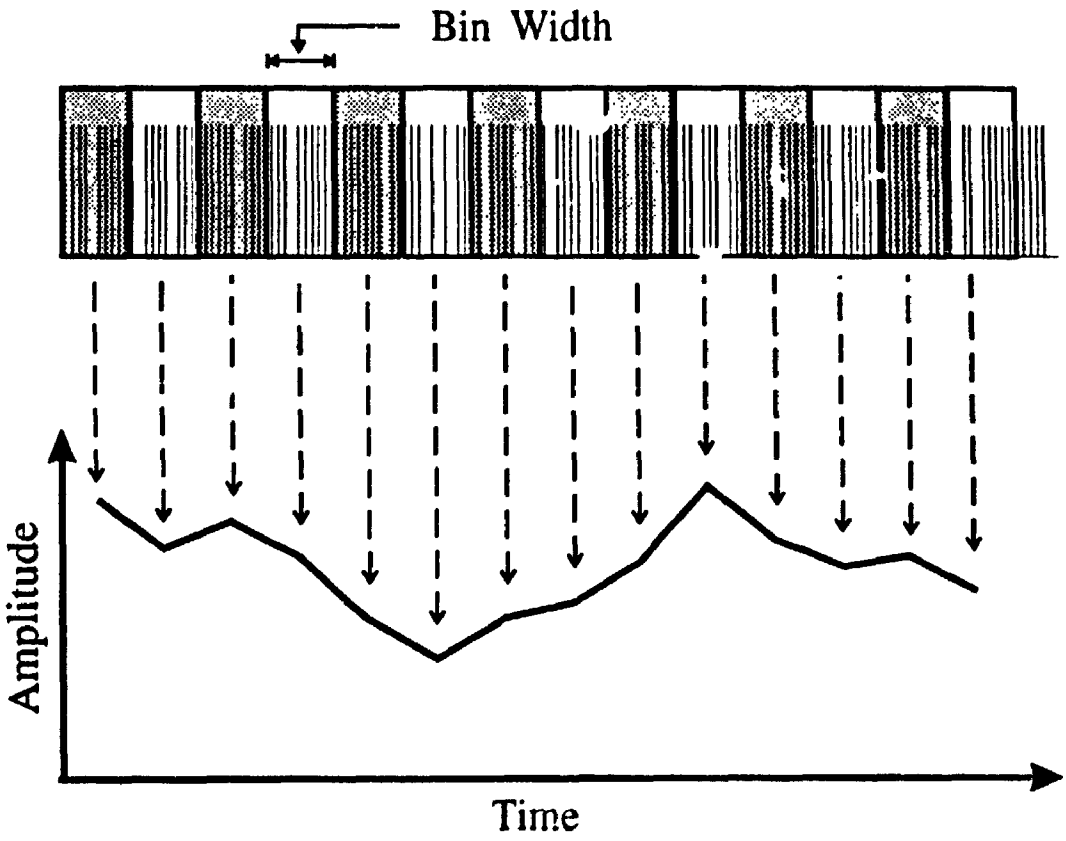

Figure 5.4: Binning of the aftershock sequence to make a suitable time series for spectral analysis. Events are counted in each time interval (bin) and assigned as the amplitude at the mid point of the bin.

data set is that of an exponentially decaying time series, the foremost part of the data contains the most important information. Therefore, we require a taper which would reduce the spectral leakage without discarding much of the initial portion of the binned data set. It is for this reason that a 10% Tukey window is chosen to taper the data set prior to frequency domain transformation. In the time domain, a 10% Tukey window is defined as

$$\begin{aligned} w(t) &= \frac{A}{2}\left[1 - cos\frac{2\pi\left(t+\frac{T_0}{2}\right)}{2\alpha T_0}\right] &&, \frac{-T_0}{2} \le t \le \frac{-T_0}{2}(1-2\alpha) \\ &= A &&, \frac{-T_0}{2}(1-2\alpha) \le t \le \frac{T_0}{2}(1-2\alpha) \\ &= \frac{A}{2}\left[1 - cos\frac{2\pi\left(\frac{T_0}{2}-t\right)}{2\alpha T_0}\right] &&, \frac{T_0}{2}(1-2\alpha) \le t \le \frac{T_0}{2} \\ &= 0 &&, \text{otherwise} \end{aligned} \qquad (5.1)$$

where α=1/10.

The tapered time series is then transformed into the frequency domain using a multi-radix FFT routine (Childers & Durling, 1975) to give the spectrum.

Commonly, any spectral method requires tests of significance to distinguish the true spectral peaks from the spurious ones. These tests are not very useful in studies like the present one. The reason is that every test for the significance of a spectral peak relies on an assumption of stationarity of the noise. Stationarity means that the statistical properties of the noise process do not depend on time; they are invariant with respect to shifts in time. Aftershock sequences cannot be considered stationary, so the common significance tests may not be valid. In order to verify the results from the spectral analysis, we used a different time domain method, which is described next.

5.4 The KORRECT Method

We developed a method of detecting periods and phase in event sequence in the time domain, which is named as KORRECT (CORrelation with a RECTangular pulse). KORRECT is basically a correlation of the occurrence times of the aftershocks with a rectangular pulse series. The pulse series is formed by repeating a finite width rect-

angular pulse of unit amplitude at regular intervals. The pulse width has been varied from 5 minutes to 15 minutes in the current usage. In order to have a conformity with the spectral method, the separation between two consecutive pulses (the period) is limited to the equivalent harmonic periods, t_n, given by $t_n = T/n, n = 1,2,3...N/2$, where T is the total duration of the sequence and N is the number of samples. Figure 5.5 is an example of the rectangular pulse formed for two different harmonic periods for a given pulse width. For each harmonic period, a rectangular pulse series is formed and overlaid on the aftershock data set.

All the aftershocks falling within the pulses are counted, added together, and divided by the number of pulses to provide a measure of aftershock density at a specific phase of the period t_n. The pulse series is then shifted in time (by a fraction of the period t_n) and the aftershock density calculated at a different phase for the same period (Figure 5.6). Each period is divided into several parts which decides the time (phase) shift. At each period, 36 computations were carried out at regular time shifts, giving a value at every 10° in phase, to provide coverage over whole cycle of 360°. This "phase variation curve" gives the aftershock density as a function of the phase at a particular period t_n. Similar phase variation curves are obtained for all the harmonic periods for further interpretation.

We tried the statistical tests of significance for harmonic peaks (Fisher, 1929) in a modified form for geophysical time series (Shimshoni, 1971). This test is commonly used in identifying the normal modes of the earth. This method depends on the rank order of the peak, thus allowing lower order peaks to be accepted. The tests of significance were not found very useful in the present study for the reasons stated in section 5.3, therefore we used a combination of a cyclic phase variation curve and a high spectral peak for the identification of significant peaks.

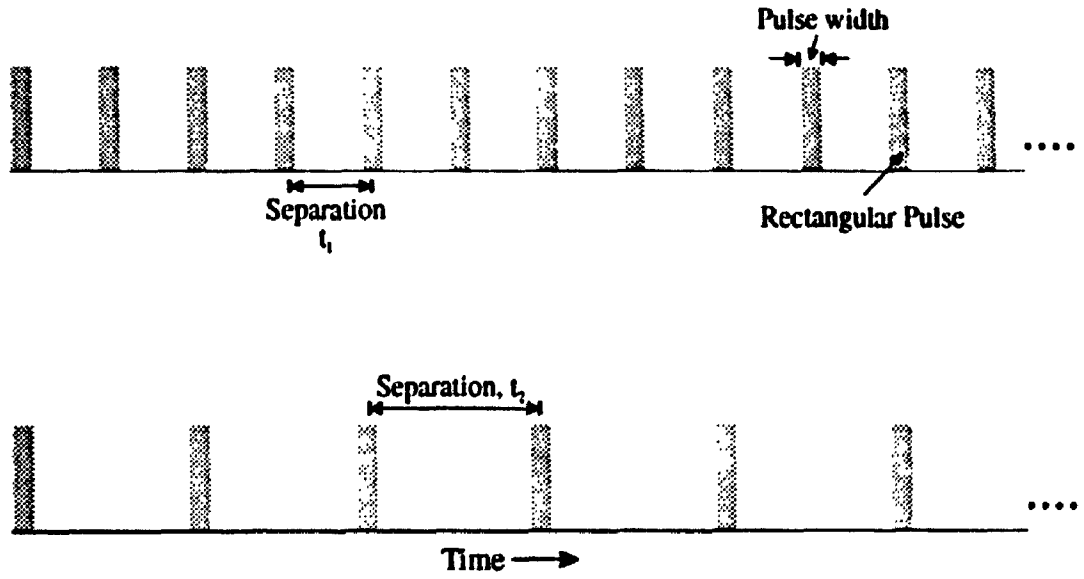

Figure 5.5: Rectangular pulse series for two different periods for use in KORRECT method. The period corresponds to the separation between the pulses.

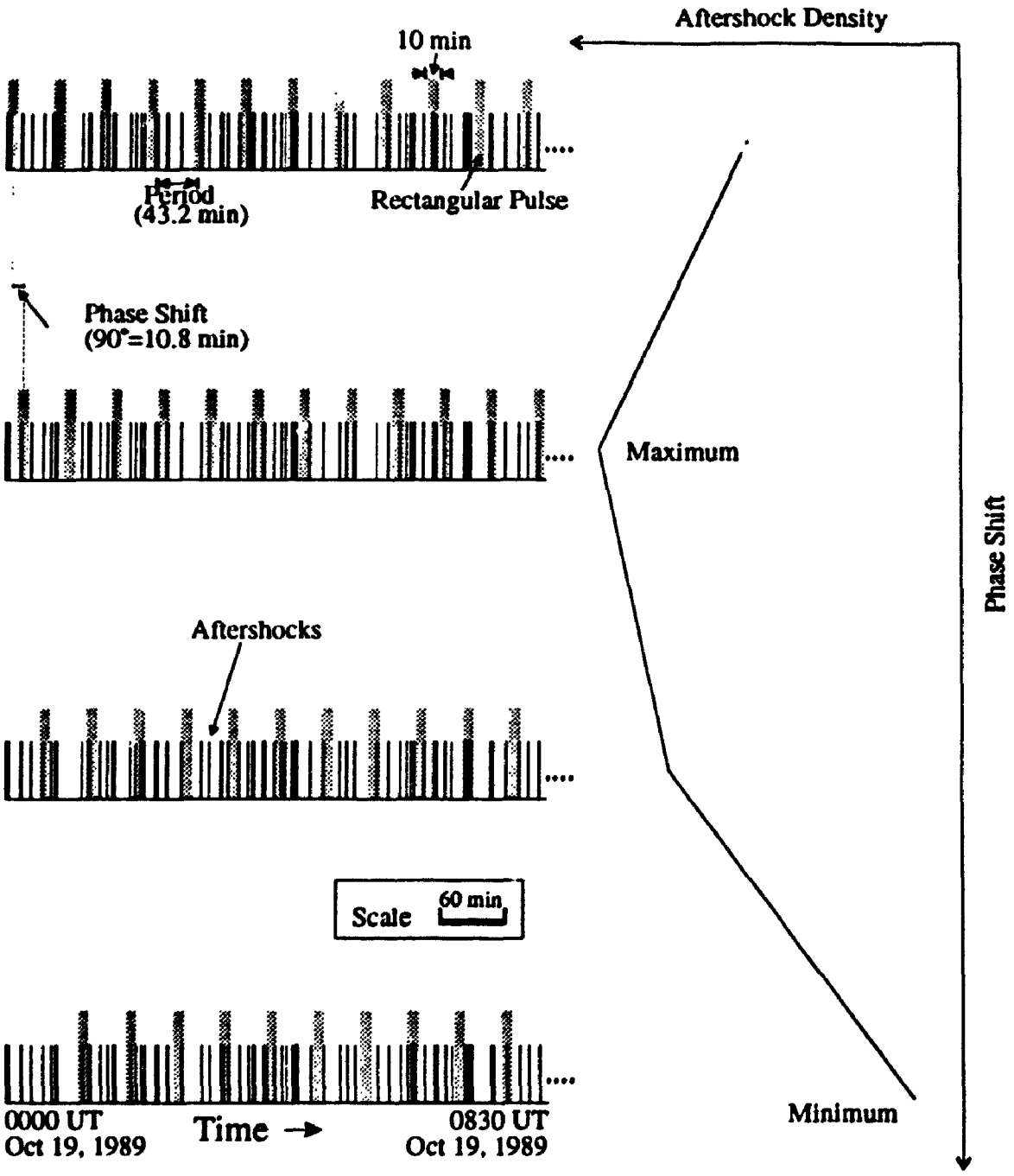

Figure 5.6: The KORRECT method for detecting periodicities and phase information in the aftershock sequence. The vertical lines are the origin times of the aftershocks. A rectangular pulse series (shaded) is overlaid on the data set; the events lying in the shaded regions are counted and divided by the number of pulses (aftershock density).

Chapter 6

The Answer

So easy it seemed
Once found, which yet unfound most would have
Thought impossible.

John Milton.

The following criteria are chosen for a positive identification of a triggering process:

1. A spectral peak above the background noise level in the amplitude spectrum.
2. The period of this peak corresponds to a known physical process (a possible trigger).
3. A distinct and systematic variation in the phase plots, for this period, obtained by the KORRECT method.

Should all of the above conditions be satisfy together for a single period, we can conclusively identify the periodicity (therefore triggering) in the aftershock sequence.

6.1 Tidal Triggering

The periods of largest solid earth tides are approximately 24.06, 12.00 and 8.28 hours. Among these, the 12 hour (2 cycles/day) tide is the largest in amplitude, which makes it the most likely candidate for the tidal triggering of earthquakes.

To examine the tidal triggering hypothesis in the Loma Prieta aftershock sequence, several time series were formed from the aftershock data set during Day 2 to Day 30 following the mainshock. The bin width in these series were varied from 60 minutes to 15 minutes. One of such data set was shown in Figure 5.1. Amplitude spectra of these binned time series are shown in Figures 6.1, 6.2 and 6.3. These spectra are estimated with a multi-radix Fast Fourier Transform (FFT) using a 30 day (720 hours) 10% Tukey window. The spectra do not exhibit any preferential behavior for the tidal frequencies (1, 2 or 3 cycles/day). We do see some peaks in the spectra, but none of these peaks have any physical meaning. If the tidal triggering hypothesis were valid, the spectra should exhibit peaks (in order of decreasing amplitude) at 2 cycles/day (semidiurnal tide), 1 cycle/day (diurnal tide) and 3 cycles/day (terdiurnal tide).

There are some distinct peaks in these spectra, which are above the background noise. These peaks correspond to 38.6 hours, 9.8 hours, 5.75 hours, 4.16 hours and 3.5 hours respectively. These periods do not point to any known physical phenomenon, hence they cannot be associated to any physical process. The persistence of these peaks in the spectra is intriguing and needs detailed study. Based on these spectra, we conclude that the solid earth tides do not trigger aftershocks in the Loma Prieta earthquake sequence.

6.2 Modal Triggering

Normal modes decay exponentially with time. After a large earthquake, they can be observed for a week or so on long period seismometers or accelerometers. Thus, the triggering effect of the normal modes on the aftershocks is expected to be seen during the first 10 days following the mainshock. The aftershock data from Day 2 (the catalog is not complete for the first 24 hours) to Day 10 is analysed for the detection of the normal mode periodicities. Compared to the tidal analysis, narrower bin widths (higher sampling rate) have to be used to examine the normal mode periods. 5 minute and 10 minute bin widths are used to form several series from the aftershock data set of first 10 days following the mainshock. Only the earthquakes occurring

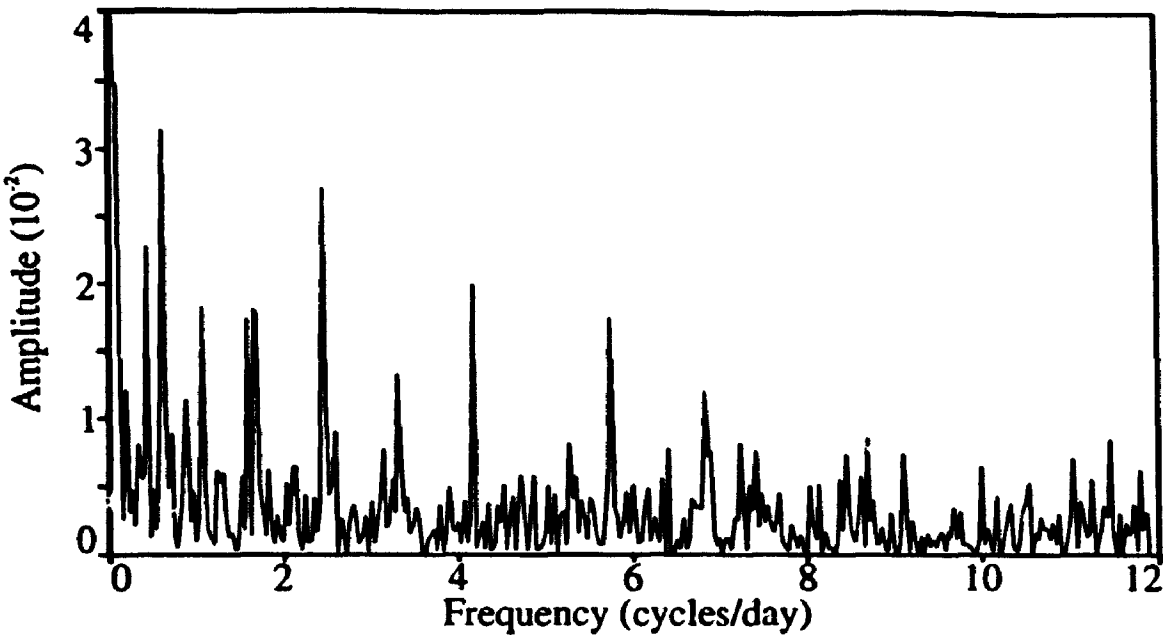

Figure 6.1: Amplitude spectrum of 30 day time series constructed from the Loma Prieta aftershock sequence using 1 hour bin size (720 points). There are no significant peaks at 1, 2 or 3 cycles/day (tidal periods).

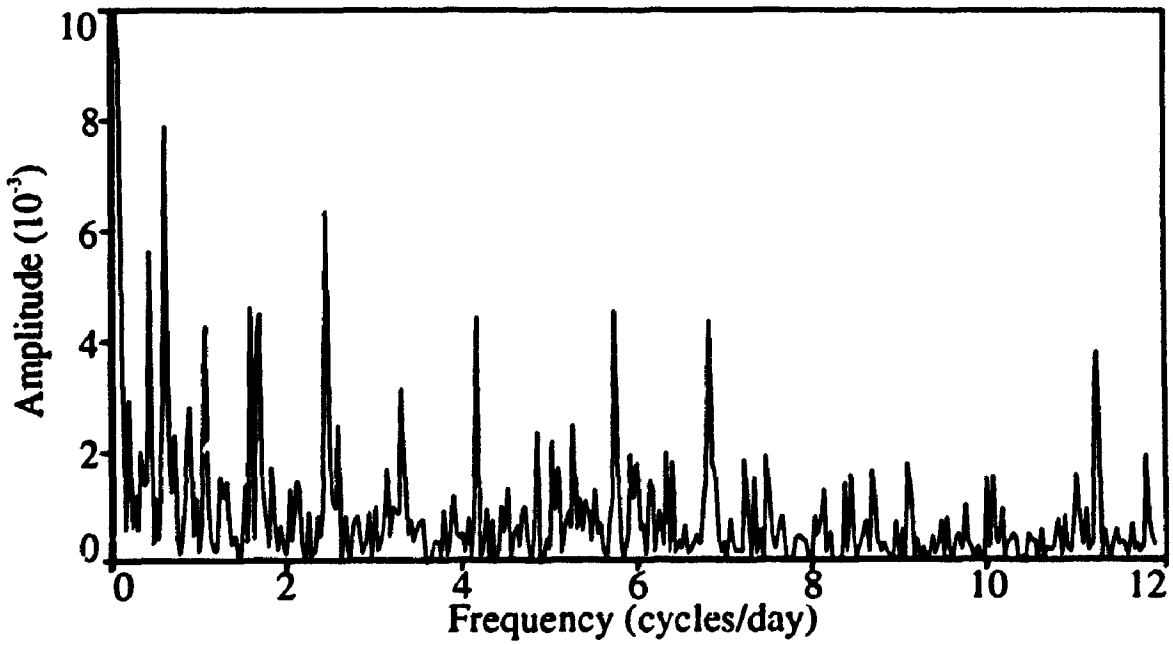

Figure 6.2: Amplitude spectrum of 30 day time series constructed from the Loma Prieta aftershock sequence using 30 minutes bin size (1440 points). There are no significant peaks at 1, 2 or 3 cycles/day (tidal periods).

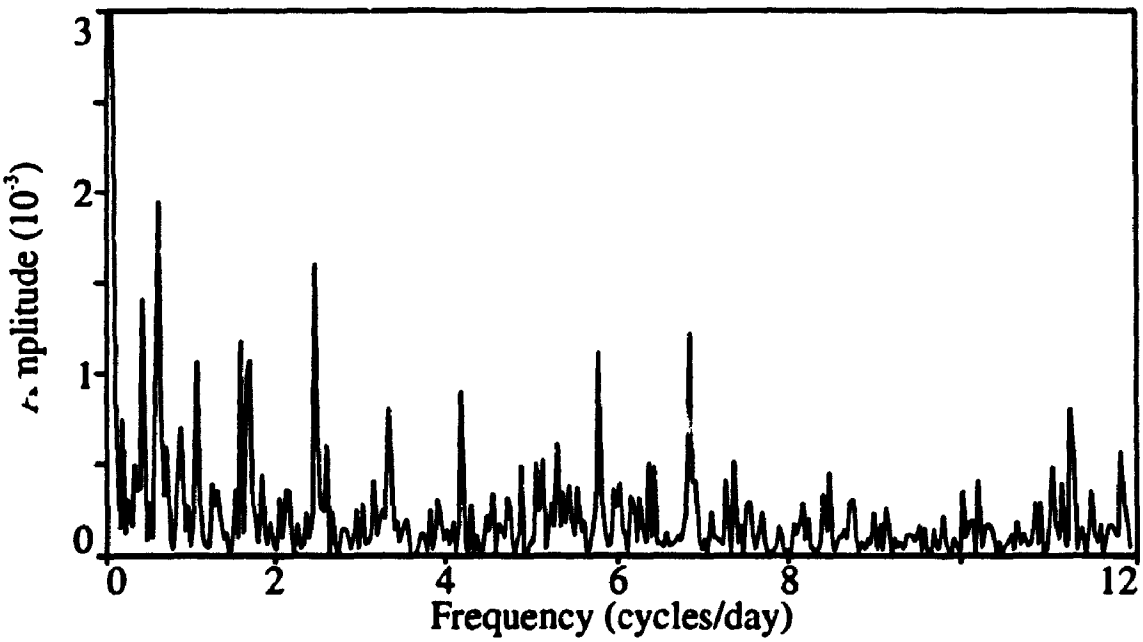

Figure 6.3: Amplitude spectrum of 30 day time series constructed from the Loma Prieta aftershock sequence using 15 minutes bin size (2880 points). There are no significant peaks at 1, 2 or 3 cycles/day (tidal periods).

within 60 km radius of the mainshock epicenter are considered. The aftershocks are also subdivided according to their focal depths and magnitudes. The spectra were estimated using a 72 hour, 10% Tukey window. This 72 hour window is then shifted forward in steps and the spectrum is estimated at each location. We found that the peaks in the spectra due to the normal modes are undetectable due to background noise after 144 hours (6 days) following the mainshock. Two factors, the declining number of aftershocks and the decay of modal amplitudes with time makes it difficult to detect the modal periodicities in the data set after Day 6. Figures 6.4, 6.5 and 6.6 show the spectra of the aftershock data set in successive windows. It can be seen that the modal peaks also decay in amplitude as time progresses and they become undetectable after 144 hours.

The series formed by the aftershocks of magnitudes ($1 \leq M_L \leq 2$) within the fault zone (5 to 15 km depth) show periodicities at the two longest period normal modes, spheroidal mode ${}_0S_2$ (frequency 26 cycles/day or 55.4 minutes) and the torroidal mode ${}_0T_2$ (frequency 33 cycles/day or 43.2 minutes).

Figure 6.4 shows a prominent periodicity at the frequency of 33 cycles/day (period of ${}_0T_2$). At the period of ${}_0S_2$ (26 cycles/day), there is a visible peak barely above the noise level. There is another strong peak in the spectrum at 52 cycles/day which is exactly double the frequency of the ${}_0S_2$ or half the period. The reason for the ${}_0S_2$ peak at half of its period will be clear from the results of the KORRECT method.

Aftershocks from different depth ranges exhibit different behavior. Figures 6.7, 6.8 and 6.9 compare the amplitude spectra of the aftershock data sets formed using different depth zones. The modal periodicities are only visible in the set containing aftershocks from the main fault zone (5 to 15 km depth).

The amplitude spectra of the series formed using large aftershocks of Loma Prieta earthquake are shown in Figure 6.10 ($2 < M_L \leq 3$) and Figure 6.11 ($3 < M_L \leq 5$). These spectra do not show high peaks at modal frequencies, indicating that the normal modes do not trigger large aftershocks. The apparent lack of triggering for larger aftershocks may be due to a decrease in the number of events.

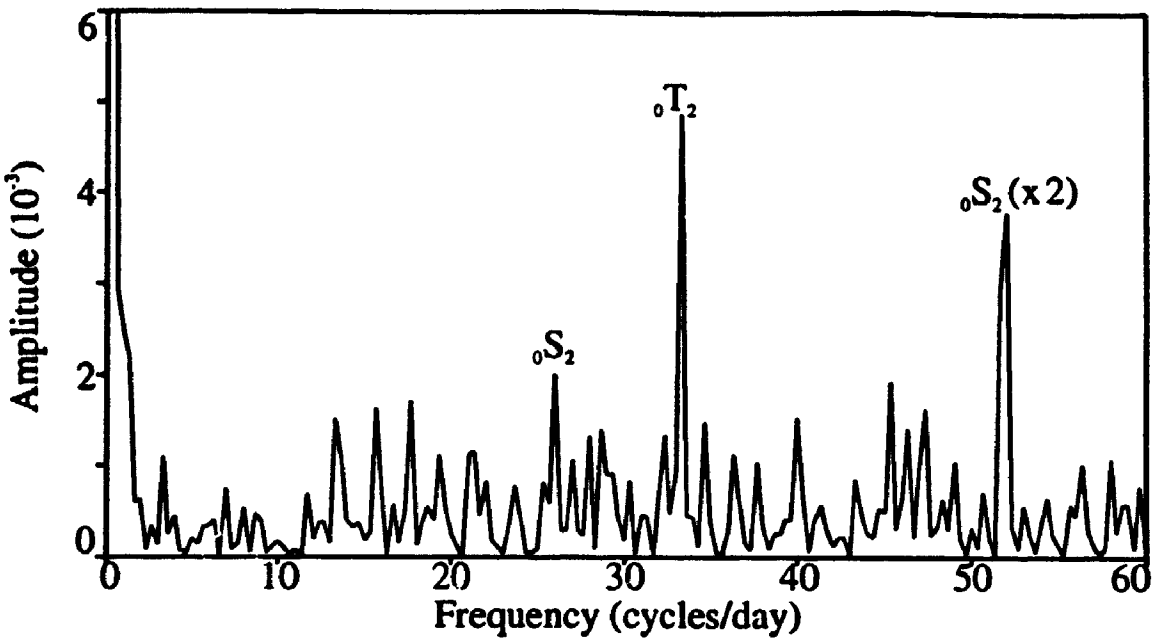

Figure 6.4: Amplitude spectra of 72 hours time series constructed by binning (bin width= 5 minutes) the Loma Prieta aftershock sequence. The beginning of the time series is 24 hours following the mainshock ($1 \leq M_L \leq 2$; 5 ≤depth≤ 15km).

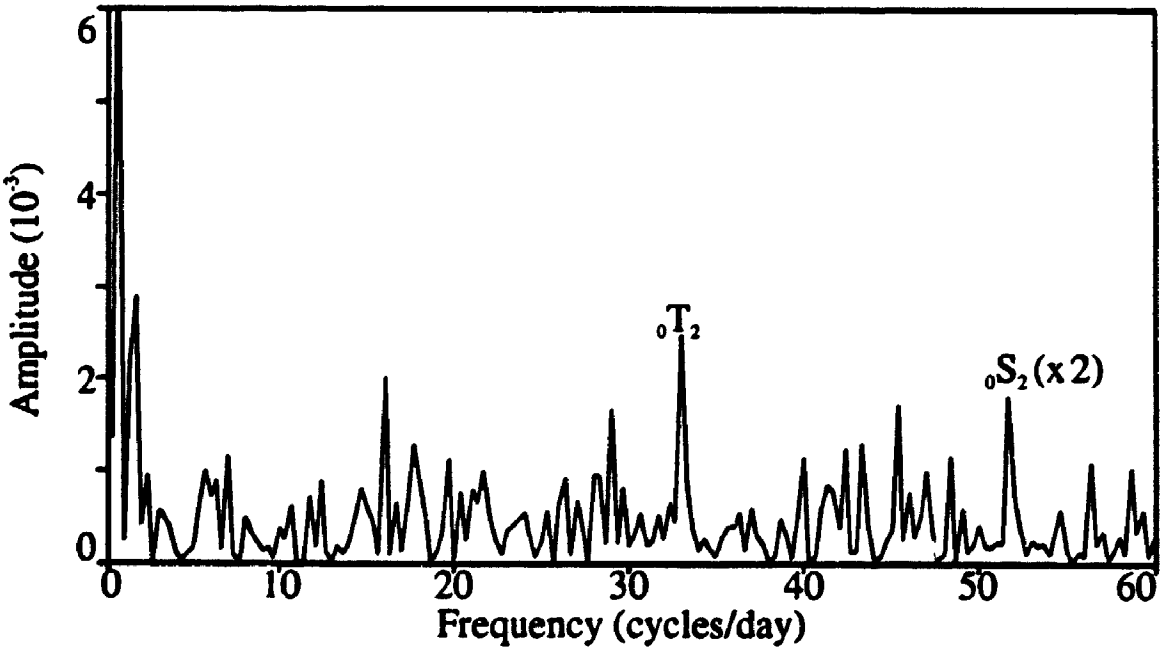

Figure 6.5: Amplitude spectra of 72 hours time series constructed by binning (bin width= 5 minutes) the Loma Prieta aftershock sequence. The beginning of the time series is 48 hours following the mainshock ($1 \leq M_L \leq 2$; 5 ≤depth≤ 15km).

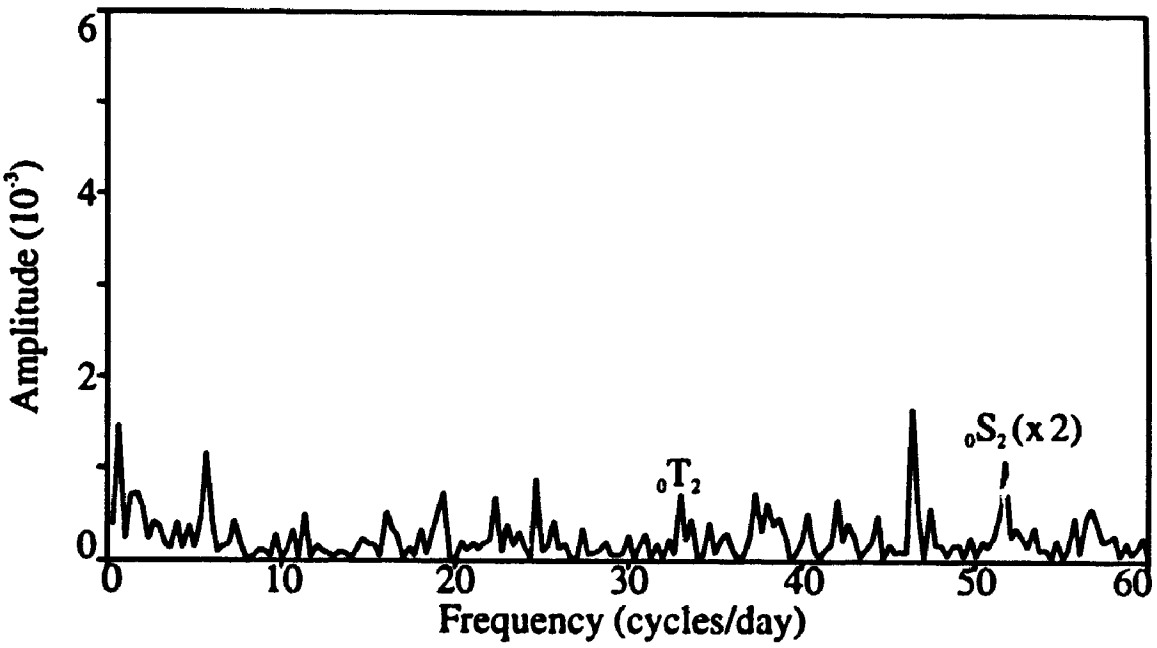

Figure 6.6: Amplitude spectra of 72 hours time series constructed by binning (bin width= 5 minutes) the Loma Prieta aftershock sequence. The beginning of the time series is 144 hours following the mainshock ($1 \leq M_L \leq 2$; $5 \leq$depth≤ 15km).

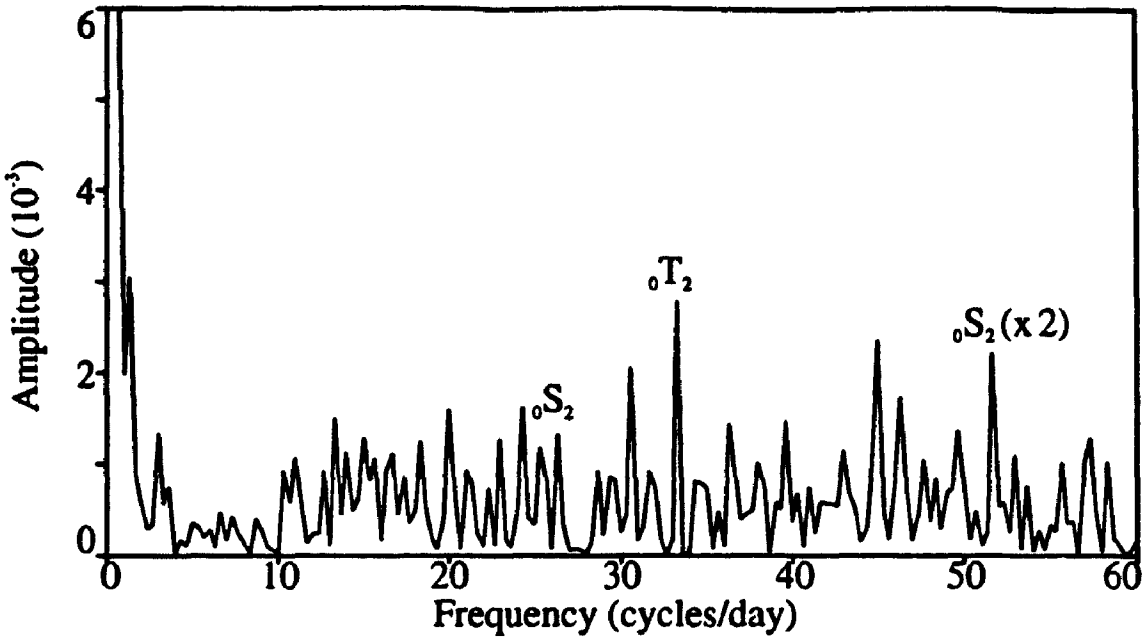

Figure 6.7: Amplitude spectra of 72 hours time series constructed by binning (bin width= 5 minutes) the Loma Prieta aftershock sequence. The beginning of the time series is 24 hours following the mainshock ($1 \leq M_L \leq 2$; 0 ≤depth≤ 10km).

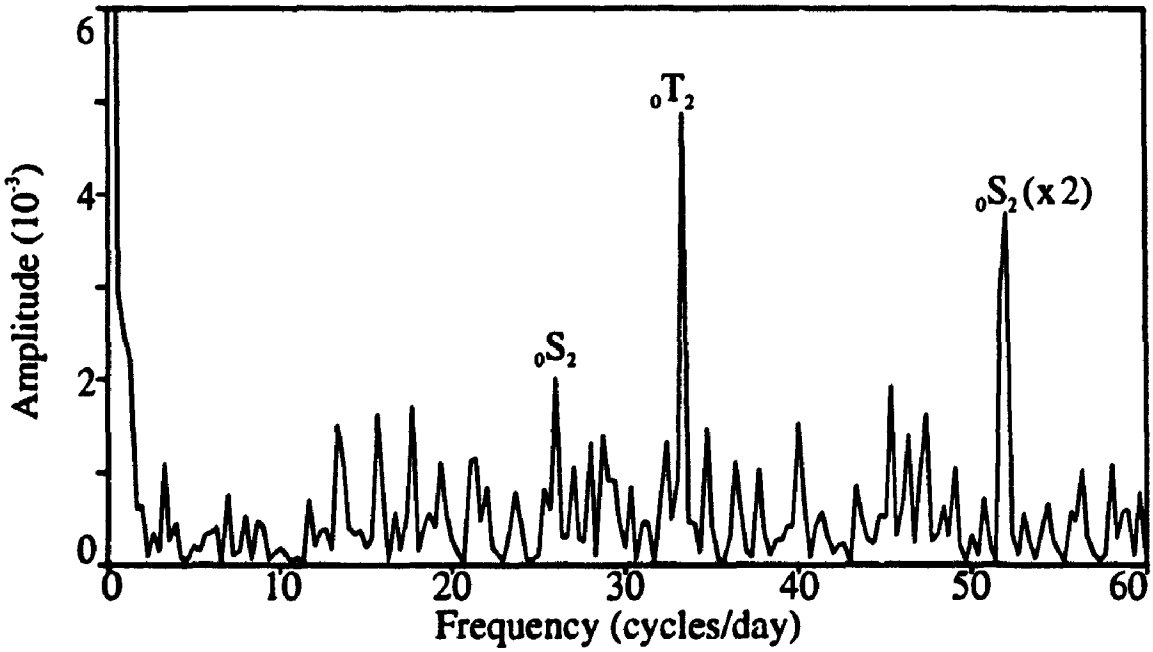

Figure 6.8: Amplitude spectra of 72 hours time series constructed by binning (bin width= 5 minutes) the Loma Prieta aftershock sequence. The beginning of the time series is 24 hours following the mainshock ($1 \leq M_L \leq 2$; 5 ≤depth≤ 15km).

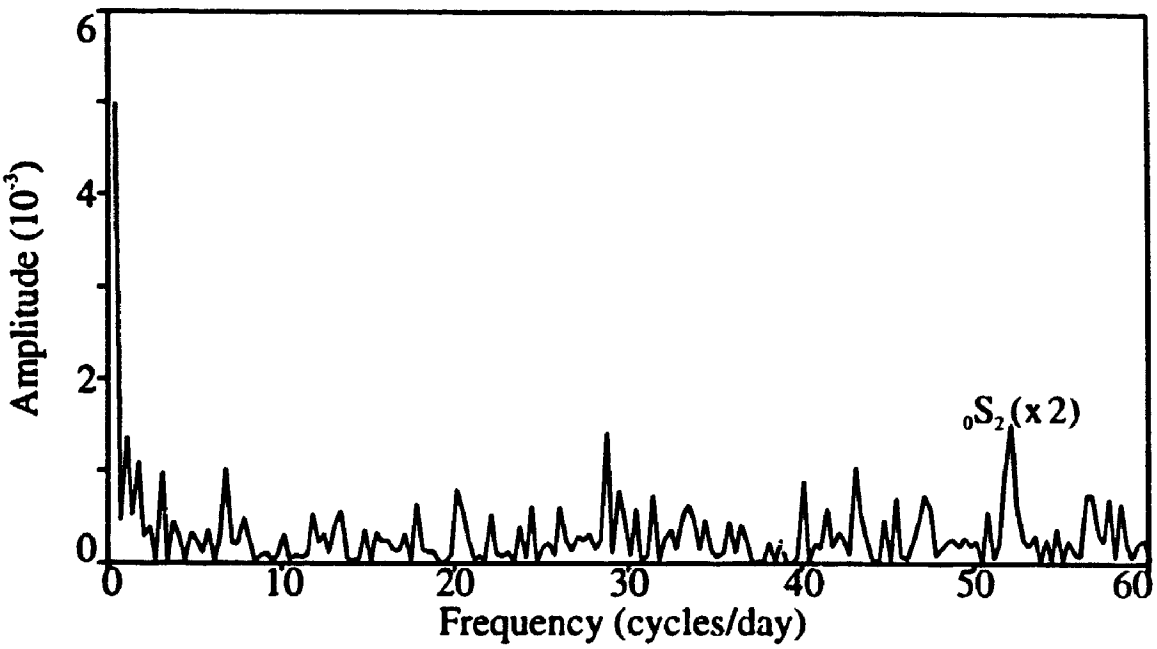

Figure 6.9: Amplitude spectra of 72 hours time series constructed by binning (bin width= 5 minutes) the Loma Prieta aftershock sequence. The beginning of the time series is 24 hours following the mainshock ($1 \leq M_L \leq 2$; $10 \leq$depth≤ 20km).

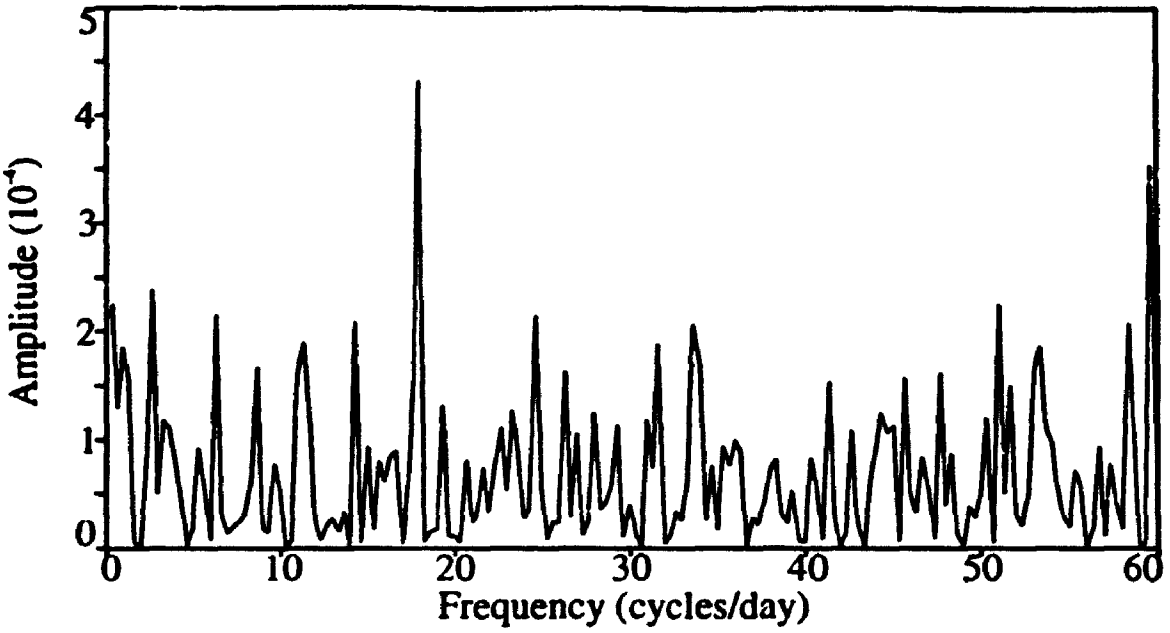

Figure 6.10: Amplitude spectra of 72 hours time series constructed by binning (bin width= 5 minutes) the Loma Prieta aftershock sequence. The beginning of the time series is 24 hours following the mainshock ($2 < M_L \leq 3$; 5 ≤depth≤ 15km).

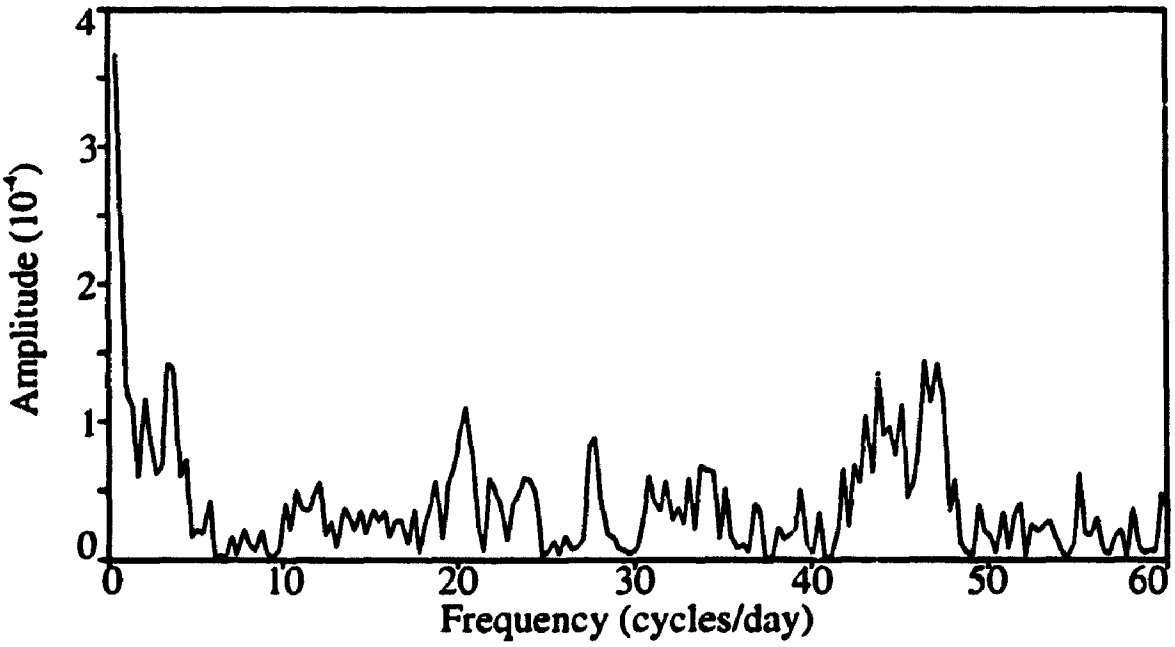

Figure 6.11: Amplitude spectra of 72 hours time series constructed by binning (bin width= 5 minutes) the Loma Prieta aftershock sequence. The beginning of the time series is 24 hours following the mainshock ($3 \leq M_L \leq 5$; 5 ≤depth≤ 15km).

6.3 Phase Variation Curves

Figures 6.12 to 6.16 and 6.21 to 6.25 show phase variation curves for several frequencies near the two normal mode frequencies, obtained by using the time domain method, KORRECT. For comparison with the results from the spectral analysis, 72 hours of data are used and the pulse separations correspond to the Fourier components for the sampling interval (in this case, the width of the rectangular pulse). Most of these phase variation curves show more or less a flat earthquake density around a mean value, indicating that almost the same number of earthquakes occur independent of the phase at these periods. In other words, there are no specific phases of these periods, which advance or inhibit aftershocks in the sequence. However, near the periods corresponding to the two fundamental modes ${}_0T_2$ (Figure 6.14) and ${}_0S_2$ (Figure 6.23), there are systematic variations in the phase plots. This indicates distinct physical mechanism of triggering at these periods, which will be discussed next.

6.3.1 Toroidal Mode ${}_0T_2$

At the period of ${}_0T_2$, the phase plot (Figure 6.14) shows a systematic cyclic behavior in the aftershock density with a distinct minimum (inhibition) and a maximum (advancement). These are separated by about 180° in phase. A plausible physical mechanism behind this triggering is shown in Figure 6.17. In the toroidal mode ${}_0T_2$, the earth is divided into two contra oscillating hemispheres separated by a nodal plane containing the focal region, with the newly opened fault surface. The stresses associated with this free oscillation mode are amplified by virtue of the sharp edge at the periphery of the newly opened fault surface. When the sense of the free oscillation is antiparallel to the original first motion, inhibition of aftershocks occurs. With the sense of oscillation parallel to the first motion, advancement of the aftershock onset times takes place.

Figures 6.18, 6.19 and 6.20 show the phase variation curves for the ${}_0T_2$ period using 72 hour data starting at different times. We note that the triggering effect in form of the cyclic behavior in the phase plots can be seen upto 5 days following

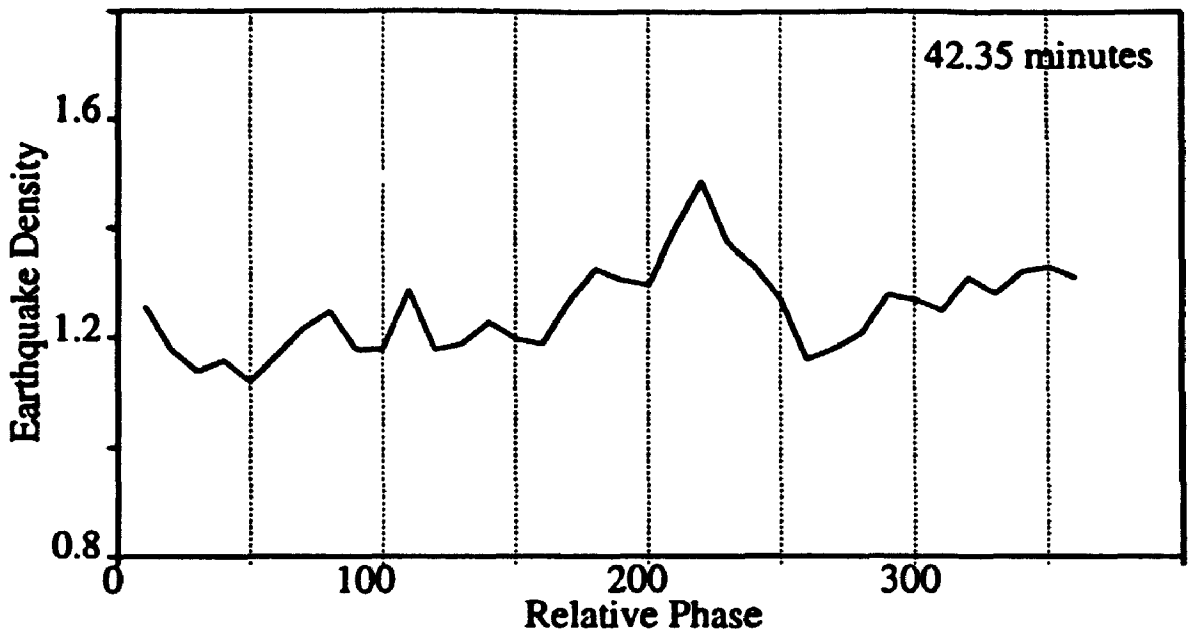

Figure 6.12: Phase variation curve for the 42.35 minute period in the Loma Prieta aftershock sequence, obtained using KORRECT method. There is no systematic behavior in the curve, indicating that almost equal number of aftershocks occur at different phases of this period.

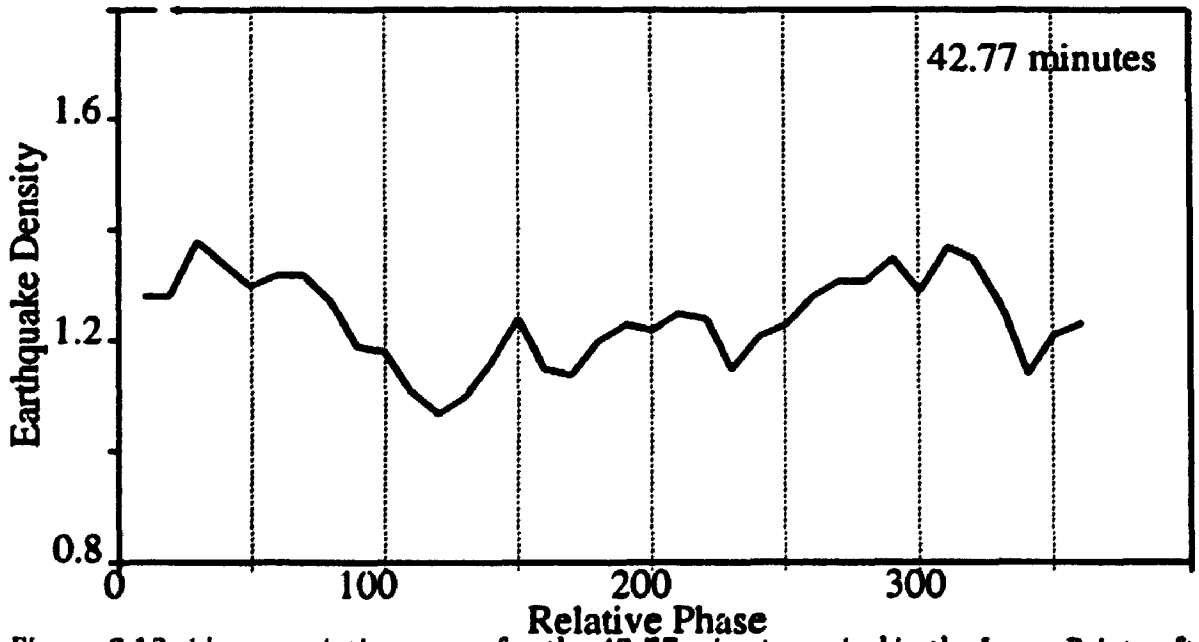

Figure 6.13: Phase variation curve for the 42.77 minute period in the Loma Prieta aftershock sequence, obtained using KORRECT method. There is no systematic behavior in the curve, indicating that almost equal number of aftershocks occur at different phases of this period.

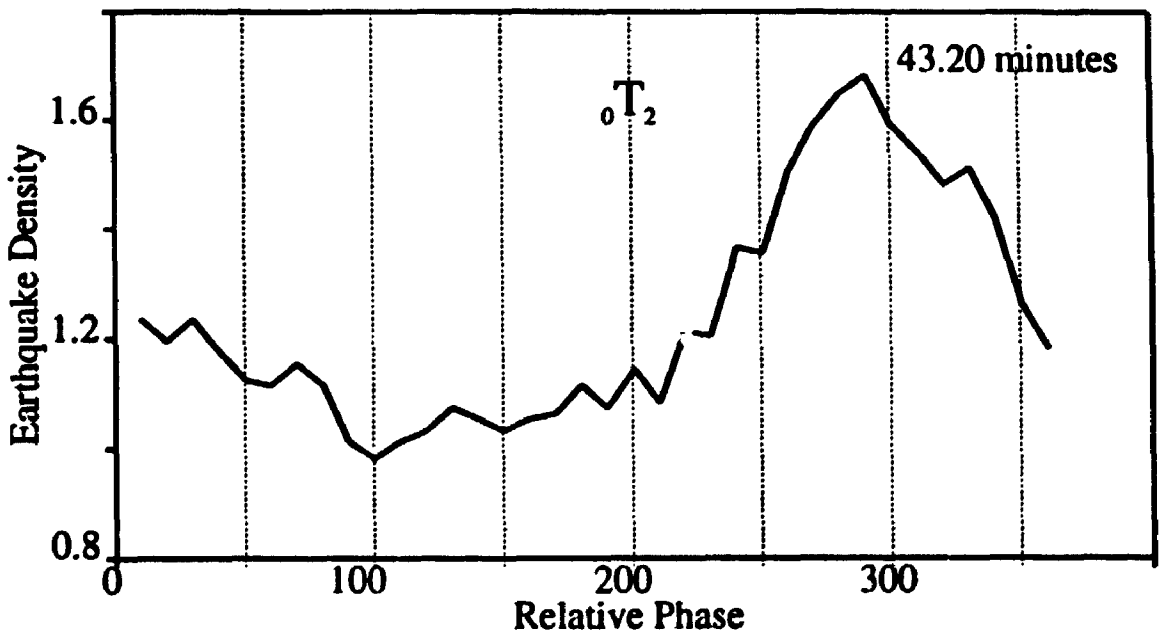

Figure 6.14: Phase variation curve for the 43.2 minute period in the Loma Prieta aftershock sequence, obtained using KORRECT method. Note the systematic variation in the curve. More aftershocks occur at certain phase of this period, while 180° apart in phase one can see a minimum (inhibition).

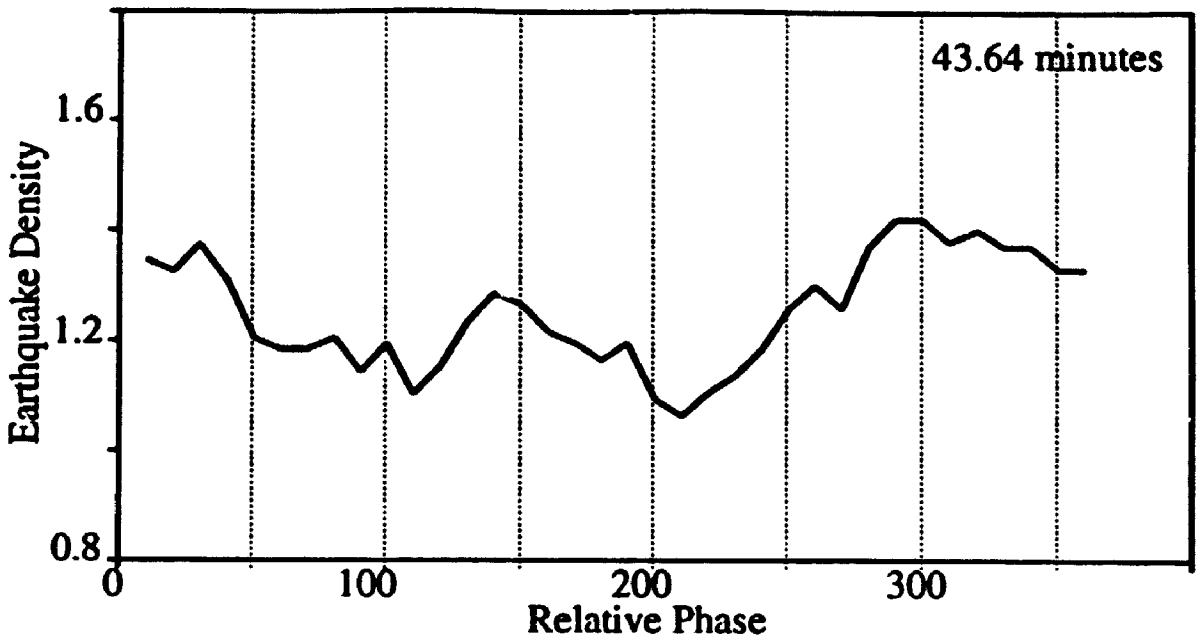

Figure 6.15: Phase variation curve for the 43.64 minute period in the Loma Prieta aftershock sequence, obtained using KORRECT method. There is no systematic behavior in the curve, indicating that almost equal number of aftershocks occur at different phases of this period.

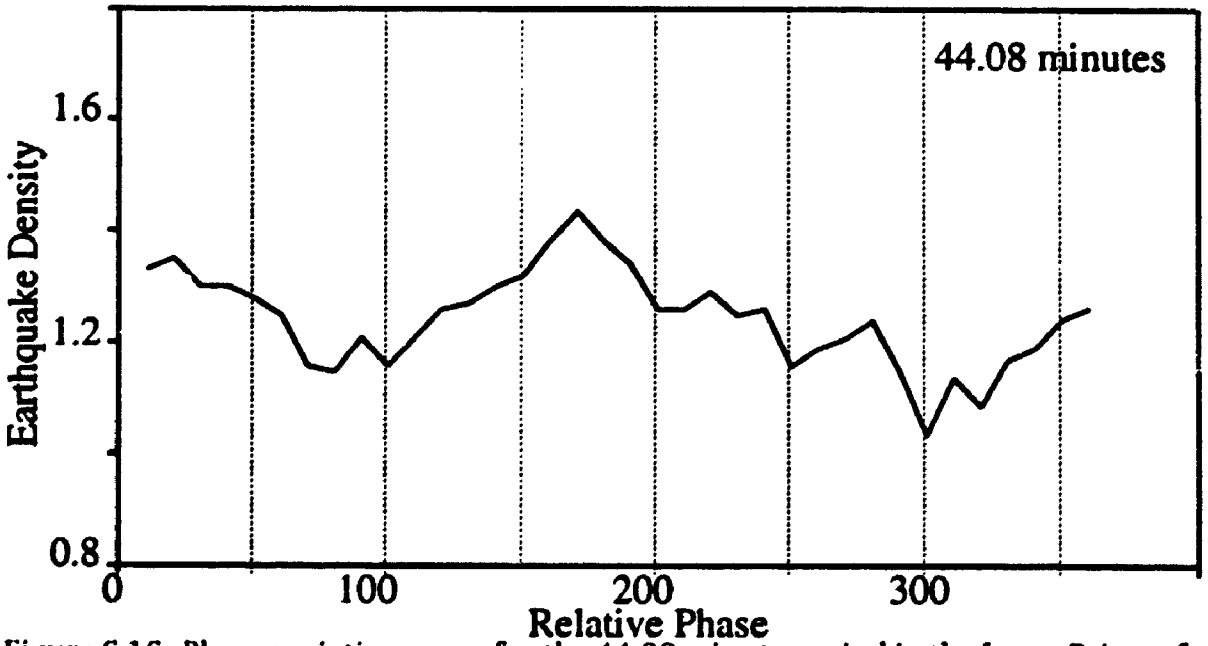

Figure 6.16: Phase variation curve for the 44.08 minute period in the Loma Prieta aftershock sequence, obtained using KORRECT method. There is no systematic behavior in the curve, indicating that almost equal number of aftershocks occur at different phases of this period.

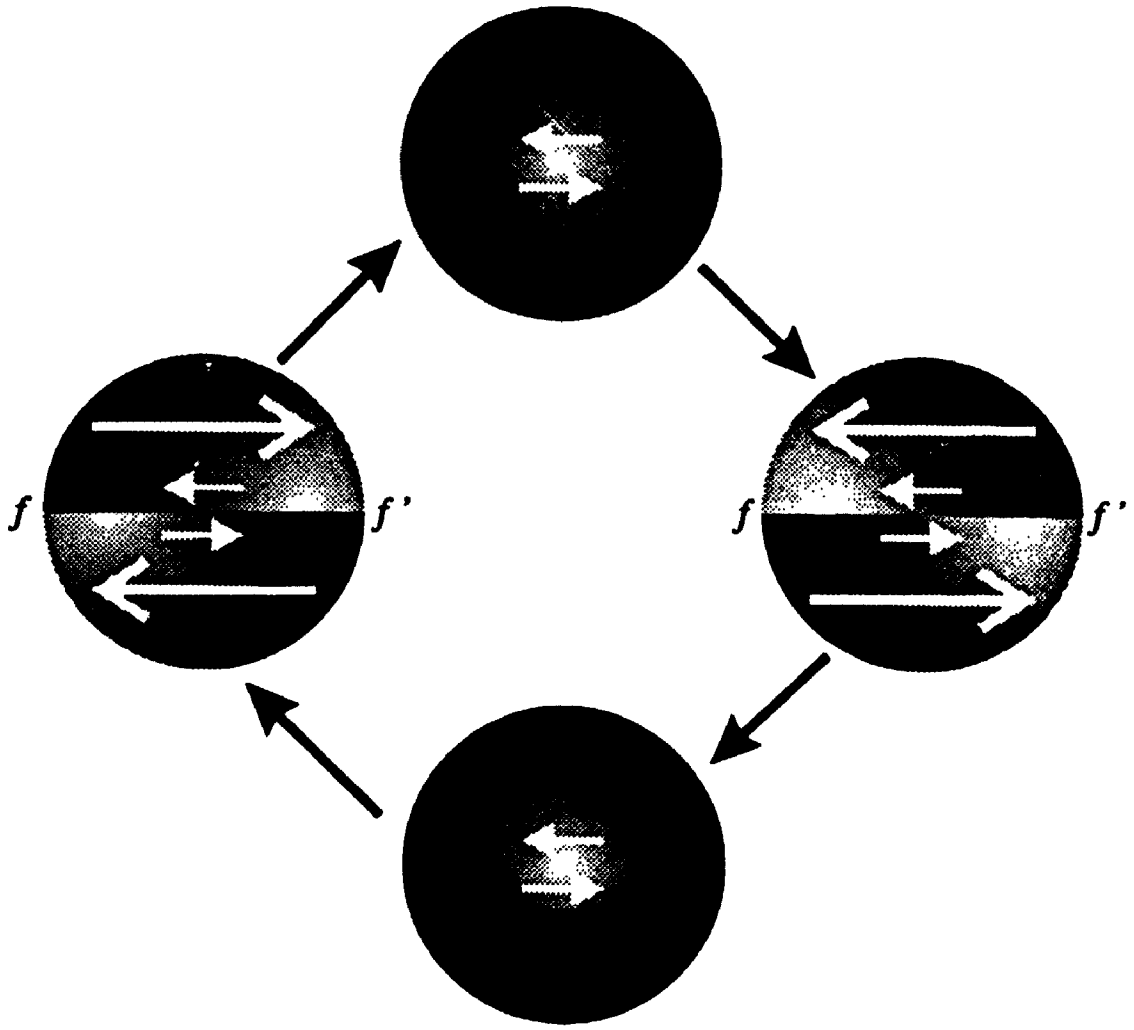

Figure 6.17: The physical mechanism of the triggering due to ${}_0T_2$. Large arrows indicate the sense of motion due to the ${}_0T_2$ mode while the little arrows show the sense of initial slip on the fault plane ff'.

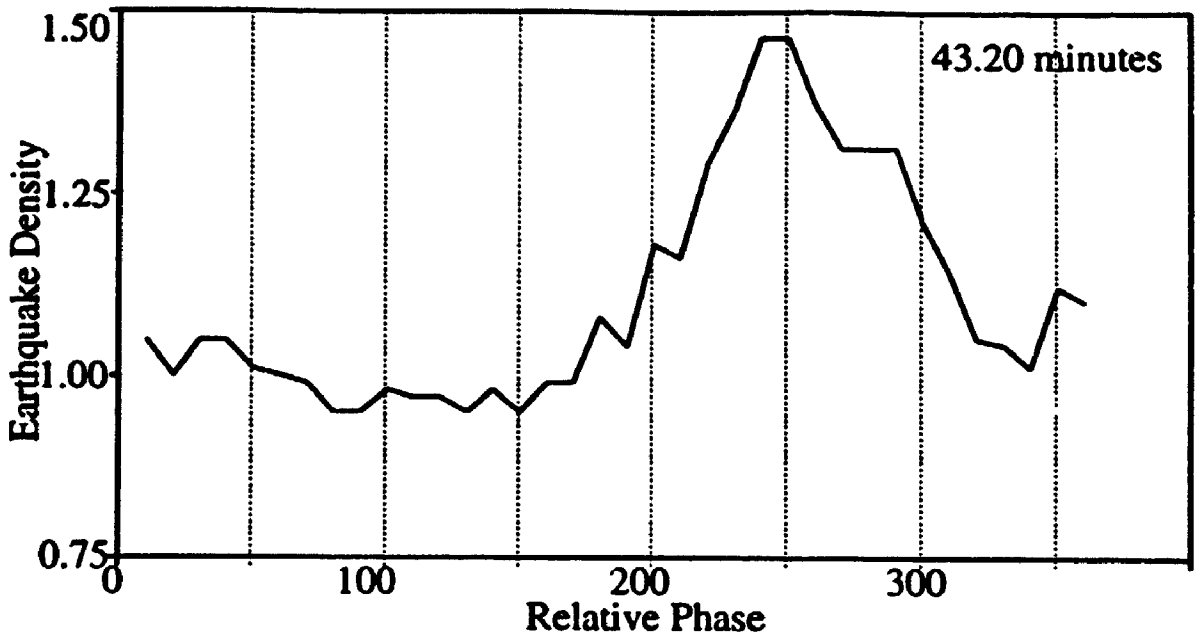

Figure 6.18: Phase variation curve for the period of ${}_0T_2$ (43.2minutes) calculated from the 72 hours of aftershock data starting at 24 hours following the mainshock.

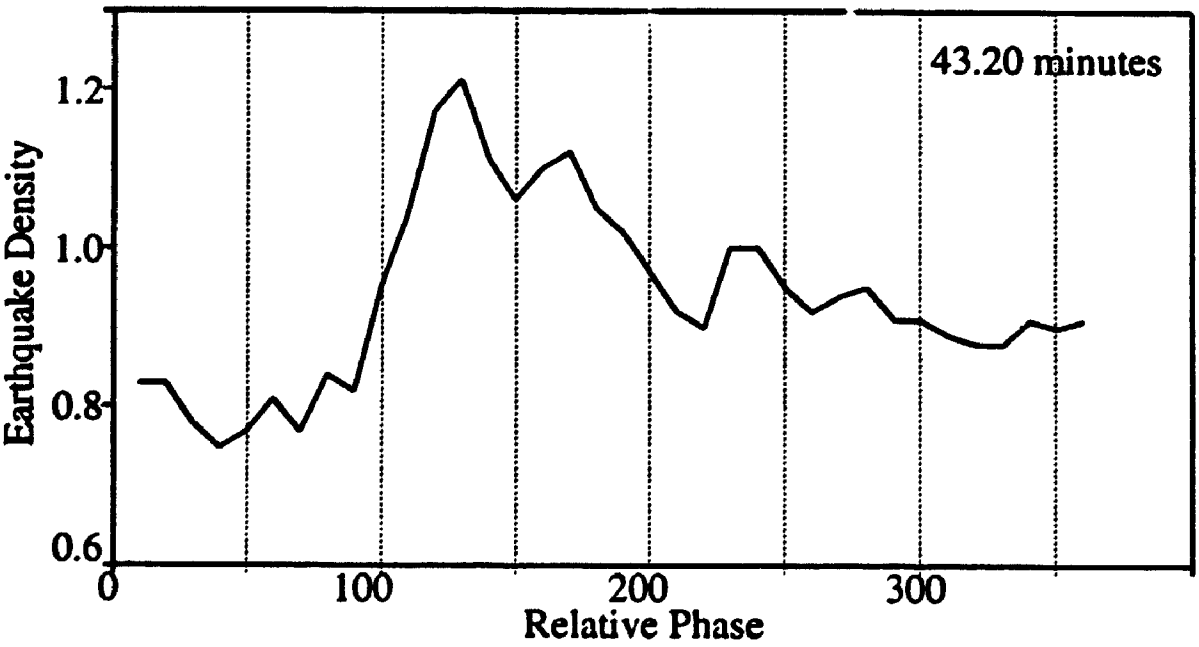

Figure 6.19: Phase variation curve for the period of ${}_0T_2$ (43.2minutes) calculated from the 72 hours of aftershock data starting at 48 hours following the mainshock.

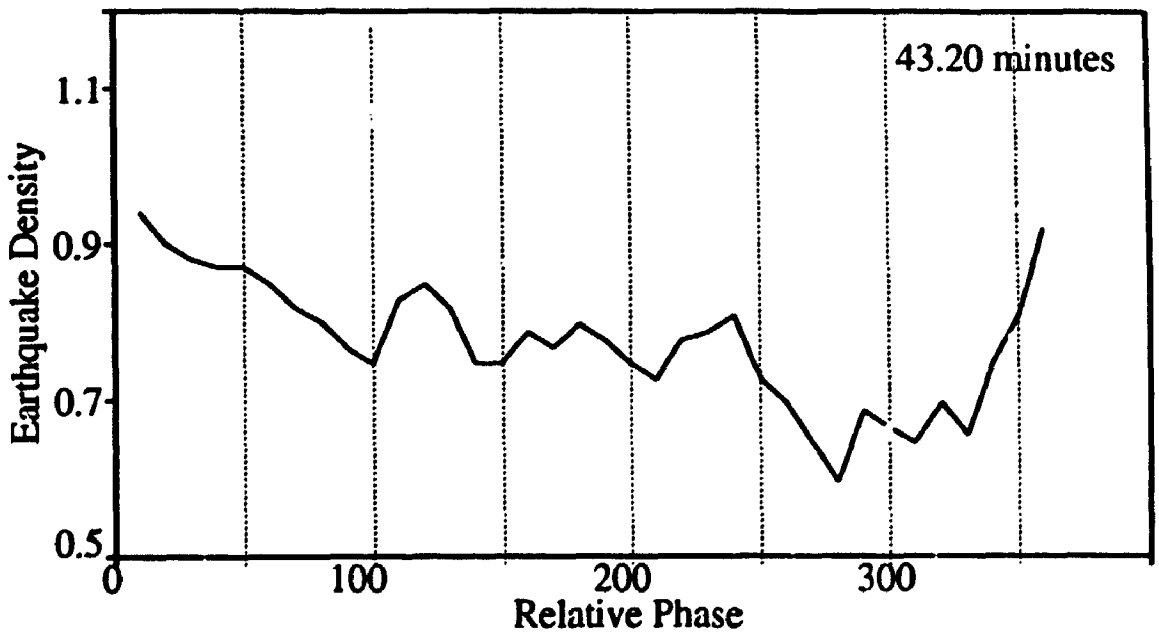

Figure 6.20: Phase variation curve for the period of ${}_0T_2$ (43.2minutes) calculated from the 72 hours of aftershock data starting at 60 hours following the mainshock.

the mainshock. After that, background aftershock activity makes it impossible to see the effect in the phase variation curves.

6.3.2 Spheroidal Mode ${}_0S_2$

At the period of ${}_0S_2$, the second order fundamental spheroidal mode, the phase plot is even more interesting (Figure 6.23). In this case, a cyclic behavior with two local maxima and minima is being observed (each separated by approximately 90° in phase). We speculate on a different triggering mechanism due to ${}_0S_2$ (Figure 6.26). In the football mode (${}_0S_2$) the earth is divided into four quadrants by two nodal planes, one of which contains the focal region. During oscillation, each pair of opposing quadrants undergo tension-compression cyclically, giving rise to two such cycles during each complete oscillation period. During the initial rupture, a number of cracks or zones of weakness of various orientation must have been created in the neighborhood of the fault. During the tension part of the cycle in a quadrant, a number of these small cracks rupture, giving rise to aftershocks. Hence we have two maxima and two minima, one for each quadrantal pair. This also implies that there will be a peak at half the period of ${}_0S_2$, in the spectrum.

The phase variation curves for the ${}_0S_2$ period at different times are shown in Figures 6.27, 6.28 and 6.29. In this case also the triggering effects are visible 120 hours (5 days) after the mainshock.

6.3.3 Spheroidal Mode ${}_0S_3$

The next largest period in the fundamental normal mode spectrum correspond to the spheroidal mode ${}_0S_3$ (period 36.00 minutes or 40 cycles/day). We examined the spectra of binned series for the ${}_0S_3$ mode. In Figure 6.4, a peak at this period is visible slightly above the background noise level. However, the phase plot from the KORRECT method (Figure 6.30) does not indicate any preferential triggering effect at any phase of the corresponding period. Therefore, the triggering due to ${}_0S_3$ mode cannot be conclusively identified.

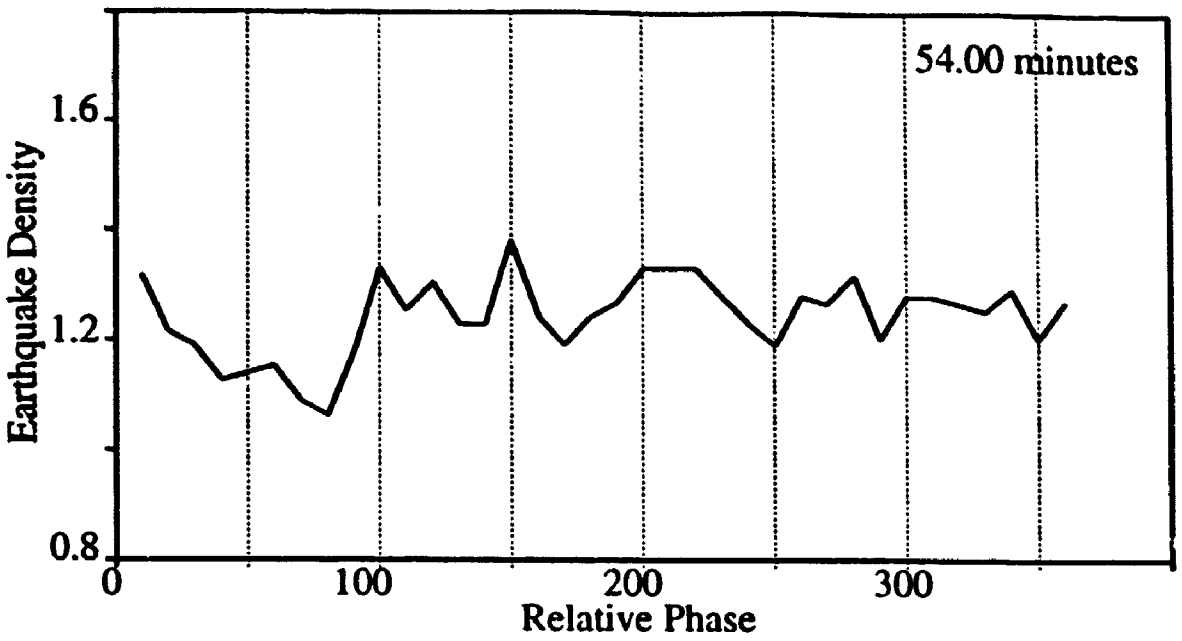

Figure 6.21: Phase variation curve for the 54.00 minute period in the Loma Prieta aftershock sequence, obtained using KORRECT method. There is no systematic behavior in the curve, indicating that almost equal number of aftershocks occur at different phases of this period.

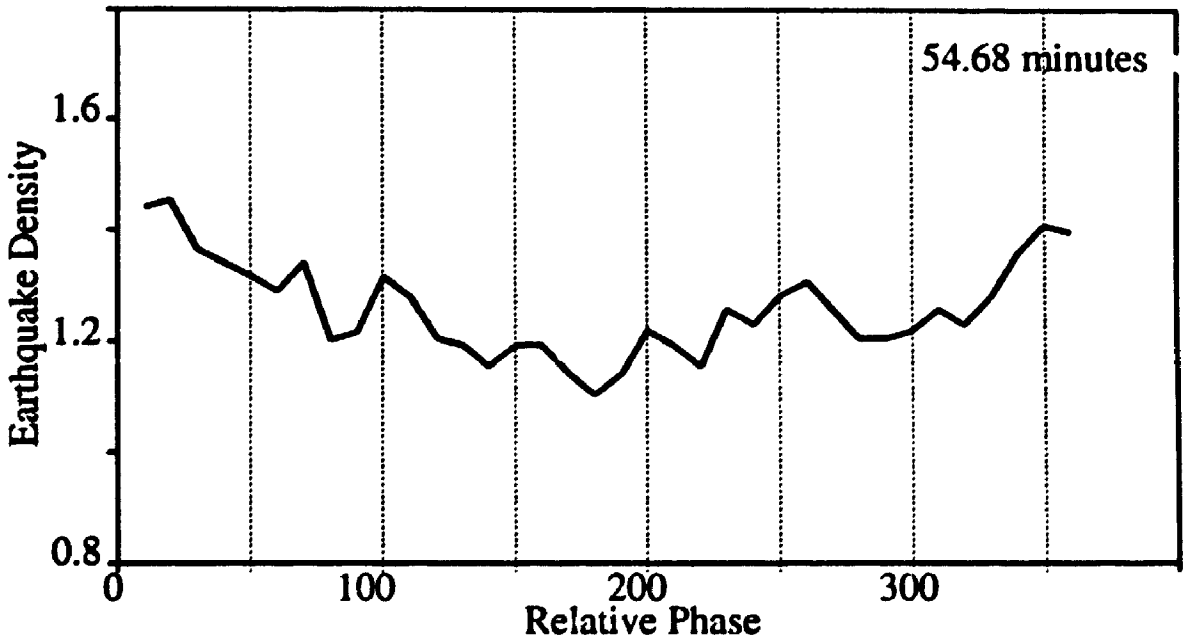

Figure 6.22: Phase variation curve for the 54.68 minute period in the Loma Prieta aftershock sequence, obtained using KORRECT method. There is no systematic behavior in the curve, indicating that almost equal number of aftershocks occur at different phases of this period.

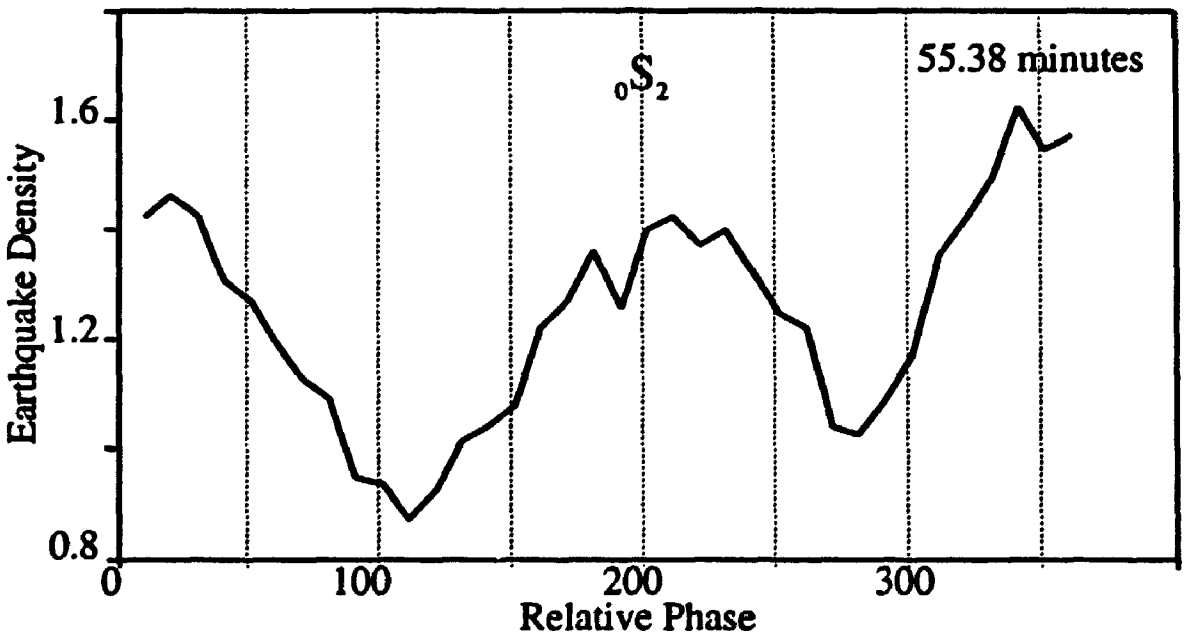

Figure 6.23: Phase variation curve for the 55.38 minute period in the Loma Prieta aftershock sequence, obtained using KORRECT method. Note the systematic variation in the curve. More aftershocks occur at two phases of this period, while one can see minima (inhibition) 90° apart in phase.

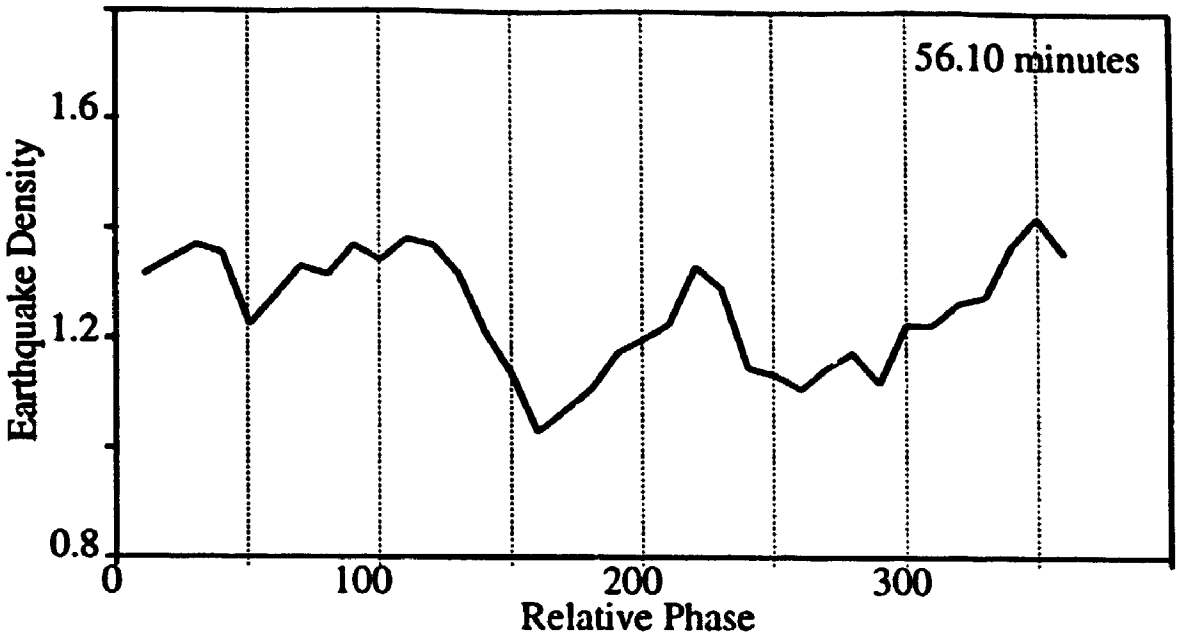

Figure 6.24: Phase variation curve for the 56.10 minute period in the Loma Prieta aftershock sequence, obtained using KORRECT method. There is no systematic behavior in the curve, indicating that almost equal number of aftershocks occur at different phases of this period.

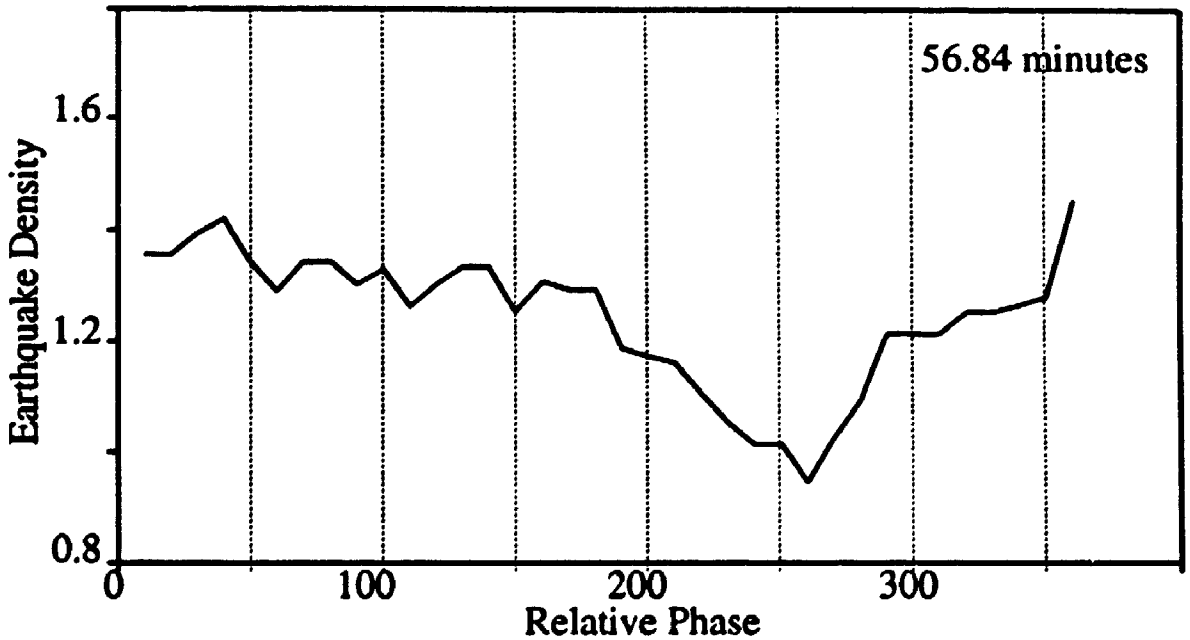

Figure 6.25: Phase variation curve for the 56.84 minute period in the Loma Prieta aftershock sequence, obtained using KORRECT method. There is no systematic behavior in the curve, indicating that almost equal number of aftershocks occur at different phases of this period.

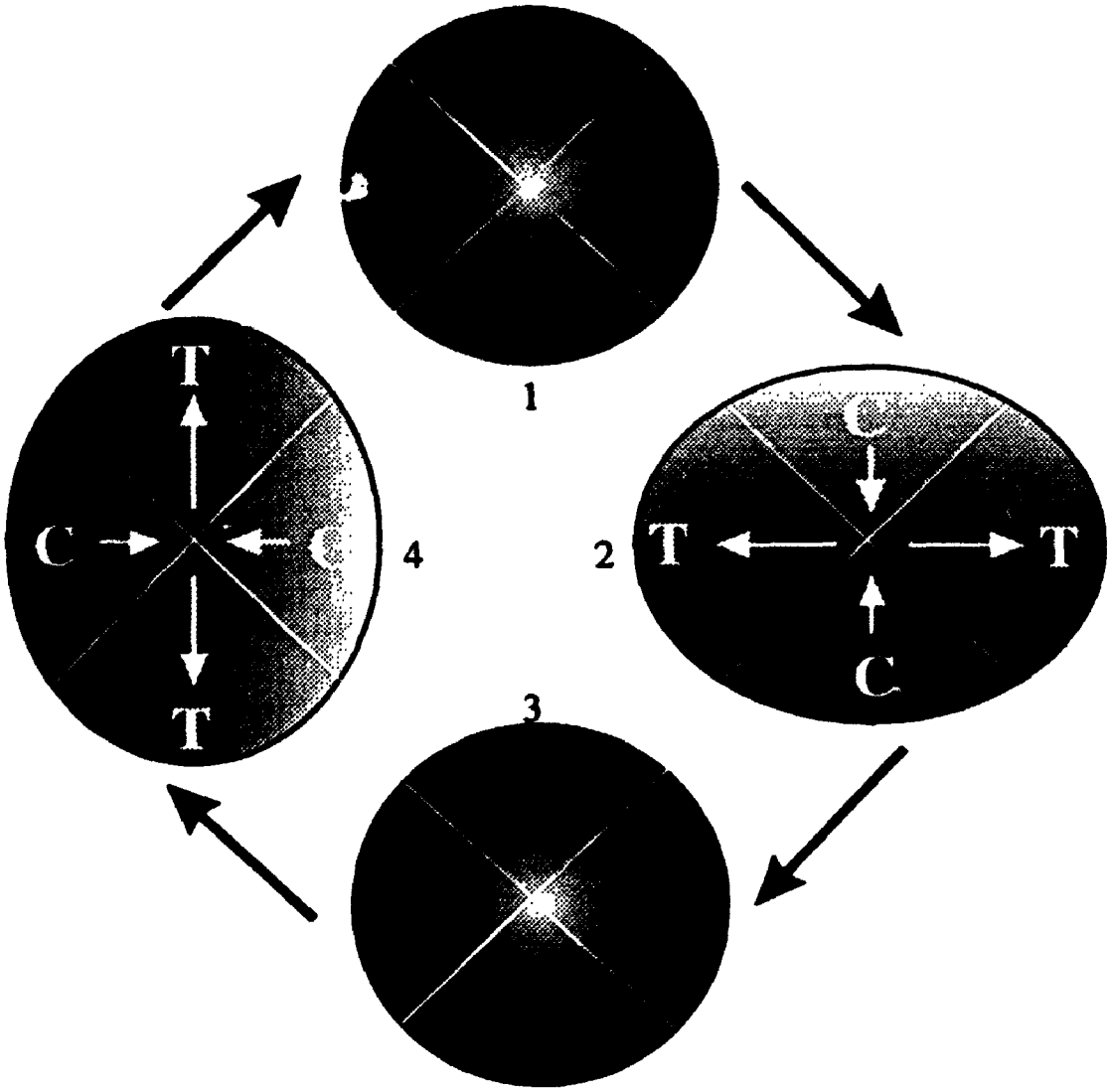

Spheroidal Mode $_0S_2$

Figure 6.26: The physical mechanism due to $_0S_2$ for the triggering effect. Aftershocks are triggered on those faults or cracks, which are perpendicular to the tension axis. During one cycle of $_0S_2$, two particular phases (2 and 4, 180° apart) are responsible for triggering.

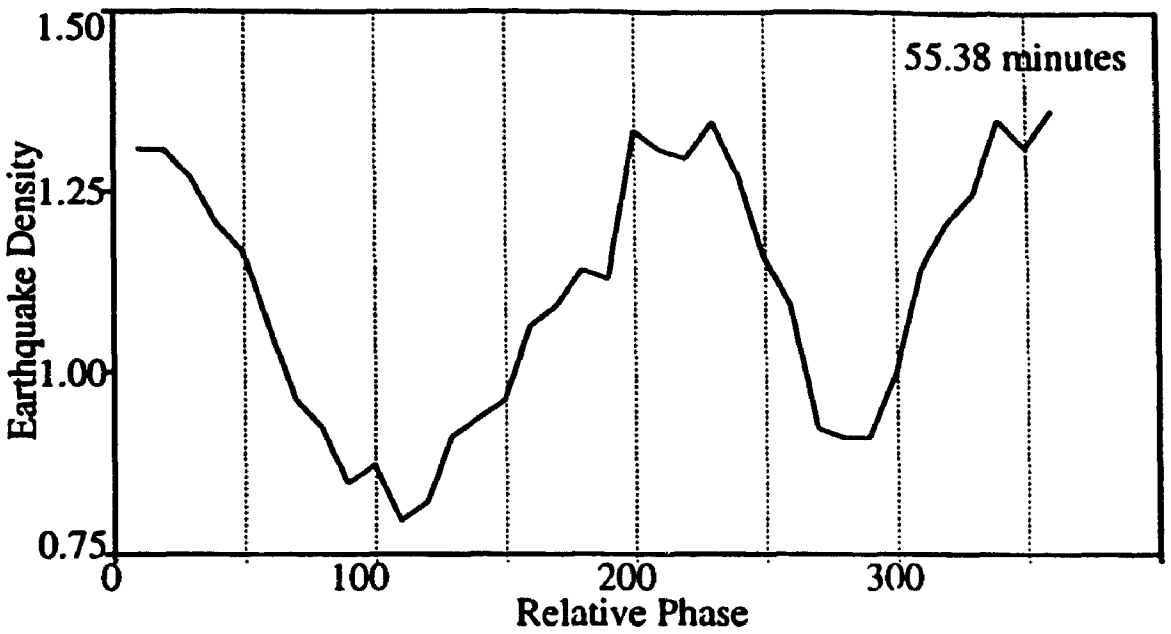

Figure 6.27: Phase variation curve for the period of ${}_0S_2$ (55.38 minutes) calculated from the 72 hours of aftershock data starting at 24 hours following the mainshock.

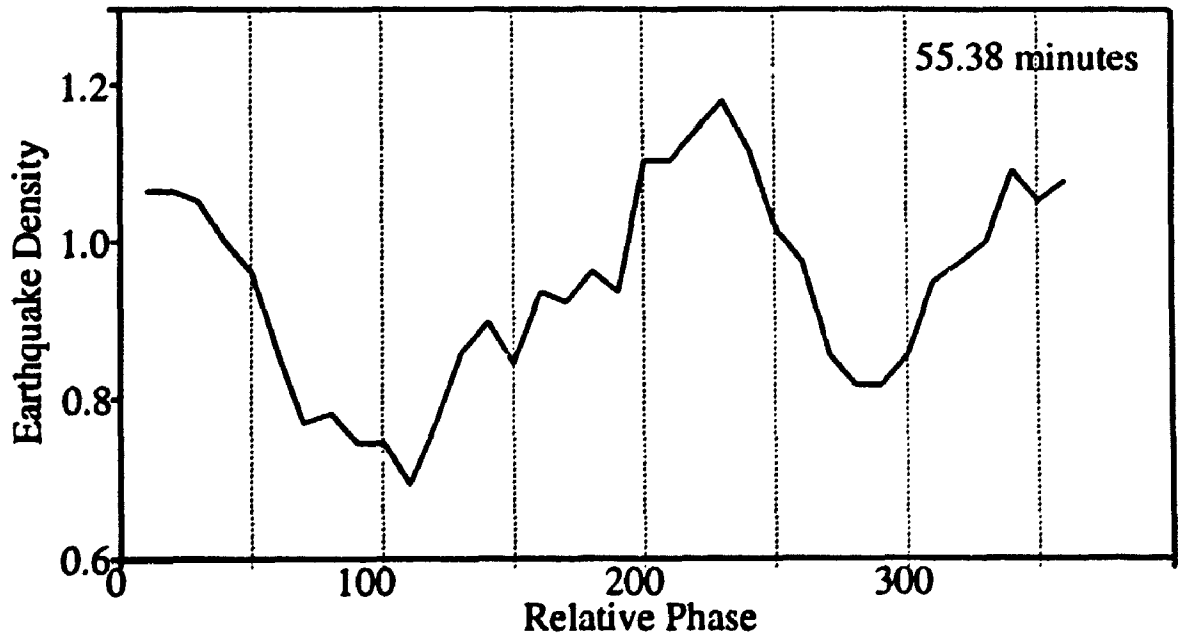

Figure 6.28: Phase variation curve for the period of ${}_0S_2$ (55.38 minutes) calculated from the 72 hours of aftershock data starting at 48 hours following the mainshock.

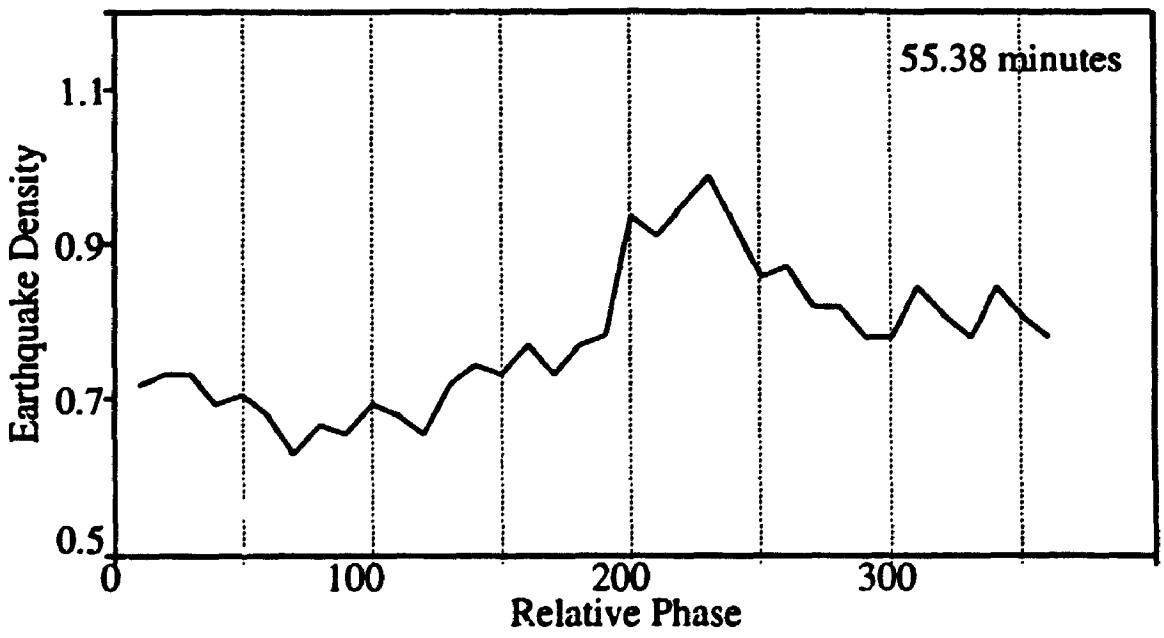

Figure 6.29: Phase variation curve for the period of ${}_0S_2$ (55.38 minutes) calculated from the 72 hours of aftershock data starting at 60 hours following the mainshock.

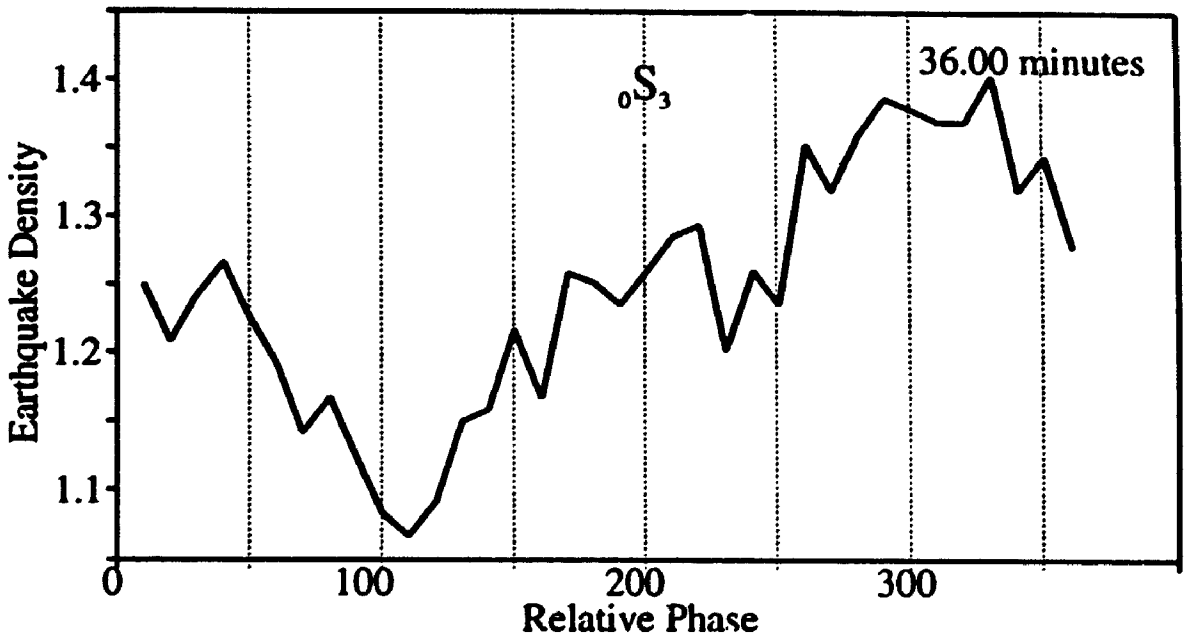

Figure 6.30: Phase variation curve for the 36 minute period (40 cycles/day), which corresponds to $_0S_3$ mode. The curve is computed using 72 hours of data starting at 24 hours following the mainshock. The curve does not show conclusive indication of the triggering.

6.4 Number of Triggered Shocks

KORRECT method also provides an estimate of the numbers of earthquakes that are either advanced or inhibited by the modes. The results show that about 5-10% of the aftershocks during the 144 hours (6 days) following the Loma Prieta mainshock were triggered by the modes ${}_0T_2$ and ${}_0S_2$. Spatially, these triggered aftershocks (Figure 6.31) lie along the periphery of the fault zone (non triggered shocks also tend to confine along the edges).

6.5 Results from the Global Aftershocks

The strong evidence of modal triggering in the Loma Prieta aftershock sequence prompted us to search for a similar effect in the global set of aftershocks.

The USGS NEIC catalogs were analysed for the aftershocks of large earthquakes occurring during 1970-1990. These aftershocks are in the magnitude range ($3 \leq M_L < 7$) occuring within 100 km of their initial earthquakes during first 10 days following the mainshocks.

The criterion for a definite identification of modal periodicities is the combination of a high frequency peak in the amplitude spectrum and a meaningful phase variation curve obtained by KORRECT method. The amplitude spectrum (Figure 6.32) of a 120 hour time series (starting at time $t = 0$) formed by binning the global aftershock sequence (bin width = 10 minutes) shows no evidence of the modal periodicities.

We wanted to examine if the timing of the large aftershocks occur at some multiples of the known normal mode periods *i.e.*, ~55 minutes and ~43 minutes. The KORRECT method described in section 5.4 is naturally suited for this purpose. It describes the phase behavior of the time series at a particular period. By studying the phase behavior of some phase variation curves in the vicinity of two modal periods, one can examine the hypothesis of modal triggering as was shown in the case of the Loma Prieta aftershocks.

The KORRECT method with 10 minutes pulse width is used to obtain

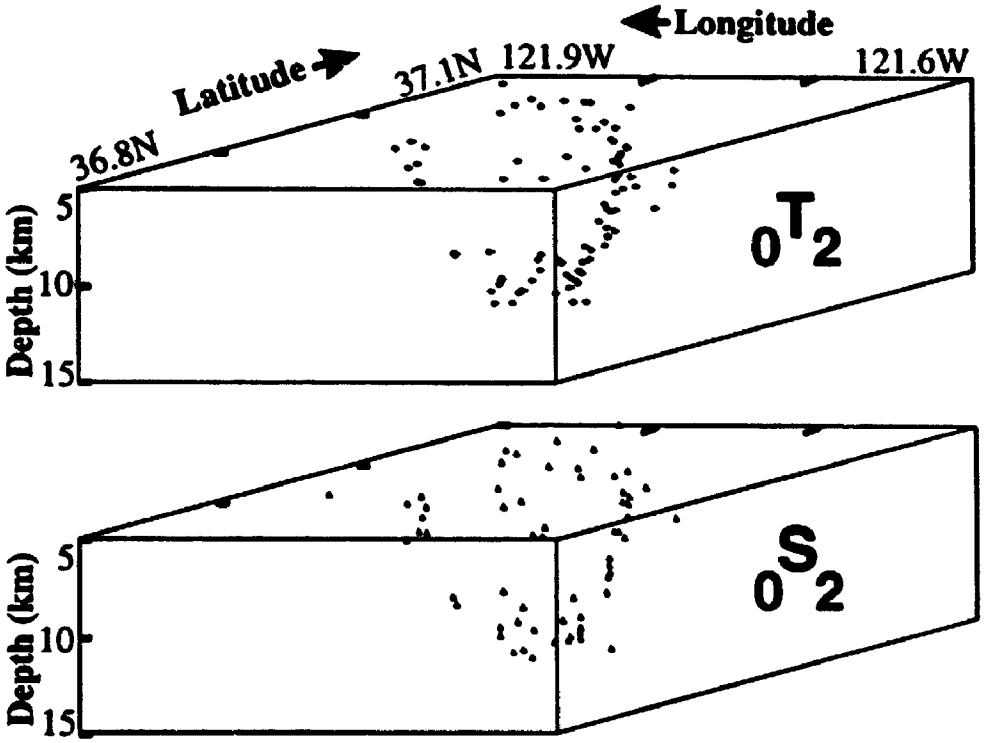

Figure 6.31: Spatial distribution of the triggered aftershocks of the Loma Prieta earthquake. These aftershocks tends to lie along the periphery of the fault zone.

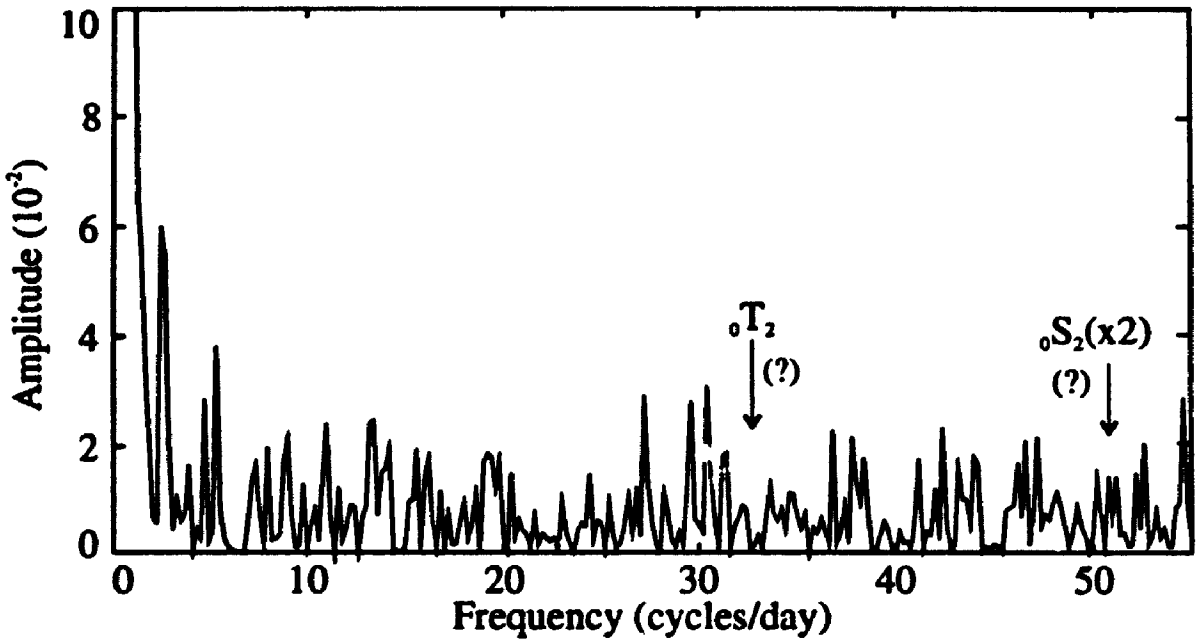

Figure 6.32: Amplitude spectrum of 5 day time series constructed from the Global aftershock sequence using 10 minutes bin size (720 points). There are no significant peaks at modal periods.

phase variation curves. These phase variation curves, corresponding to several frequencies in vicinity of two normal modes ${}_0T_2$ and ${}_0S_2$ are shown in Figures 6.33 and 6.34. These curves do not show strong evidence of the triggering effect as seen in case of the Loma Prieta aftershock sequence. It may seem from figures 6.33(b) and 6.34(c) that distinct maxima and minima exist, but the separation of these extrema do not follow a systematic pattern (as in the case of the Loma Prieta aftershock sequence, the extrema were 90° apart). The little hills and valley visible in the phase plots have little meaning until they are associated with a corresponding high peak in the amplitude spectrum. Modal triggering of large global aftershocks cannot be supported on the basis of phase plots only. The spectrum in Figure 6.32 shows a peak at 2.6 cycles/day, but this frequency does not correspond to any known physical process.

In the case of the Loma Prieta aftershock sequence, we observed that the triggering effects are important only for small aftershocks ($1 \leq M_L < 2$). Larger aftershocks do not show the modal triggering phenomenon (See Figures 6.10 and 6.11). Similarly, globally distributed large aftershocks also seem to be self triggered.

6.6 Concluding Remarks

We have shown that two free oscillation n · ·des ${}_0S_2$ and ${}_0T_2$ excited by the Loma Prieta earthquake influence the occurrence times of its aftershocks during the first 6 days. These results are valid for the low magnitude ($1 \leq M_L < 2$) aftershocks. In terms of actual numbers, about 5-10% of the small aftershocks are influenced by these two normal modes. Large aftershocks for the global earthquake data set, on the other hand, do not show any influence of the normal modes, neither in the Loma Prieta sequence nor in global aftershock data set. However, it should be noted that the number of events decreases remarkably as one considers larger magnitude aftershocks. It is possible that the triggering effects are not detectable for larger events due to the lack of number of events. No evidence was found to support solid earth tidal triggering.

Complete aftershock sequence catalogs that include all the low magnitude events are not common. The Loma Prieta aftershock sequence is the first, and perhaps the only such data set in existence. Even this catalog is incomplete for the

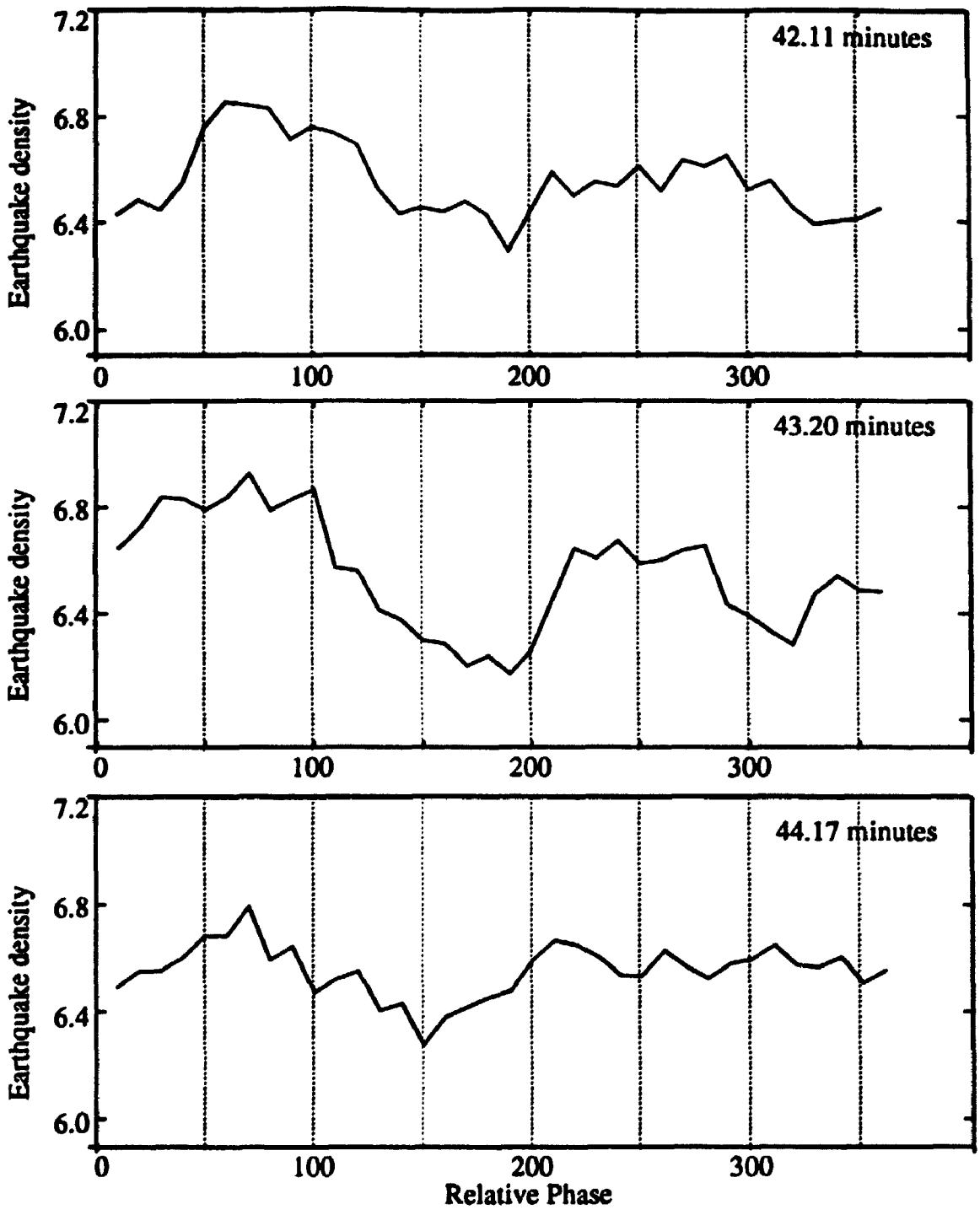

Figure 6.33: Phase variation curves obtained by KORRECT method for the global aftershock data set. These are the curves for the periods in the near vicinity of the ${}_0T_2$ mode.

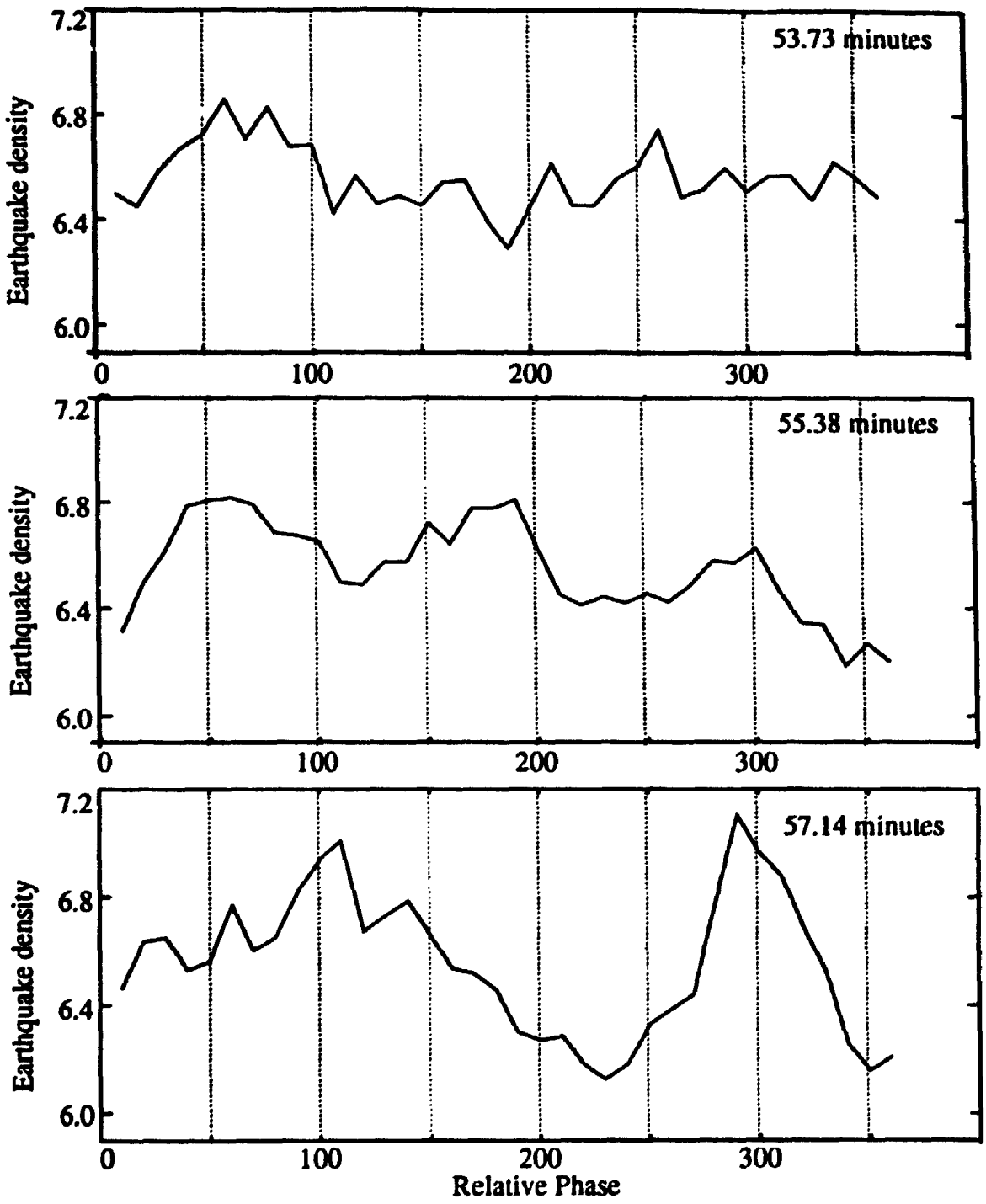

Figure 6.34: Phase variation curves obtained by KORRECT method for the global aftershock data set. These are the curves for the periods in the near vicinity of the ${}_0S_2$ mode.

events of magnitude $M_L < 1$. Hence, these small events could not be included in the analysis.

The results presented here also indicate that the response of the fault surface to the normal modes excited by the mainshock has not been completely understood and rethinking of certain assumptions in the near field calculations is needed. It is not inconceivable, in the vicinity of the hypocenter, that the freshly opened fault surface responds to some well excited modes and results in either the amplification of the modal amplitudes or a change in the seismic activity or both. In routine calculations of the modal amplitudes, the presence of this free surface is ignored. This assumption is not valid in the immediate vicinity of the fault surface.

Evidence from other studies

1. Recently, in a study of TERRAscope data, anomalously high amplitudes of normal modes have been observed in the near vicinity of the epicenter of the Landers earthquake (Kanamori *et al*,1992). Figure 6.35 compares theoretical and observed spectra of normal modes from the seismograms recorded at three different stations (Watada *et al*,1993). Note that at the station PAS (epicentral distance $\Delta = 1.4°$), the modes show very high amplitudes than theoretically expected (dotted curves). These anomalies are partially explained by Watada *et al* (1993) as the effect of the rotation of the earth and lower mantle heterogeneity. This is a intriguing observation and may be due to the modal amplification because of the freshly opened fault surface. Whatever the cause is, its effect may be reflected in the form of a triggering of small events in the aftershock sequence.

2. The Landers earthquake (June 28, 1992; $M_S = 7.3$) triggered a widespread increase in earthquake activity throughout the western United States (Hill *et al*, 1993) as far as 1250 km from the epicenter of the mainshock. Hill *et al* (1993) speculated that static stresses due to the low period Love and Rayleigh waves (1-2 orders of magnitude less than the tidal stress) triggered earthquakes ($1.7 \leq$ magnitude ≤ 4.4) on favorably oriented faults, in areas further from the

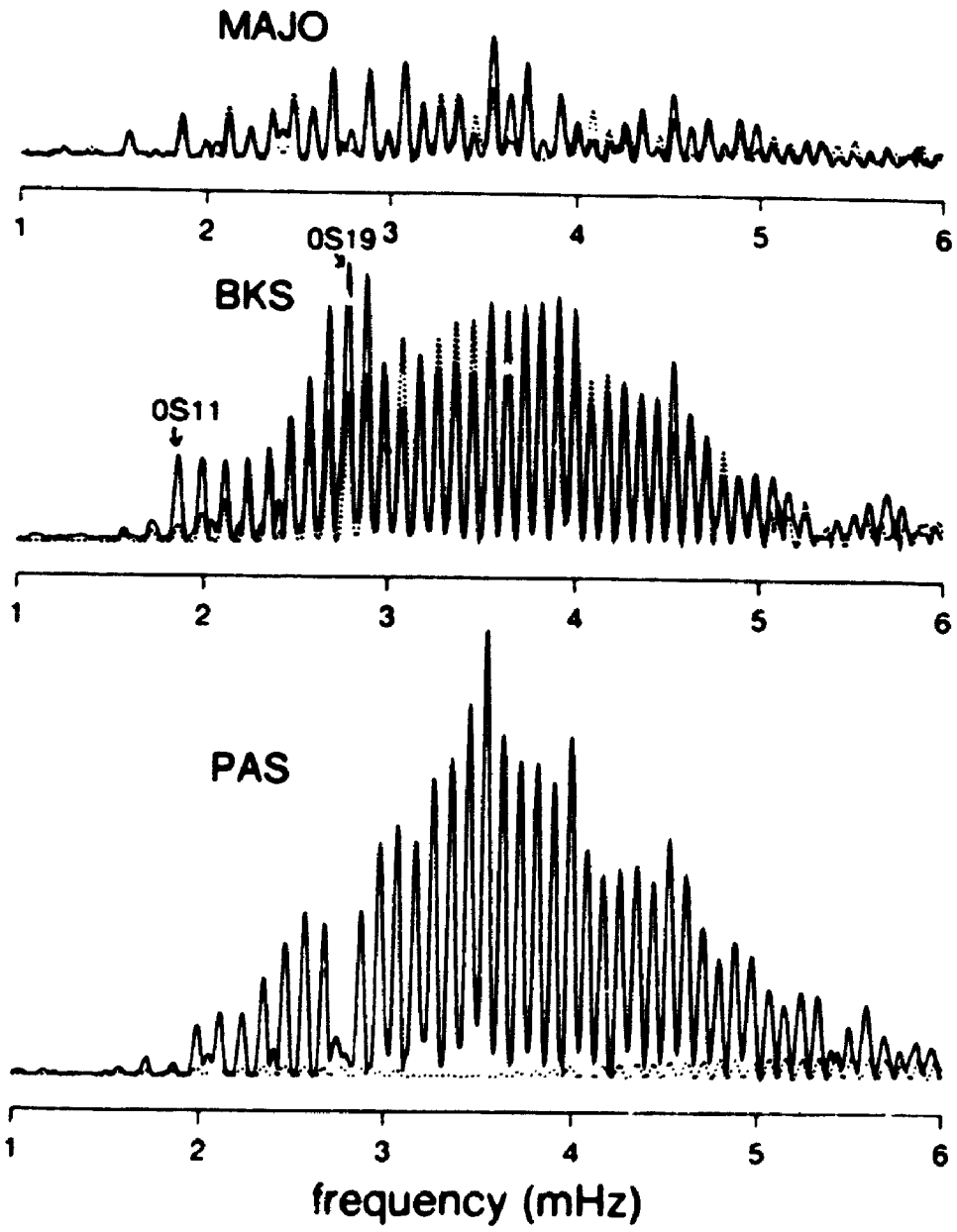

Figure 6.35: The Fourier spectra of Hanning tapered VLP vertical channel records (solid line) after Landers earthquake and spherical earth synthetic seismograms (dashed line) at MAJO (Δ = 81°), BKS (Δ = 6°) and PAS (Δ = 1.4°)[after Watada *et al* (1993)].

epicenter of the mainshock (as far as 17 times greater than the fault length). This study strongly suggests that the stresses due to the normal modes may also be able to trigger small aftershocks.

Epilogue
(Discussion and Conclusions)

The woods are lovely, dark, and deep,
But I have promises to keep,
And miles to go before I sleep,
And miles to go before I sleep.

Robert Frost, *Stopping by the Woods on a Snowy Evening.*

Motivation

In 1989, the Canadian superconducting gravimeter (SG) was installed to support the theoretical investigations of long period behavior of the earth's fluid outer core and to analyse the gravity tides with high accuracy. In an earlier study, we used the SG as a long period seismometer and determined parameters of normal modes from the April 18, 1990, Minahasa Peninsula earthquake (Kamal & Mansinha, 1992) using the STFT method. During the analysis of SG records, two important things were noted:

- The STFT method should not be the method of choice for the determination of normal mode parameters because of some inherent difficulties (Part I) in amplitude estimation.
- Earthquake occurrences at almost regular intervals were noted in some of the SG recordings. This prompted us to do a search for triggering of earthquakes

(Part II).

Results

In the first part of this dissertation, we demonstrated the superiority of the modal fitting over the STFT method. Even for a signal-to-noise ratio as low as 1.3, the modal fitting provides much more accurate (error upto 10%) values of the parameters than those obtained by the STFT method (error upto 500%). Also, the length of the time series required in the modal fitting is at least 4.5 times less than that in STFT method. The method is still in its infancy and application to the real data requires further work.

The amplification of the local displacements caused by the normal modes due to the presence of a freshly opened free surface may trigger aftershocks in the near vicinity of the hypocenter (Part II). The small ($1 \leq M_L \leq 2$) aftershocks of the October 18, 1989 Loma Prieta earthquake show the triggering effect due to two fundamental normal modes ${}_0S_2$ and ${}_0T_2$ (and probably ${}_0S_3$) during the first 6 days following the mainshock. After 6 days, the decay of the normal modes and the decrease in the number of aftershocks make it difficult to detect such an effect. On the other hand, large ($M_s \geq 3$) aftershocks of earthquakes ($M_s \geq 7$) occurring globally during 1970-1990 do not show such triggering effects conclusively. The triggered seismicity by small static stresses ($\sim 10^{-4}$ bar) due to Landers earthquake (Hill *et al*, 1993) also supports the possibility of modal triggering of small aftershocks.

The two modes, which trigger some of the aftershocks in the Loma Prieta earthquake sequence, are the longest period modes and are not commonly observed except for some of the largest earthquakes. Perhaps, the study of aftershock sequences is the only way to study these modes in the vicinity of the epicenter.

Future Work

1. Prior to the application of Marquardt's approach for minimization, one may carry out a Monte Carlo method (computing the merit function at several random points in parameter space) to roughly locate the global minimum. Hope-

fully, it will then be easy to pinpoint the absolute minimum through Marquardt's approach in a smaller region of parameter space.

2. A realistic modelling of split modes is definitely needed for analysing real seismic time series and should be tried. A possible approach would be to narrow band pass filter the time series and fit for all possible split peaks.

3. The background seismic noise also contributes in the poor estimates of the values of the parameters. The results may improve if the seismic noise can be appropriately modelled and filtered out before fitting.

4. The Loma Prieta aftershock sequence was a unique catalog, almost complete for the low magnitude aftershocks. The catalogs of similar quality should be examined in future for the triggering due to normal modes.

5. Quantification of the stresses due to these modes, on and around the fault plane are yet to be carried out. These calculations will enable us to verify our hypothesis of the amplification of the local modal displacements due to the presence of newly opened free surface after the mainshock.

APPENDIX A

U.S. GEOLOGICAL SURVEY
GLOBAL HYPOCENTER DATA BASE CD-ROM

GLOBAL SEARCH

DATE RANGE (Yr:Mo): 1970AD: JAN - 1990AD:DEC

MAGNITUDE RANGE: 7.0 - 9.0

CATALOGS: PDE

YEAR	MO	DA	ORIG-TIME	LAT	LON	DEP	MAGNITUDE
1970	01	04	170040.20	24.14	102.50	31	7.5
1970	01	08	171239.10	-34.74	178.57	179	7.0
1970	01	10	120708.60	6.82	126.74	73	7.3
1970	01	20	071951.20	-25.80	-177.35	80	7.3
1970	03	28	210223.40	39.18	29.49	20	7.3
1970	04	07	053405.60	15.76	121.72	37	7.5
1970	04	12	040144.00	15.06	122.05	24	7.0
1970	04	29	140132.80	14.52	-92.60	33	7.3
1970	05	27	120506.00	27.22	140.12	382	7.1
1970	05	31	202327.30	-9.18	-78.82	43	7.8
1970	06	11	164638.30	-59.11	157.77	33	7.2
1970	06	15	111452.40	-54.34	-63.65	33	7.0
1970	06	24	130908.30	51.75	-131.02	12	7.0
1970	07	25	224110.70	32.18	131.70	34	7.0
1970	07	31	170805.40	-1.46	-72.56	651	7.1
1970	08	11	102220.00	-14.12	166.65	33	7.5
1970	08	30	174609.00	52.38	151.60	645	7.2
1970	10	31	175309.30	-4.93	145.47	42	7.0

1970	12	02	155419.90	-10.97	163.29	33	7.0
1970	12	10	043438.80	-3.99	-80.72	25	7.6
1971	01	03	173540.20	-55.50	-2.58	33	7.1
1971	01	10	071703.70	-3.13	139.70	33	8.1
1971	02	04	153328.60	.65	98.84	33	7.1
1971	02	08	210421.80	-63.45	-61.22	33	7.0
1971	05	02	060827.30	51.43	-177.21	43	7.1
1971	06	17	210040.90	-25.48	-69.15	93	7.0
1971	07	09	030318.70	-32.54	-71.15	58	7.5
1971	07	14	061129.10	-5.47	153.88	47	7.9
1971	07	19	001445.30	-5.69	153.80	42	7.1
1971	07	26	012321.30	-4.94	153.17	48	7.9
1971	07	27	020249.60	-2.75	-77.43	135	7.5
1971	08	02	072456.80	41.38	143.46	51	7.0
1971	08	05	015851.70	- 85	-22.13	33	7.0
1971	09	05	183525.00	46.50	141.17	9	7.1
1971	09	14	052029.30	-6.48	151.52	35	7.1
1971	10	27	175836.90	-15.50	167.22	40	7.1
1971	11	06	220000.10	51.47	179.11	2	7.4
1971	11	21	055711.90	-11.82	166.53	115	7.1
1971	11	24	193529.10	52.90	159.19	106	7.5
1971	12	15	082955.30	56.00	163.29	33	7.8
1972	01	23	211752.10	-13.17	166.38	33	7.1
1972	01	25	020623.30	22.45	122.26	33	7.5
1972	01	25	034123.70	23.03	122.15	33	7.0
1972	02	14	232951.70	-11.36	166.34	102	7.4
1972	02	29	092259.80	33.34	140.78	56	7.2
1972	04	10	020653.20	28.43	52.83	33	7.1
1972	04	24	095721.70	23.64	121.55	33	7.2
1972	04	25	193009.30	13.37	120.31	50	7.3
1972	05	22	204557.30	-1[illegible].69	-175.19	227	7.1

1972	06	11	164100.90	3.94	124.32	325	7.5
1972	07	30	214514.10	56.82	-135.68	25	7.6
1972	08	17	234405.90	-5.96	152.90	10	7.1
1972	11	02	195522.10	-20.05	168.84	32	7.0
1972	12	02	001947.20	6.47	126.60	33	7.4
1972	12	04	101612.00	33.33	140.68	66	7.4
1973	01	30	210112.50	18.48	-103.00	43	7.5
1973	02	06	103710.10	31.40	100.58	33	7.7
1973	02	28	063749.50	50.49	156.58	27	7.2
1973	03	17	083051.80	13.37	122.79	33	7.5
1973	06	17	035502.90	43.23	145.79	48	7.7
1973	06	24	024325.50	43.32	146.44	50	7.1
1973	07	23	012257.80	49.99	78.85	0	7.1
1973	08	28	095040.00	18.27	-96.60	84	7.2
1973	09	29	004400.80	41.89	130.87	575	7.0
1973	10	06	150737.30	-60.82	-21.55	33	7.5
1973	10	27	065957.40	70.78	54.18	0	7.6
1973	12	28	134145.80	-14.46	166.60	26	7.8
1973	12	29	001931.10	-15.12	166.90	47	7.2
1974	01	10	085113.30	-14.43	166.86	34	7.2
1974	01	31	233005.30	-7.46	155.89	34	7.0
1974	02	01	031233.10	-7.38	155.57	40	7.1
1974	07	02	232626.60	-29.08	-175.95	33	7.3
1974	07	13	011822.80	7.75	-77.69	12	7.3
1974	07	30	051240.60	36.35	70.76	211	7.4
1974	08	11	011355.50	39.46	73.83	9	7.3
1974	08	18	104412.80	-38.45	-73.43	36	7.1
1974	10	03	142129.10	-12.27	-77.79	13	7.6
1974	10	08	095058.10	17.30	-62.00	47	7.5
1974	10	16	054509.80	52.64	-32.07	33	7.3
1974	10	23	061454.00	-8.42	154.03	48	7.2

1974	11	09	125949.80	-12.50	-77.79	6	7.2
1974	11	20	041446.90	-15.02	167.14	33	7.0
1975	02	02	084339.10	53.11	173.50	10	7.6
1975	02	04	113607.50	40.64	122.58	33	7.4
1975	05	10	142738.70	-38.18	-73.23	6	7.8
1975	05	26	091151.50	36.00	-17.65	33	8.1
1975	06	10	134714.50	43.02	147.73	15	7.0
1975	07	10	182916.00	6.51	126.64	86	7.0
1975	07	20	143739.90	-6.59	155.05	49	7.9
1975	07	20	195427.70	-7.10	155.15	44	7.7
1975	10	01	032958.90	-4.88	102.20	33	7.0
1975	10	06	222416.20	-12.52	166.50	54	7.0
1975	10	11	143515.00	-24.89	-175.12	9	7.8
1975	10	31	082802.60	12.54	125.99	50	7.6
1975	11	0[illegible]	011733.90	13.84	144.75	113	7.1
1975	11	29	144740.40	19.33	-155.02	5	7.2
1975	12	26	155638.70	-16.26	-172.47	33	7.8
1976	01	14	155634.90	-29.21	-177.89	69	7.8
1976	01	14	164733.50	-28.43	-177.66	33	8.2
1976	01	21	100524.10	44.92	149.12	41	7.0
1976	02	04	090143.40	15.32	-89.10	5	7.5
1976	04	08	024027.00	40.31	63.77	33	7.1
1976	05	17	025840.60	40.38	63.47	10	7.1
1976	05	29	140018.50	24.53	98.71	10	7.0
1976	06	20	205313.40	3.40	96.32	33	7.0
1976	06	25	191856.90	-4.60	140.09	33	7.1
1976	07	11	204147.50	7.41	-78.13	3	7.0
1976	07	27	194254.60	39.57	117.98	23	8.0
1976	07	28	104535.20	39.66	118.40	26	7.4
1976	08	02	105525.70	-20.61	169.27	52	7.0
1976	08	16	161107.30	6.26	124.02	33	7.9

1976	10	29	025107.60	-4.52	139.92	33	7.2
1976	11	24	122218.80	39.12	44.03	36	7.3
1976	11	30	004057.80	-20.52	-68.92	82	7.3
1977	03	04	192154.1[illegible]	45.77	26.76	94	7.2
1977	03	18	214352.40	16.77	122.33	37	7.0
1977	03	21	211854.20	27.61	56.39	29	7.0
1977	04	02	071522.70	-16.70	-172.10	33	7.6
1977	04	20	234250.50	-9.89	160.35	19	7.6
1977	04	20	234913.10	-9.84	160.82	33	7.5
1977	04	21	042409.60	-9.97	160.73	33	8.1
1977	06	22	120833.40	-22.88	-175.90	65	7.2
1977	07	29	111545.30	-8.03	155.54	33	7.2
1977	08	19	060855.20	-11.09	118.46	33	8.0
1977	08	26	195001.40	-59.43	-20.51	33	7.1
1977	10	10	115353.60	-25.86	-175.41	33	7.2
1977	11	23	092624.70	-31.03	-67.77	13	7.4
1978	02	09	213512.70	-30.68	-177.36	33	7.7
1978	03	07	024847.60	32.01	137.61	439	7.0
1978	03	23	031520.30	44.93	148.44	33	7.5
1978	03	24	194750.70	44.24	148.86	33	7.6
1978	03	24	210548.20	42.84	78.61	33	7.1
1978	06	12	081426.40	38.19	142.03	44	7.7
1978	06	17	151133.50	-17.10	-172.26	33	7.2
1978	07	23	144236.90	22.28	121.51	17	7.4
1978	08	03	181117.10	-26.51	-70.54	58	7.0
1978	08	23	003832.20	10.20	-85.22	56	7.2
1978	09	16	153556.60	33.39	57.43	33	7.8
1978	11	05	220207.10	-11.13	162.14	33	7.4
1978	11	29	195247.60	16.01	-96.59	18	7.9
1978	12	06	140201.00	44.59	146.58	91	7.5
1978	12	12	114416.00	7.33	123.49	33	7.4

1978	12	23	112312.00	23.25	122.07	33	7.2
1979	02	28	212706.10	60.64	-141.59	15	7.4
1979	03	14	110716.30	17.81	-101.28	49	7.6
1979	04	10	014222.00	2.96	126.93	37	7.2
1979	04	15	061944.10	42.10	19.21	10	7.3
1979	05	01	130337.10	-21.24	169.80	79	7.2
1979	08	26	143122.10	19.07	122.10	15	7.1
1979	09	12	051751.40	-1.68	136.04	5	7.9
1979	10	12	102522.30	-46.67	165.71	33	7.5
1979	10	15	231654.50	32.63	-115.33	12	7.0
1979	10	23	095106.70	-10.61	161.28	22	7.2
1979	11	16	152125.70	-16.76	-179.98	33	7.0
1979	11	27	171032.90	33.96	59.73	10	7.5
1979	12	12	075903.30	1.60	-79.36	24	7.7
1980	01	01	164240.00	38.81	-27.78	10	7.2
1980	02	23	055103.20	43.53	146.75	44	7.1
1980	03	08	221210.30	-22.67	171.36	38	7.1
1980	03	24	035951.30	52.97	-167.67	33	7.1
1980	04	13	180431.90	-23.47	-177.30	79	7.2
1980	06	18	171454.50	9.48	126.66	54	7.2
1980	07	08	231919.80	-12.41	166.38	33	7.8
1980	07	17	194223.20	-12.52	165.92	33	8.0
1980	07	29	031156.30	-13.10	166.34	48	7.2
1980	10	10	122523.50	36.19	1.35	10	7.7
1980	10	24	145335.10	18.21	-98.24	72	7.0
1980	10	25	110005.10	-21.89	169.85	33	7.2
1980	11	08	102734.00	41.12	-124.25	19	7.2
1980	11	23	183453.80	40.91	15.37	10	7.2
1981	01	23	215441.60	-29.68	60.84	10	7.0
1981	01	30	085244.10	51.74	176.27	33	7.1
1981	04	24	215006.00	-13.43	166.42	33	7.3

1981	05	25	052514.40	-48.79	164.36	33	7.6
1981	07	06	030824.18	-22.29	171.74	33	7.0
1981	07	15	075908.47	-17.26	167.60	30	7.1
1981	07	28	172224.62	30.01	57.79	33	7.3
1981	09	01	092931.54	-14.96	-173.09	25	7.9
1981	10	16	032542.22	-33.13	-73.07	33	7.5
1981	10	25	032215.57	18.05	-102.08	33	7.4
1981	12	19	141050.72	39.24	25.23	10	7.6
1981	12	24	053320.71	-29.97	-177.61	28	7.0
1981	12	26	170532.52	-29.93	-177.74	33	7.1
1982	01	11	061006.49	13.75	124.36	45	7.4
1982	01	18	192724.45	40.00	24.32	10	7.0
1982	06	07	065237.37	16.61	-98.15	40	7.2
1982	06	07	105940.16	16.56	-98.36	33	7.0
1982	06	19	062158.00	13.31	-89.34	81	7.0
1982	06	30	015734.15	44.68	151.14	33	7.1
1982	07	07	104303.74	-51.22	160.51	10	7.3
1982	08	05	203252.95	-12.60	165.93	30	7.5
1982	08	19	155901.53	6.72	-82.68	10	7.0
1982	12	19	174354.85	-24.13	-175.86	33	7.7
1983	01	17	124129.70	38.03	20.23	14	7.2
1983	01	24	081739.61	16.15	-95.23	56	7.0
1983	03	18	090550.00	-4.88	153.58	88	7.9
1983	04	03	025001.18	8.72	-83.12	37	7.3
1983	05	26	025959.60	40.46	139.10	23	7.8
1983	07	11	125628.37	-60.89	-53.02	10	7.0
1983	08	06	154351.24	40.14	24.77	2	7.3
1983	08	17	105554.13	55.87	161.29	62	7.0
1983	10	04	185213.30	-26.53	-70.56	14	7.4
1983	10	28	140606.61	44.06	-113.86	10	7.3
1983	11	24	053034.23	-7.48	128.17	178	7.1

1983	11	30	174600.67	-6.85	72.11	10	7.7
1983	12	02	030905.66	14.07	-91.92	67	7.1
1983	12	30	235239.93	36.37	70.74	214	7.2
1984	02	07	213321.49	-10.01	160.47	18	7.7
1984	03	19	202838.24	40.32	63.35	14	7.1
1984	03	24	094402.60	44.12	148.19	44	7.0
1984	10	15	102107.50	-15.86	-173.64	128	7.1
1984	11	01	044850.27	8.19	-38.79	10	7.4
1984	11	17	064930.02	.20	98.03	33	7.4
1984	11	23	044606.38	-14.31	171.28	33	7.1
1984	12	28	103753.76	56.19	163.46	33	7.0
1985	03	03	224707.28	-33.13	-71.87	33	7.8
1985	03	03	233831.43	-32.74	-71.21	33	7.0
1985	04	09	015659.48	-34.13	-71.62	37	7.5
1985	05	10	153550.59	-5.60	151.04	26	7.3
1985	06	03	120621.13	-15.29	-173.52	33	7.0
1985	07	03	043651.73	-4.44	152.83	33	7.4
1985	08	23	124156.16	39.43	75.22	6	7.5
1985	09	19	131747.35	18.19	-102.53	27	8.1
1985	09	21	013713.47	17.80	-101.65	30	7.6
1985	09	26	072751.13	-34.69	-178.66	51	7.0
1985	11	17	094021.29	-1.64	134.91	10	7.1
1985	11	28	022542.34	-14.04	166.24	33	7.2
1985	11	28	034954.15	-13.99	166.18	33	7.6
1985	12	21	011322.41	-13.97	166.52	43	7.6
1986	04	30	070718.12	18.40	-102.97	26	7.0
1986	05	07	224710.87	51.52	-174.78	33	7.9
1986	06	24	031130.93	-4.45	143.94	102	7.1
1986	08	14	193913.67	1.79	126.52	33	7.4
1986	10	20	064609.98	-28.12	-176.37	29	8.3
1986	11	14	212010.55	23.90	121.57	33	7.8

1987	01	30	222942.09	-60.06	-26.92	47	7.0
1987	02	08	183358.39	-6.09	147.69	54	7.6
1987	03	05	091705.28	-24.39	-70.16	62	7.3
1987	03	06	041041.96	.15	-77.82	10	7.0
1987	07	06	024942.78	-14.07	167.83	47	7.1
1987	09	03	064013.91	-58.89	158.51	33	7.7
1987	10	06	041906.08	-17.94	-172.23	16	7.3
1987	10	16	204801.64	-6.27	149.06	47	7.7
1987	10	25	165405.69	-2.32	138.36	33	7.0
1987	11	17	084653.32	58.59	-143.27	10	7.0
1987	11	30	192319.59	58.68	-142.79	10	7.7
1988	02	24	035203.29	13.48	124.62	24	7.1
1988	03	06	223538.14	56.95	-143.03	10	7.6
1988	04	12	231955.57	-17.19	-72.31	33	7.0
1988	06	18	224942.37	26.86	-111.00	10	7.0
1988	08	06	003624.65	25.15	95.13	90	7.3
1988	08	10	043826.17	-10.37	160.82	34	7.4
1988	11	06	130319.34	22.79	99.61	17	7.3
1988	12	07	074124.20	40.99	44.19	5	7.0
1989	04	25	142900.51	16.77	-99.33	19	7.1
1989	05	23	105446.32	-52.34	160.57	10	8.2
1989	10	18	000415.24	37.04	-121.88	18	7.1
1989	10	27	210451.82	-11.02	162.35	24	7.1
1989	11	01	182534.94	39.84	142.76	28	7.4
1989	12	15	184345.03	8.34	126.73	24	7.4
1989	12	30	231851.64	-3.41	145.97	38	7.0
1990	03	03	121627.96	-22.12	175.16	33	7.4
1990	03	05	163812.57	-18.32	168.06	20	7.0
1990	03	25	132255.60	9.92	-84.81	22	7.0
1990	04	05	211235.55	15.13	147.60	11	7.5
1990	04	18	133919.01	1.19	122.86	25	7.4

1990	05	20	022201.62	5.12	32.15	14	7.4
1990	05	24	200008.19	5.36	31.85	16	7.0
1990	05	30	104006.14	45.84	26.67	89	7.1
1990	06	14	074056.21	11.76	121.90	18	7.1
1990	06	20	210009.98	36.96	49.41	18	7.7
1990	07	16	072634.61	15.68	121.17	25	7.8
1990	11	06	201429.74	53.45	169.87	24	7.0

APPENDIX B

The computer programs used in the thesis are available on a disk and can be obtained from the Dept of Earth Sciences, University of Western Ontario, London, Ontario, CANADA. N6A 5B7. I, or anyone else, is not responsible for any undetected bugs, errors etc.

Description of Computer Programs

Part I

```
FFT.f       : Fortran program for computing Fourier transform and
              Amplitude spectrum.

Filter.f    : Fortran program for band pass filtering the SG data.

Lsq_det.dat: Input to Lsqfit.f

Lsqfit.f    : Fortran Program for fitting customised wavelets.

param.dat   : Starting guess parameters
               Period    : Fourier periods from FFT.f  column 1
               Amplitude: 1.0                          column 2
               Phase     : 0.0                         column 3
               Q         : 100.0                       column 4

Resample.f : Fortran program for resampling the SG data.
```

syndata.dat: Input to Synth.f

synmode.dat: Input periods to make synthetic data.

Synth.f : Fortran program to make synthetic data.

A flow diagram for the usage of these routines is given on next page.

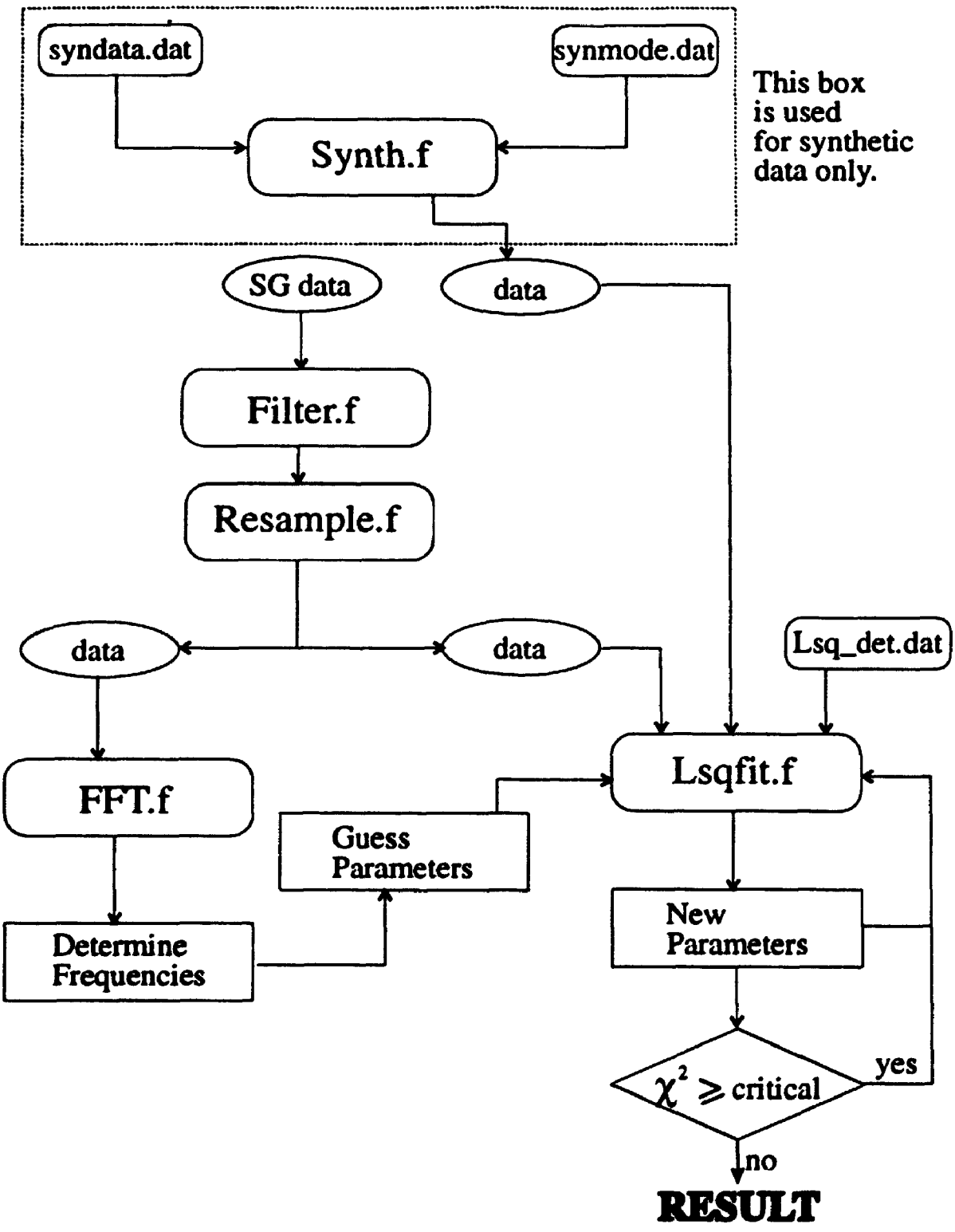
syndata.dat
synmode.dat
Synth.f
This box is used for synthetic data only.
SG data
data
Filter.f
Resample.f
data
data
Lsq_det.dat
FFT.f
Lsqfit.f
Guess Parameters
Determine Frequencies
New Parameters
$\chi^2 \geq$ critical
yes
no
RESULT

Part II

Analyze.f : Fortran program to compute the spectrum of various time series obtained using Make.f.

Eqden.f : Fortran program to apply KORRECT method (enclosed).

Lom.dat : Data file containing aftershock information (from USGS).

Make.f : Fortran program to make time series from the aftershock data set using different bin size, magnitude range, depth range, distance from the mainshock etc.

```
!                    Program EQDEN.F                    !
!                    ---------------                    !
!                                                       !
! Program for the cross correlation analysis of         !
! aftershock sequences with the Normal Modes excited    !
! by the mainshock.                                     !
!                                                       !
! kamal: 19921116 to 19930318                           !
!                                                       !
! Input:                                                !
!         (A) Aftershocks:-                             !
!                1. Occurence time                      !
!                2. Focal depth                         !
!                3. Magnitude                           !
!        (B) Additional:-                               !
!                1. Bin Size                            !
!                2. Depth Bounds                        !
!                3. Magnitude Bounds                    !
!                4. Time Bounds                         !
!                5. Phase Shift                         !
!                                                       !
! Output:                                               !
!         Returns the maximum and minimum Amplitude and !
!        Phase information for different frequencies.   !
!                                                       !

parameter (npt = 10000, Ndays = 120, Npts = Ndays*24*60)
real depth(npt), Magnitude(npt), Phase_min(npt)
real azigap, dist, herror, lngdeg, lngmin, Ave_den(npt)
real resdul, sec, verror, latdeg, latmin, longitude(npt)
real latitude(npt), Events_info(36,400,6)
```

```
      real TimeEq(npt), Frequency(npt), Amp_max(npt),Amp_min(npt)
      real DepthLower, DepthUpper, MagLower, MagUpper,Phase_shift
      real Bin_start, Bin_end, No_of_events, Phase_max(npt)
      integer year, month, day,hour,min,PST, DayOfYear,Total_eq
      integer Spectral_points, Scale_factor, Points_to_plot
      character*1 latdir, lngdir
      character*3 stn
      character*20 Input_file, Output_file
      character*36 Data_field

      open(unit=1, file='eqden.dat',status='old')
      open(unit=7,file='Phase.var')
      open(unit=8,file='0s2.eve')
      open(unit=9,file='0t2.eve')
      open(unit=10,file='events.dat')
      read (1,*) Data_field, Input_file    ! Input_file is the
                                           ! Data file containing
                                           ! aftershock data
      open(unit=50, file=Input_file, status='old')
      read(1,*) Data_field, Bin_size         ! in Minutes
      Bin_size = 60.*Bin_size                ! in seconds

      write(6,101) Input_file
      do i = 1, npt
         if (mod(i,100) .eq. 0) write(6,102)
         read(50, 10) year, month, day, hour, min, sec, latdeg,
     &              latdir, latmin, lngdeg, lngdir, lngmin,
     &              depth(i), Magnitude(i), PST, azigap, dist,
     &              resdul, herror, verror, stn
         call TimeSinceEarthquake(year,month,day,hour,min,sec,
     &          DayOfYear, TimeEq(i),lngdeg,lngmin,latdeg,latmin,
```

```
     &                longitude(i), latitude(i))
           write(10,*)TimeEq(i),Magnitude(i),depth(i),longitude(i),
     &                latitude(i)
           if(DayOfYear.gt.Ndays) go to 100
                                    ! Make series upto Ndays only
                                    ! (See parameter statement)
           end do
101        format(' Reading ',a15,'....',$)
100        write(6,*)  ' Done'
102        format(' .',$)
10         format(3i2, 1x, 2i2, f6.2, f3.0, a1, f5.2, f4.0, a1, f5.2,
     &       f7.2, 2x, f5.2, i3, f4.0, f5.1, f5.2, f5.1, f5.1, a3)
           close(50)
30         format(10f8.0)
           Total_eq = i
           write(10,*) Total_eq
           close(10)
           write(6,*) Data_field, Bin_size
           write(7,*) Data_field, Bin_size
           read(1,*) Data_field, DepthLower, DepthUpper   ! in km
           write(6,*) Data_field, DepthLower, DepthUpper
           write(7,*) Data_field, DepthLower, DepthUpper
           read(1,*) Data_field, MagLower, MagUpper       ! M_L
           write(6,*) Data_field, MagLower, MagUpper
           write(7,*) Data_field, MagLower, MagUpper
           read(1,*) Data_field, Start_time, End_time     ! in hours
           write(6,*) Data_field, Start_time, End_time
           write(7,*) Data_field, Start_time, End_time
           read(1,*) Data_field, Phase_shift              ! in Degrees
           write(6,*) Data_field, Phase_shift
           write(7,*) Data_field, Phase_shift
```

```
      close(1)

      write(7,*) '  Period(min)     Phase_Shift     Total_events'
      Start_time = Start_time *60.*60.                ! in Seconds
      End_time = End_time *60.*60.                    ! in Seconds
      Total_time = End_time - Start_time
      Spectral_points = nint( Total_time/Bin_size )
      Points_to_plot = 0
      do i = 1, Spectral_points/2
        Frequency(i) =(float(i)*86400.)/          ! Frequency in
     &           (Bin_size*float(Spectral_points)) ! cycles/day
        if (Frequency(i) .lt. 36.) then
          Points_to_plot = Points_to_plot + 1  ! Limit
        else                                   ! the Frequencies
          write(6,*) ' Points to plot = ' ,Points_to_plot
          go to 20                             ! to
        end if                                 ! 50 cycles/day
      end do
20      write(6,110)
110      format(' Computing....',$)
      do i = 1, Points_to_plot
        Period = Bin_size * float(Spectral_points)/float(i)
        Shift = amod(Start_time,Period)           ! To force
        if (Shift.gt.(Period/2.)) then            ! the starting
          Shift = (-1.0) * (Period - Shift)       ! point to be
        end if                                    ! at a complete
        Start_instant = Start_time + Shift        ! cycle
        call EarthquakeDensity(Amp_max(i),Amp_min(i),Bin_size,
     &       Period,TimeEq,Magnitude,depth,End_time,Phase_max(i),
     &       Bin_start, Bin_end, MagLower, MagUpper,Phase_min(i),
     &       DepthLower, DepthUpper, Total_eq, No_of_events,
```

```
     &       Phase_shift, Start_instant, longitude, latitude)
           write(6,120)
         end do
120        format(' #',$)
         write(6,*) ' Done'
         close(7)
         close(8)
         close(9)
         open(unit=2, file='outputft')
         do i = 1, Points_to_plot
           write(2,*) Frequency(i), Amp_max(i), Phase_max(i),
     &                          Amp_min(i), Phase_min(i)
         end do
         close(2)
                        ! Plotting of Amplitude and Phase !
         call plots(1, 4, 6)
         call factor(0.75)
         call note(500,25)
         call note(750,25)
         call note(1000,100)
         call color(2)
         call PLOTIT(Frequency,Amp_max,Points_to_plot,0.5,0.2,
     &       6.0,3.0,'FREQ (CYCLES/DAY)',17,'POWER',5)
         call color(3)
         call PLOTIT(Frequency,Amp_min,Points_to_plot,7.5,0.2,
     &       6.0,3.0,'FREQ (CYCLES/DAY)',17,'POWER',5)
         call symbol(3.5,4.2,0.1,' BIN SIZE (MIN)= ',0.,+17)
         call number(999.,999.,0.1,Bin_size/60.,0.,2)
         call symbol(999.,999.,0.1,21,0.,1)
         call symbol(999.,999.,0.1,' DEPTH LOWER= ',0.,+14)
         call number(999.,999.,0.1,DepthLower,0.,2)
```

```
      call symbol(999.,999.,0.1,' DEPTH UPPER= ',0.,+14)
      call number(999.,999.,0.1,DepthUpper,0.,2)
      call symbol(999.,999.,0.1,21,0.,1)
      call symbol(999.,999.,0.1,' MAG LOWER= ',0.,+12)
      call number(999.,999.,0.1,MagLower,0.,2)
      call symbol(999.,999.,0.1,'   MAG UPPER= ',0.,+14)
      call number(999.,999.,0.1,MagUpper,0.,2)
      call symbol(999.,999.,0.1,21,0.,1)
      call symbol(999.,999.,0.1,' START POINT= ',0.,+14)
      call number(999.,999.,0.1,Start_time/3600.,0.,0)
      call symbol(999.,999.,0.1,'  END POINT= ',0.,+13)
      call number(999.,999.,0.1,End_time/3600.,0.,0)
      call symbol(999.,999.,0.1,21,0.,1)
      read(5,*)
      call plot(0.,0.,999)
      stop
      end
*************************************************************************
      subroutine EarthquakeDensity(Amp_max,Amp_min, Bin_size,
     &      Period, TimeEq, Magnitude, depth, End_time, Phase_max,
     &      Bin_start, Bin_end, MagLower, MagUpper, Phase_min,
     &      DepthLower, DepthUpper, Total_eq, No_of_events,
     &      Phase_shift, Start_time, longitude, latitude)
      real TimeEq(1), Magnitude(1), depth(1), No_of_events
      real DepthLower, DepthUpper, MagLower, MagUpper
      real Bin_start, Bin_end, Psuedo_amp(100), Phase
      real langitude(1), latitude(1), Events_info(36,400,6)
      integer Total_eq, Phase_counter, events
      Phase_counter = 0
      Time_shift = 0.0
      Bin_width = Bin_size
```

```
      Shift_time = 360. / Phase_shift  ! Convert Degrees in time
      events = 0
10       if( Phase_counter .ge. nint(Shift_time) ) go to 30
      Phase_counter = Phase_counter + 1
      Time_shift = float(Phase_counter-1) * Period/Shift_time
      Total_events = 0.0
      Bin_counter = 1.0
20      Bin_start = Start_time +  Period*(Bin_counter-1.0)
     &                    + Time_shift
      Bin_end = Bin_start + Bin_width
      call CountEvents(No_of_events, Time_eq, Magnitude, depth,
     &       Bin_start, Bin_end, MagLower, MagUpper, DepthLower,
     &        DepthUpper, Total_eq, longitude, latitude, Period,
     &              Events_info, Phase_counter, events)
      Total_events = Total_events + No_of_events
      events=nint(Total_events)
      if((Bin_end+Period+Bin_width).gt. End_time) then
         Psuedo_amp(Phase_counter) = Total_events /
     &                (Bin_width*Bin_counter)
            write(7,*) Period/60., Phase_counter*Phase_shift,
     &                        Total_events/Bin_counter
      else
         Bin_counter = Bin_counter + 1.0
         go to 20
      end if
      go to 10
30      Amp_max = Psuedo_amp(1)
      Amp_min = Psuedo_amp(1)
      Phase_max = 0.0
      Phase_min = 0.0
      do i = 2, nint(Shift_time)
```

```
          if( Psuedo_amp(i) .gt. Amp_max) then
            Amp_max = Psuedo_amp(i)
            Phase_max = float(i)*Phase_shift          ! in Degrees
          end if
          if( Psuedo_amp(i) .lt. Amp_min ) then
            Amp_min = Psuedo_amp(i)
            Phase_min = float(i)*Phase_shift          ! in Degrees
          end if
        end do
        do i = 1, Phase_counter
            if (Period.gt.3315. .and. Period.lt.3330.) then
            if (Psuedo_amp(i).eq.Amp_max) then     ! OS2
              do j = 1, events
                write(8,*) (Events_info(i,j,k), k= 1, 6)
              end do
            end if
          end if
          if (Period.gt.2580. .and. Period.lt.2600.) then
            if (Psuedo_amp(i).eq.Amp_max) then     ! OT2
              do j = 1, events
                write(9,*) (Events_info(i,j,k), k= 1, 6)
              end do
            end if
          end if
        end do
        return
        end
*************************************************************************
        subroutine CountEvents(No_of_events, TimeEq, Magnitude,
     &    depth,Bin_start, Bin_end, MagLower, MagUpper, DepthLower,
     &    DepthUpper, Total_eq, longitude, latitude, Period,
```

```
&     Events_info, Phase_counter,events)
      real TimeEq(1), Magnitude(1), depth(1), No_of_events
      real DepthLower, DepthUpper, MagLower, MagUpper, Period
      real Bin_start, Bin_end, longitude(1), latitude(1)
      real Events_info(36,400,6)
      integer Total_eq, Phase_counter, events
      No_of_events = 0.0
      do j = 1, Total_eq
       if(TimeEq(j).gt.Bin_start .and.
&      TimeEq(j).le.Bin_end)then
        if (depth(j).ge.DepthLower) then
         if (depth(j).le.DepthUpper) then
          if (Magnitude(j).ge.MagLower) then
           if (Magnitude(j).le.MagUpper) then
            No_of_events = No_of_events + 1.0
            events = events + 1
            Events_info(Phase_counter,events,1) = TimeEq(j)/60.
            Events_info(Phase_counter,events,2) = Magnitude(j)
            Events_info(Phase_counter,events,3) = depth(j)
            Events_info(Phase_counter,events,4) = longitude(j)
            Events_info(Phase_counter,events,5) = latitude(j)
            Events_info(Phase_counter,events,6) = float(j)
           end if
          end if
         end if
        endif
       end if
      end do
      return
      end
*************************************************************************
```

```
      subroutine TimeSinceEarthquake(year,month,day,hour,min,sec,
     &          DayOfYear, TimeEq, lngdeg, lngmin, latdeg, latmin,
     &          longitude, latitude)
      real sec, TimeEq, longitude, latitude, lngdeg, lngmin
      real latdeg, latmin
      integer DaysInMonth(12)
      integer year, month, day, hour, min
      integer YearInit, DayInit, DayOfYear
      data DaysInMonth/31, 28, 31, 30, 31, 30, 31,
     &                 31, 30, 31, 30, 31/
      YearInit = 89                    ! Starting Year, 1989
      DayInit = 291                    ! Starting Day, October 18
      DayOfYear = (year - YearInit)*365
      if (mod(year,4).eq.0) DaysInMonth(2) = 29
      do i = 1, month-1
         DayOfYear = DayOfYear + DaysInMonth(i)
      end do
      DayOfYear = DayOfYear + day
         longitude = lngdeg + lngmin/60.
         latitude = latdeg + latmin/60.
         TimeEq = float(DayOfYear-DayInit)*24.* 60.* 60.
     &                     + float(hour)* 60.* 60.
     &                     + float(min) * 60.
     &                     + sec
     &                     - (4.* 60. + 15.34)  ! Eq Origin Time
      DayOfYear = DayOfYear- DayInit
      return
      end
*****************************************************************
      subroutine PLOTIT(xplt,yplt,npt,Xorigin,Yorigin,
     &                  Xlength,Ylength,xtitle,xchr,ytitle,ychr)
```

```
      integer xchr, ychr
      real xplt(1), yplt(1), Xlength, Ylength, Xorigin, Yorigin
      character xtitle, ytitle
      call plot(Xorigin,Yorigin,-3)
      call scale(xplt, Xlength, npt,+1)
      call scale(yplt, Ylength, npt, +1)
      call axis(0.,0.,xtitle,-xchr,Xlength,0.,xplt(npt+1),
     &          xplt(npt+2))
      call axis(0.,0.,ytitle,+ychr,Ylength,90.,yplt(npt+1),
     &          yplt(npt+2))
      call line(xplt, yplt, npt, 1, 0, 1)
      call plot(-Xorigin,-Yorigin,-3)
      return
      end
*****************************************************************************
```

References

[1] Aki, K. and Richards, P.G., 1980. *Quantitative Seismology: Theory and Methods*, W.H.Freeman, San Francisco, CA. 577 p.

[2] Allen, M.W., 1936. The lunar triggering effect on earthquakes in Southern California. *Bull. Seismol. Soc. Am.*, **26**, 147-157.

[3] Alsop, L.E., 1964. Spheroidal free periods of the earth observed at eight stations around the world. *Bull. Seismol. Soc. Am.*, **54**, 755-776.

[4] Alsop, L.E., Sutton, G.H. and Ewing M., 1961. Measurements of Q for very long period free oscillations. *Jour. Geophys. Res.*, **66**, 2911-2915.

[5] Anderson, D.L. and Archambeau, C.B., 1964. The anelasticity of the earth. *Jour. Geophys. Res.* , **70**, 1441.

[6] Anderson, D.L. and Dziewonski, A.M., 1982. Upper Mantle anisotropy: evidence from free oscillations, *Geophy. Jour. Roy. astr. Soc.*, **69**, 383-404.

[7] Benioff, H.,Press, F. and Smith, S., 1961. Excitation of the free oscillations of the earth by earthquakes. *Jour.Geophys.Res.*, **66**, 605.

[8] Ben-Menahem, A.,and Israel, M., 1970. Effect of major seismic events on the rotation of the earth. *Geophy. Jour. Roy. astr. Soc.*, **19**, 367-393.

[9] Bevington, P.R. , 1969. *Data Reduction and Error Analysis for the Physical Sciences*, McGraw-Hill Book Co., NY, 336 p.

[10] Block, B., Dratler, J., and Moore, R.D., 1970. Earth normal modes from a 6.5 magnitude earthquake. *Nature*, **226**, 343-344.

[11] Bolt, B.A. and Brillinger, D.R., 1979. Estimation of uncertainties in eigenspectral estimates from decaying geophysical time series. *Geophys.J.R.astr.Soc.*, **59**, 593-603.

[12] Buland, R. and Gilbert, F., 1978. Improved resolution of complex eigen frquencies in analytically continued seismic spectra. *Geophys.J.R.astr.Soc.*, **52**, 457-470.

[13] Burr, E.J., 1960. Earthquakes and Uranus: Misuse of a statistical test of significance. *Nature*, **186**, 336.

[14] Cauchy, A., 1848. Méthode générale pour la résolution des systèmes déquations simultanées. *C. R. Acad. Sci. Paris*, **27**, 536-538.

[15] Chao, B.F. and Gilbert, F., 1980. Autoregressive estimation of complex eigenfrequencies in low frequency seismic spectra. *Geophys.J.R.astr.Soc.*, **44**, 77-105.

[16] Childers, D. and Durling, A., 1975. *Digital filtering and signal processing.* West publishing co., 539 p.

[17] Dahlen, F.A., 1982. The effect of data windows on the estimation of free oscillation parameters. *Geophys. J. R. astr. Soc.*, **69**, 537-549.

[18] Davison, C., 1927. Clustering and periodicity of Earthquakes. *Nature*, **120**, 587.

[19] Davison, C., 1934. The origin of earthquakes as illustrated by their periodicity. *Geological Magazine*, **71**, 493.

[20] Davison, C., 1935. Periodic variations in the mean focal depth of Japanese earthquakes. *Nature*, **135**, 76-77.

[21] Delauney, J., 1880. Planets an.. earthquakes. *Am. Journ. Sci.*, **119**, 162.

[22] Dietz, L.D., and Ellsworth, W.L., 1990. The October 17, 1989, Loma Prieta, California, Earthquake and its aftershocks: Geometry of the sequence from high-resolution locations. *Geophys. Res. Lett.*, **17**, 1417-1420.

[23] Dratler, J., Farrell, W.E., Block, B. and Gilbert, F., 1971. High-Q overtone modes of the earth. *Geophys.J.R.astr.Soc.*, **23**, 399-410.

[24] Dziewonski, A.M. and Anderson, D.L., 1981. Preliminary reference earth model. *Phys. Earth Plan. Int.*, **25**, 297-356.

[25] Eaton, J.P., O'neill, M.E. and Murdock, J.N., 1970. Aftershocks of 1966 Parkfield-Chalome, California, earthquake - a detailed study. *Bull. Seismol. Soc. Am.*, **60**, 1151.

[26] Fadeli, A., Rydelek, P.A., Emter, D. and Zürn, W., 1991. On volcanic shocks at Merapi and tidal triggering. *in* Volcanic tremor and magma flow edited by R.Schick and R. Mugiono. Forschungszentrum Jülich.

[27] Fisher, R.A., 1929. Test of significance in harmonic analysis. *Proc. R. Soc.*, **A 125**, 54-59.

[28] Fraser-Smith, A.C., Bernardi, A., McGill, P.R., Ladd, M.E., Helliwell, R.A. and Villard, O.G.(Jr.), 1990. Low frequency magnetic field measurements near the epicenter of the M_S7.1 Loma Prieta earthquake, *Geophys. Res. Lett.*, **17**, 1465-1468.

[29] Geller, R.J. and Stein, S., 1979. Time domain attenuation measurements for fundamental spheroidal modes (${}_0S_6$ to ${}_0S_{28}$) for the 1977 Indonesian earthquake. *Bull. Seismol. Soc. Am.*, **69**, 1671-1691.

[30] Gilbert, F., 1973. Derivation of source parameters from low-frequency spectra. *Phil. Trans. R. Soc. Lond.*, **A 274**, 369-371.

[31] Gilbert, F. and Dziewonski, A.M., 1975. An application of normal mode theory to the retrieval of structural parameters and source mechanisms from seismic spectra. *Phil. Trans. R. Soc. London*, **A 278**, 187-269.

[32] Goulty, N.R., 1979. Tidal triggering of deep moonquakes. *Phys. Earth. Plan. Int.*, **19**, 52-58.

[33] Gribbin, J., 1971. Relation of Sunspot and earthquake activity. *Science*, **173**, 558.

[34] Gribbin, J.R. and Plagemann, S.H., 1974. *The Jupiter effect.* Walker and Company, New York, 134 p.

[35] Gubbins, D., 1990. *Seismology and Plate Tectonics.* Cambridge Univ Press, Cambridge, 339 p.

[36] Gupta, H.K. and Rastogi, B.K., 1976. *Dams and Earthquakes*, Amsterdam: Elsevier, 299 pp.

[37] Hanks, T.C., 1977. Earthquake stress drops, ambient tectonic stresses and stress that drive plate motions. *Pageoph*, **115**, 441-458.

[38] Hansen, R.A., 1982. Observational study of terrestrial eigenvibrations. *Phys. Earth Plan. Int.*, **28**, 27-69.

[39] Hartley, H.O., 1961. The modified Gauss-Newton method for the fitting of non linear regression functions by least squares. *Technometrics*, **3**, 269-280.

[40] Hartzell, S.H., Stewart, G.S. and Mendoza, C., 1991. Comparison of L_1 and L_2 norms in a teleseismic waveform inversion for the slip history of the Loma Prieta, California, Earthquake. *Bull. Seismol. Soc. Am.*, **81**, 1518-1539.

[41] Hazard, D.L., 1909. Peculiar magnetic distribution in December, 1908. *Terrestrial magnetism and atmospheric electricity*, **14**, 37.

[42] Healy, J.H., Rubey, W.W., Griggs, D.T. and Raleigh, C.B., 1968. The Denver earthquake, *Science*, **161**, p 1301-1310.

[43] Heaton, T.H., 1975. Tidal triggering of earthquakes. *Geophys. J. R. astr. Soc.*, **43**, 307-326.

[44] Hill, D.P., Reasenberg, P.A., Michael, A., Arabaz, W.J., Beroza, G., Brumbaugh, D., Brune, J.N., Castro, R., Davis, S., dePolo, D., Ellsworth, W.L., Gomberg, J., Harmsen, S., House, L., Jackson, S.M., Johnston, M.J.S., Jones, L., Keller, R., Malone, S., Munguia, L., Nava, S., Pechmann, J.C., Sanford, A., Simpson, R.W., Smith, R.B.,

Stark, M., Stickney, M., Vidal, A., Walter, S., Wong, V. and Zollweg, J., 1993. Seismicity remotely triggered by the magnitude 7.3 Landers, California, earthquake. *Science*, **260**, 1617-1623.

[45] Hori, S., Fukao, Y., Kumazawa, M., Furumoto, M. and Yamamoto, A., 1989. A new method of spectral analysis and its applications to the earth's free oscillations: The "Sompi" method. *Jour. Geophys. Res.*,**94**, 7535-7553.

[46] Hughes, D.W., 1977. Planetary alignments don't cause earthquakes. *Nature*, **265**, 13.

[47] Ip, W.H., 1976. Chinese Records on the correlation of heliocentric planetary alignments and earthquake activities. *Icarus*, **29**, 435.

[48] Johnston, M., 1978. Tectonomagnetic effects. *Earthquake Information Bulletin*, **10**, 82.

[49] Kamal and Mansinha, L., 1992. A test of the superconducting gravimeter as along period seismometer. *Phys. Earth Plan. Int.*, **71**, 52-60.

[50] Kanamori, H., 1976. Are earthquakes a major cause of the Chandler Wobble. *Nature*, **262**, 254.

[51] Kanamori, H., 1977. The energy release in great Earthquakes *J. Geophy. Res.*, **82**, 2981-2987.

[52] Kanamori, H. and Anderson, D.L., 1975. Theoretical basis of some empirical relations in seismology. *Bull. Seismol. Soc. Am.*, **65**, 1073-1095.

[53] Kanamori, H., Hauksson, E. and Heaton, T., 1992. TERRAscope. *EOS*, **73**, 371.

[54] Kanamori, H. and Satake, K., 1990. Broadband study of the 1989 Loma Prieta Earthquake. *Geophy. Res. Lett.*, **17**, 1179-1182.

[55] Kelvin, Lord (Sir William Thomson), 1864. Dynamical problems regarding elastic spherical shells and spheroids of incompressible liquid. *Phil. Trans. Roy. Soc.*, **153**, 563-616.

[56] Kilston, S. and Knopoff, L., 1983. Lunar-Solar periodicities of large earthquakes in southern California. *Nature*, **304**, 21-25.

[57] Klein, F.W., 1976. Earthquake swarms and the semidiurnal solid earth tide. *Nature*, **304**, 21-25. *Geophys. J. R. astr. Soc.*, **45**, 245-295.

[58] Klein, F.W., 1989. User's guide to HYPOINVERSE, a program for VAX computer to solve earthquake locations and magnitudes. *U. S. Geol. Surv., Open-File Rep.*, **89-314**, 58.

[59] Knopoff, L., 1964a. Q. *Rev. Geophys.*, **2**, 625-660.

[60] Knopoff, L., 1964b. Earth tides as a triggering mechanism for earthquakes. *Bull. Seismol. Soc. Am.*, **54**, 1865-1870.

[61] Knopoff, L., 1969. The triggering of large earthquakes by earth tides. *EOS*, **50**, 399.

[62] Knott, C.G., 1886. Earthquake frequency. *Trans. Seis. Soc. Japan*, **9**

[63] Knott, C.G., 1897. On lunar periodicities in earthquake frequency. *Proc. Roy. Soc.*, **60**, 457-466.

[64] Lake, J.J., 1875. Earthquake and their causes. *English Mechanic*, **21**, 51.

[65] Lamb, H., 1882. On the vibrations of an elastic sphere. *London Math. Soc. Proc.*, **13**.

[66] Lamé, M.G., 1853. Memoire sur l'équilibre d'élasticitié des envelopes sphériques. *Comptes Rendus*, **37**.

[67] Lammelein, D.R., Latham, G.V., Dorman, J., Nakamura, Y. and Ewing, M., 1974. Lunar seismicity, stucture and tectonics. *Rev. Geophy. Space Phy.*, **12**, 1-21.

[68] Lamont, J., 1892. Connexion between earthquakes and magnetic disturbances. *Philosophical Magazine*, **what**, 559.

[69] Lapwood, E.R. and Usami, T., 1981. *Free Oscillations of the Earth.* Cambridge Univ Press, Cambridge, 243 p.

[70] Latham, G., Ewing, M., Dorman, J., Lammelein, D., Press, F., Töksoz, N., Sutton, G., Duennebier, F. and Nakamura, Y., 1971. Moonquakes. *Science*, **174**, 687-692.

[71] Lindberg, C.R. and Park, J., 1987. Multiple-taper spectral analysis of terrestrial free oscillations: part II. *Geophys. J. R. astr. Soc.*, **91**, 795-836.

[72] Love, A.E.H., 1911. *Some Problems of Geodynamics.* Cambridge University Press.

[73] Mandelbrot, B., 1983. *The Fractal Geometry of Nature.* W.H.Freeman & Co., p 408.

[74] Mansinha, L., Smylie, D.E., 1967. Effect of earthquakes on the Chandler Wobble and the secular pole shift. *J. Geophys. Res.*, **72**, 4731-4743.

[75] Mansinha, L., Smylie, D.E., 1968. Earthquakes and the earth's Wobble. *Science*, **161**, 1127.

[76] Marquardt, D.W., 1963. An algorithm for least-square estimation of nonlinear parameters. *J. Soc. Ind. Appl. Math.*, **II(2)**, 431-441.

[77] Marshall, G.A., Stein, R.S. and Thatcher, W., 1991. Faulting geometry and slip from co-seismic elevation changes: the 18 October, 1989, Loma Prieta, California, Earthquake. *Bull. Seismol. Soc. Am.*, **81**, 1660-1693.

[78] Masters, G. and Gilbert, F., 1983. Attenuation in the earth at low frequencies. *Phil. Trans. Roy. Soc. London*, **A 308**, 479-522.

[79] McNally, K.C., Lay, T., Protti-Quesada, M., Valensise, G., Orange, D. and Anderson, R.S., 1989. Santa Cruz mountains (Loma Prieta) earthquake. *EOS*, **70**, 1463-1467.

[80] Meeus, Jean, 1976. Sunspots and earthquakes. *Physics Today*, **29**, 11.

[81] Mendiguren, J.A., 1980. Inversion of free oscillation data for an elliptical rotating earth in source moment tensor studies. *Pageoph*, **118**, 1192-1208.

[82] Meyerson, R.J., 1970. Long term evidence for the association with the excitation of the Chandler wobble. *Jour. Geophy. Res.*, **75**, 6612-6617.

[83] Milne, John, 1886. *Earthquakes*. Kegan Paul, Trench & Co. , London.

[84] Mohler, Amy S., 1980. Earthquake/Earth-tide correlation and other features of the Susanville, California, earthquake sequence of June-July 1976. *Bull. Seismol. Soc. Am.*, **70**, 1583-1593.

[85] Molchanov, O.A., Kopytenko, Y.A., Voronov, P.M., Kopytenko, E.A., Matiashvili, T.G., Fraser-Smith, A.C. and Bernardi, A., 1992. Results of ULF magnetic field measurements near the epicenters of the Spitak(M_S = 6.9) and Loma Prieta(M_S = 7.1) earthquakes: comparative analysis. *Geophy. Res. Lett.*, **19**, 1495-1498.

[86] Moore, George W., 1964. Magnetic disturbances preceding the 1964 Alaska earthquake. *Nature*, **203**, 508.

[87] Nowroozi, A.A., 1968. Measurements of Q values from the free oscillations of the earth. *J. Geophys. Res.*, **73**, 1407-1415.

[88] O'Connell, R.J. and Dziewonski, A.M., 1976. Excitation of the Chandler Wobble by large earthquakes. *Nature*, **262**, 259.

[89] Oldham, R.D., 1902. On the tidal periodicity in the earthquakes of Assam. *Jour. Asiatic Soc. Bengal*, **71**, 139-153.

[90] Oldham, R.D., 1903. The diurnal variation in frequency of the aftershocks of the great earthquake of June 12, 1897. *Mem. Geol. Surv. India*, **35**, 1-34.

[91] Omori, F., 1904. Note on the lunar-daily distribution of earthquakes. *Pub. Eqke. Inv. Comm. Tokyo*, **18**, 27-40.

[92] Oppenheimer, David H., 1990. Aftershock slip behavior of the 1989 Loma Prieta, California earthquake. *Geophy. Res. Lett.*, **17**, 1199-1202.

[93] Perrey, Alexis, 1847. Record of Perrey's report. *Comptes Rendus*, **24**, 822.

[94] Perrey, A., 1864. Theory of earthquakes. *Am. Jour. Sci.*, **37**.

[95] Perrey, A., 1875. Sur la fréquence des tremblents de terre relativement a l'âge de le lune. *Comptes Rendus*, **81**, 690-692.

[96] Phillips, Ed S., 1917. Great earthquakes and certain lunar longitudes. *English Mechanic*, **105**, 25.

[97] Pines, D., and Shaham, J., 1973. Seismic activity, polar tides and the Chandler Wobble. *Nature*, **245**, 77.

[98] Pollitz, F.F., 1990. Recovery of aspherical structure from the observations of normal mode amplitudes. *Geophys. J. Int.*, **102**, 313-339.

[99] Powell, M.J.D., 1975. Restart procedures for the conjugate gradient method. *CSS Report No. 23* (Harwell, UK; Computer science and systems division, Atomic Energy Research Establishment).

[100] Press, F., and Briggs, P., 1975. Chandler woobble, earthquakes, rotation and geomagnetic changes. *Nature*, **256**, 270.

[101] Press, W.H., Teukolsky, S.A., Vetterling, W.T. and Fiannery, B.P., 1992. *Numerical Recipes in FORTRAN, The art of scientific computing*, Cambridge University Press, p 963.

[102] Price, H.J., 1979. An improved Prony algorithm for exponential analysis *in* Proccedings of the IEEE International symposium on electromagnetic capability, pp 310-313, Institute of Electrical and Electronics Engineers, New York.

[103] Reid, Harry F., 1914. The influence of earthquake disturbances on suspended magnets. *Bull. Seismol. Soc. Am.*, **4**, 204.

[104] Sailor, R.V. and Dziewonski, A.M., 1978. Measurements and interpretation of normal mode attenuation. *Geophys. J. R. astr. Soc.*, **53**, 559-581.

[105] Scholz, C.H., 1990. *The Mechanics of Earthquakes and Faulting.* Cambridge Univ Press, Cambridge NY, 439 p.

[106] Schuster, Arthur, 1897. On lunar and solsr periodicities of earthquakes. *Proc. Roy. Soc.*, **61**, 455-465.

[107] Shaw, J.J., 1917. Earthquakes and lunar longitudes. *English Mechanic*, **104**, 473.

[108] Shimshoni, Michael, 1971. On Fisher's test of significance in harmonic analysis. *Geophys. J. R. astr. Soc.*, **23**, 373-377.

[109] Shlien, Seymor, 1972. Earthquake-Tide correlation. *Geophys. J. R. astr. Soc.*, **28**, 27-34.

[110] Silver, P.G. and Jordan, T.H., 1981. Fundamental spheroidal mode observations of aspherical heterogeneity. *Geophys. J. R. astr. Soc.*, **64**, 605-634.

[111] Simpson, D.W., 1986. Triggered earthquakes, *Ann.Rev.Earth Plan.Sci*, **14**, p 21-42.

[112] Simpson, D.W., Leith, W.S. and Scholz, C.H., 1988. Two types of reservoir induced seismicity. *Bull. Seismol. Soc. Am.*, **78**, 2025-2040.

[113] Smith, B.E. and Johnston, M.J.S., 1976. A tectonomagnetic effect observed before a magnitude 5.2 earthquake near Hollister, California. *Jour. Geophys. Res.*, **81**, 3556.

[114] Smith, M.F. and Masters, G., 1989. Aspherical structure constraints from free oscillation frequency and attenuation measurements. *Jour. Geophys. Res.*, **94**, 1953-1976.

[115] Snay, R.A., Neugebauer, H.C. and Prescott, W.H., 1991. Horizontal deformation associated with the Loma Prieta earthquake. *Bull. Seismol. Soc. Am.*, **81**, 1647-1659.

[116] Steidl, J.H., Archuleta, R.J. and Hartzell S.H., 1991. Rupture history of the 1989 Loma Prieta, California, earthquake. *Bull. Seismol. Soc. Am.*, **81**, 1573-1602.

[117] Stein, S and Geller R.J., 1978. Time domain observation and synthesis of split spheroidal and torsional free oscillations of 1960 Chilean earthquake- preliminary results, *Bull. Seismol. Soc. Am.*, **68**, 325-332.

[118] Thomson, D.J., 1982. Spectrum estimation and harmonic analysis. *Proc. IEEE*, **70**, 1055-1096.

[119] Tomashek, R., 1959. Great earthquakes and the astronomical positions of Uranus. *Nature*, **184**, 177.

[120] Wallace, T.C., Velasco, A., Zhang, J. and Lay, T., 1991. A broadband seismological investigation of the 1989 Loma Prieta, California, earthquake: Evidence for deep slow slip? *Bull. Seismol. Soc. Am.*, **81**, 1722-1646.

[121] Wallis, J.B., 1905. The cause of earthquakes: Is it all extra-terrestrial? *Fnglish Mechanic*, **82**, 277.

[122] Watada, S., Kanamori, H. and Anderson, D., 1993. An analysis of nearfield normal mode amplitude anomalies of the Landers earthquake. *Geophys. Res. Lett.*, **20**, 2611-2614.

[123] Woodward, R.L. and Masters, G., 1992. Upper mantle structure from long period differential travel times and free oscillation data. *Geophys. J. Int.*, **109**, 275-293.

[124] Young, D. and Zürn, W., 1979. Tidal triggering of earthquakes in the Swabian Jura? *J. Geophys.*, **45**, 171-182.